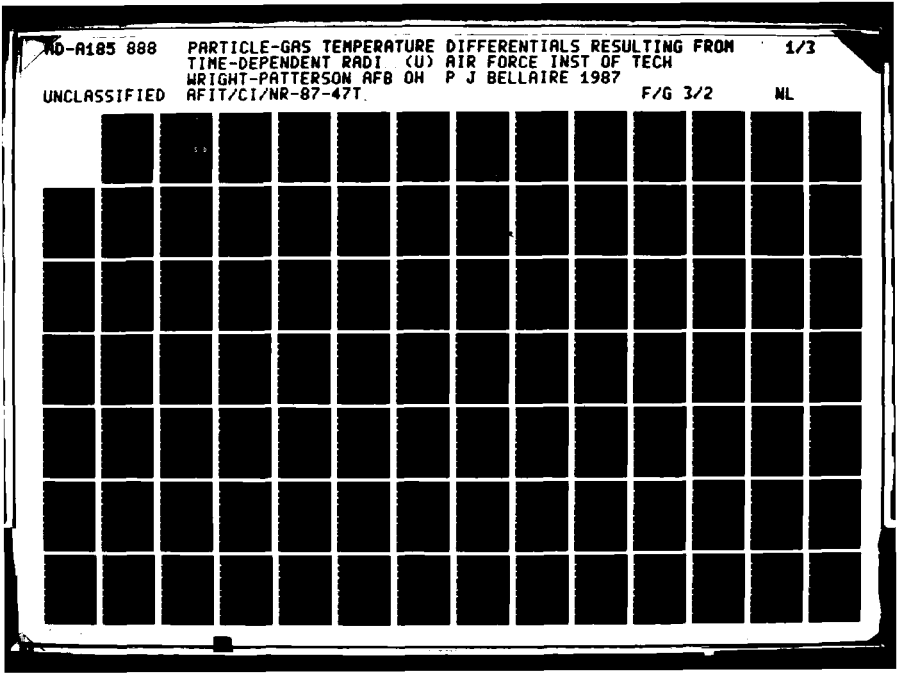
AD-A185 888 PARTICLE-GAS TEMPERATURE DIFFERENTIALS RESULTING FROM TIME-DEPENDENT RADI (U) AIR FORCE INST OF TECH WRIGHT-PATTERSON AFB OH P J BELLAIRE 1987
1/3
UNCLASSIFIED AFIT/CI/NR-87-47T
F/G 3/2
NL

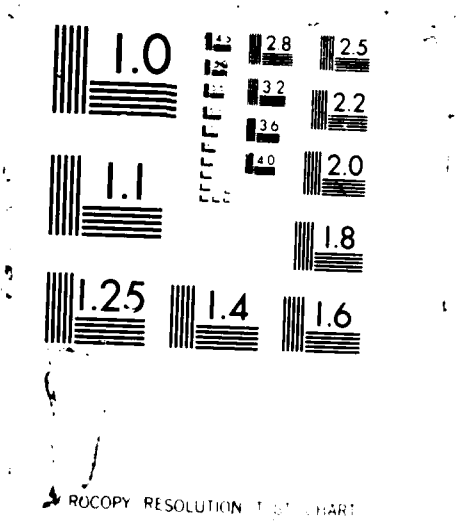
1.0
1.1
1.25
1.4
1.6
1.8
2.0
2.2
2.5
2.8
3.2
3.6
4.0
ROCOPY RESOLUTION

AD-A185 888

DTIC FILE COPY

PARTICLE-GAS TEMPERATURE DIFFERENTIALS RESULTING FROM TIME-DEPENDENT RADIATIVE-CONDUCTIVE HEAT FLUX DIVERGENCES IN THE TENUOUS DUST-LADEN ATMOSPHERE OF MARS

Paul John Bellaire, Jr.
B.S.

DTIC
ELECTE
OCT 2 7 1987
S D
H

DISTRIBUTION STATEMENT A
Approved for public release;
Distribution Unlimited

A Digest Presented to the Faculty of the Graduate School of Saint Louis University in Partial Fulfillment of the Requirements for the Degree of Master of Science (Research)

1987

87 10 14 263

SECURITY CLASSIFICATION OF THIS PAGE (When Data Entered)

REPORT DOCUMENTATION PAGE

READ INSTRUCTIONS BEFORE COMPLETING FORM

1. REPORT NUMBER: AFIT/CI/NR 87-47T	2. GOVT ACCESSION NO.
3. RECIPIENT'S CATALOG NUMBER: A125 822	
4. TITLE (and Subtitle): Particle-Gas Temperature Differentials Resulting From Time-Dependent Radiative-Conductive Heat Flux Divergences In The Tenuous Dust-Laden Atmosphere Of Mars	5. TYPE OF REPORT & PERIOD COVERED: THESIS/DISSERTATION
	6. PERFORMING ORG. REPORT NUMBER
7. AUTHOR(s): Paul John Bellaire, Jr.	8. CONTRACT OR GRANT NUMBER(s)
9. PERFORMING ORGANIZATION NAME AND ADDRESS: AFIT STUDENT AT: Saint Louis University	10. PROGRAM ELEMENT, PROJECT, TASK AREA & WORK UNIT NUMBERS
11. CONTROLLING OFFICE NAME AND ADDRESS: AFIT/NR, WPAFB OH 45433-6583	12. REPORT DATE: 1987
	13. NUMBER OF PAGES: 199
14. MONITORING AGENCY NAME & ADDRESS (if different from Controlling Office)	15. SECURITY CLASS. (of this report): UNCLASSIFIED
	15a. DECLASSIFICATION/DOWNGRADING SCHEDULE

16. DISTRIBUTION STATEMENT (of this Report)

APPROVED FOR PUBLIC RELEASE; DISTRIBUTION UNLIMITED

17. DISTRIBUTION STATEMENT (of the abstract entered in Block 20, if different from Report)

18. SUPPLEMENTARY NOTES

APPROVED FOR PUBLIC RELEASE: IAW AFR 190-1

Lynn Wolaver 17 May 87

LYNN E. WOLAVER
Dean for Research and
Professional Development
AFIT/NR

19. KEY WORDS (Continue on reverse side if necessary and identify by block number)

20. ABSTRACT (Continue on reverse side if necessary and identify by block number)

ATTACHED

DD FORM 1 JAN 73 1473 EDITION OF 1 NOV 65 IS OBSOLETE

SECURITY CLASSIFICATION OF THIS PAGE (When Data Entered)

87 [illegible] 203

PARTICLE-GAS TEMPERATURE DIFFERENTIALS RESULTING FROM TIME-DEPENDENT RADIATIVE-CONDUCTIVE HEAT FLUX DIVERGENCES IN THE TENUOUS DUST-LADEN ATMOSPHERE OF MARS

Paul John Bellaire, Jr.
B.S.

A Thesis Presented to the Faculty of the Graduate School of Saint Louis University in Partial Fulfillment of the Requirements for the Degree of Master of Science (Research)

1987

COMMITTEE IN CHARGE OF CANDIDACY:

Professor Albert J. Pallmann,
Chairperson and Advisor

Professor Yeong Jer Lin

Assistant Professor Lawrence Coy

DEDICATION

For Peter Jerome Bellaire

Stranger and Brother,
Thanks for the Clarinet.

DIGEST

For an aerosol atmosphere, disparities in gas temperature, T_g, and particle temperature, T_p, may arise over the diurnal cycle. A radiative-conductive-convective heat transfer simulation of the dusty atmosphere of Mars was developed to quantify the temporal and spatial character of the temperature difference (T_p-T_g).

This program computed thermal energy fluxes in the temporal and vertical domains in a 51-layer, vertically inhomogeneous, plane-parallel model atmosphere, with a 30-layer simulated ground structure. Observations from Mariner and Viking spacecraft were used in conjunction with other research findings to provide model input and set the boundary and initial conditions for the simulation. Temperature fields within the atmosphere were inferred from radiative-conductive-convective flux fields by means of enthalpy rate principles, while the radiation laws of Kirchhoff and Planck were applied to the flux fields to determine aerosol temperatures. Several independent methods of validation were successfully applied to the model output, including comparisons with distinct spacecraft

DTIC COPY INSPECTED 1

Accession For
NTIS GRA&I
DTIC TAB
Unannounced
Justification
By
Distribution/
Availability Codes
Dist | Avail and/or Special
A-1

observations and the separate computation of dust heating effects outside the model.

Just after local noon, dust temperatures at the highest altitudes were found to exceed ambient temperatures by at least 100 K, while in the lowest and dustiest atmospheric layers, differences were typically smaller than 10 K. The mean temperature of these lowest and thickest dust layers is about 20 to 30 K lower than surface temperature. The quantity $(T_p - T_g)$ decreased with increasing dust load; T_p attained a minimum near the 9 km level, with the altitude of this minimum seemingly independent of dust load.

ACKNOWLEDGEMENTS

I wish to express my heartfelt gratitude to my advisor, Dr. Albert J. Pallmann, whose prior research and inspirational guidance provided the tools and the direction for this thesis. "Ad astras per asperas."

I tender my appreciation and a salute to my superiors and colleagues at the Air Force Institute of Technology, whose faith in my abilities permitted me the unique opportunity of obtaining my Master's Degree unusually early in my military career. My special thanks to Lt. Col. John P. Cipriano, AFIT Chief of Meteorology Programs, and his assistant, Mrs. Peggy Malavich, for their perseverance and unwavering assistance.

Many thanks to Mr. Eric Haug, Capt. John Coover, Mr. Richard Molinaro, and Mr. Patrick Wright for their aid and counsel in the use of the departmental computer systems. The help of Mr. Haug is particularly noteworthy, since it was well outside the normal scope of his duties.

Dr. Laurence S. Rothman of the Optical Physics Branch at the Air Force Geophysics Laboratory (AFGL) graciously supplied the HITRAN database used in this research. Dr. Shepard A. Clough, also of AFGL, provided a copy of the FASCOD2 algorithm for

inspection. Ms. Patricia A. Ross, Request Coordination Manager of the NSSDC Central Data Services Facility at Goddard Space Flight Center, generously made available Mariner and Viking photography of Mars from the datasets of the following Principal Investigators: Dr. R.E. Arvidson, Dr. M.H. Carr, and Dr. R.B. Leighton. Their original and proprietary work is hereby recognized.

The following persons at the National Center for Atmospheric Research (NCAR) deserve applause and thanks for their time and kind advice: Mr. Richard Sato, Dr. Warren Washington, Dr. Stephen Schneider, Dr. Starley Thompson, Mr. Dick Valent, Dr. Richard Carbone, Dr. Julian Pike, Dr. Hal Cole, Dr. Jeffrey Kiehl, Dr. John Gille, Dr. Robert Dickinson, Dr. Stephen Bougher, and Dr. Fillipo Giorgi. My deep appreciation is given to Mrs. Betty Wilson of NCAR's Advanced Study Program, who worked very hard in arranging schedules for my NCAR visit.

The staff at the Air Weather Service Technical Library at Scott AFB, Illinois are to be commended for their diligent, efficient, and professional service. I will certainly miss my friends there.

The cheerful assistance of Meg Batchelor and Juanita Ryles, the departmental secretaries at Saint Louis University, is gratefully acknowledged.

TABLE OF CONTENTS

PAGE

Committee in Charge of Candidacy i

Dedication ii

Acknowledgements iii

Table of Contents v

List of Figures and Tables vii

CHAPTER

1. Introduction 1

   1.1 Overview 1

   1.2 Statement of the Problem 2

   1.3 Thesis Objectives 3

2. Modeling Conceptualization Based on
   Review of the Pertinent Literature 6

   2.1 Overview 6

   2.2 The Solar-Planetary System 8

   2.3 The Planetary Atmosphere-Ground
   Subsystems 12

   2.4 Modeling Radiative Transfer 17

   2.5 Modeling Convective Heat Transfer
   on Mars 21

   2.6 Optical Properties of Aerosols 22

2.7 Aerosols on Earth and Mars 25

2.8 Radiative Transfer in Aerosol Atmospheres 30

2.9 Modeling the Radiation and Heat Budgets 32

3. Methodology 37

3.1 Overview 37

3.2 Description of the Model 38

3.3 Governing Equations and Boundary Conditions 42

3.4 Initial Atmospheric Conditions of the Model 45

3.5 The Dust Temperature Algorithm 47

4. Discussion of Results 53

4.1 Overview 53

4.2 Validation of Model Output 70

5. Conclusions 76

APPENDIX 84

BIBLIOGRAPHY 193

VITA AUCTORIS 199

LIST OF FIGURES AND TABLES

FIGURE PAGE

1. The Dust Temperature Algorithm 49

2. Program MARSDUST Flowchart 52

3. Vertical Atmospheric Temperature Profile;
No Dust Load, LMST 04.00 55
Y axis: 0 to 50 000 m, X axis: 160 to 260 K

4. Vertical Atmospheric Temperature Profile;
No Dust Load, LMST 12.00 56
Y axis: 0 to 50 000 m, X axis: 160 to 260 K

5. Dust Amplitude Profiles; Dust Extinction
Coefficient = (DUSTAMP)exp[$(-1.11 \times 10^{-9})z^2$],
where z = altitude (m) 57

6. Vertical Atmospheric Temperature Profile;
Light Dust Load, LMST 04.00 59
Y axis: 0 to 50 000 m, X axis: 160 to 260 K

7. Vertical Atmospheric Temperature Profile;
Light Dust Load, LMST 12.00 60
Y axis: 0 to 50 000 m, X axis: 160 to 260 K

8. Vertical Atmospheric Temperature Profile;
Heavy Dust Load, LMST 04.00 61
Y axis: 0 to 50 000 m, X axis: 160 to 260 K

9. Vertical Atmospheric Temperature Profile;
Heavy Dust Load, LMST 12.00 62
Y axis: 0 to 50 000 m, X axis: 160 to 260 K

10. Vertical Dust Temperature Profile;

Light Dust Load, LMST 04.00 64

Y axis: 0 to 50 000 m, X axis: 190 to 290 K

11. Vertical Dust Temperature Profile;

Light Dust Load, LMST 12.00 65

Y axis: 0 to 50 000 m, X axis: 190 to 290 K

APPENDIX

A.1 Atmospheric Temperature Profile,

No Dust Load, LMST 00.00 87

A.2 Atmospheric Temperature Profile,

No Dust Load, LMST 04.00 88

A.3 Atmospheric Temperature Profile,

No Dust Load, LMST 08.00 89

A.4 Atmospheric Temperature Profile,

No Dust Load, LMST 12.00 90

A.5 Atmospheric Temperature Profile,

No Dust Load, LMST 15.90 91

A.6 Atmospheric Temperature Profile,

No Dust Load, LMST 20.00 92

A.7 Atmospheric Temperature Profile,

No Dust Load, LMST 24.00 93

A.8 Atmospheric Temperature Profile,

Light Dust Load, LMST 00.00 96

A.9 Atmospheric Temperature Profile,

Light Dust Load, LMST 04.00 97

A.10 Atmospheric Temperature Profile,
Light Dust Load, LMST 06.00 98
A.11 Atmospheric Temperature Profile,
Light Dust Load, LMST 08.00 99
A.12 Atmospheric Temperature Profile,
Light Dust Load, LMST 10.00 100
A.13 Atmospheric Temperature Profile,
Light Dust Load, LMST 12.00 101
A.14 Atmospheric Temperature Profile,
Light Dust Load, LMST 13.90 102
A.15 Atmospheric Temperature Profile,
Light Dust Load, LMST 15.90 103
A.16 Atmospheric Temperature Profile,
Light Dust Load, LMST 18.00 104
A.17 Atmospheric Temperature Profile,
Light Dust Load, LMST 20.00 105
A.18 Atmospheric Temperature Profile,
Light Dust Load, LMST 24.00 106
A.19 Dust Temperature Profile,
Light Dust Load, LMST 00.00 108
A.20 Dust Temperature Profile,
Light Dust Load, LMST 04.00 109
A.21 Dust Temperature Profile,
Light Dust Load, LMST 06.00 110
A.22 Dust Temperature Profile,
Light Dust Load, LMST 08.00 111

A.23 Dust Temperature Profile,
Light Dust Load, LMST 10.00 112
A.24 Dust Temperature Profile,
Light Dust Load, LMST 12.00 113
A.25 Dust Temperature Profile,
Light Dust Load, LMST 13.90 114
A.26 Dust Temperature Profile,
Light Dust Load, LMST 15.90 115
A.27 Dust Temperature Profile,
Light Dust Load, LMST 18.00 116
A.28 Dust Temperature Profile,
Light Dust Load, LMST 20.00 117
A.29 Dust Temperature Profile,
Light Dust Load, LMST 24.00 118
A.30 Dust-Atm Temperature Profile,
Light Dust Load, LMST 00.00 120
A.31 Dust-Atm Temperature Profile,
Light Dust Load, LMST 04.00 121
A.32 Dust-Atm Temperature Profile,
Light Dust Load, LMST 06.00 122
A.33 Dust-Atm Temperature Profile,
Light Dust Load, LMST 08.00 123
A.34 Dust-Atm Temperature Profile,
Light Dust Load, LMST 10.00 124
A.35 Dust-Atm Temperature Profile,
Light Dust Load, LMST 12.00 125

A.36 Dust-Atm Temperature Profile,
Light Dust Load, LMST 13.90 126
A.37 Dust-Atm Temperature Profile,
Light Dust Load, LMST 15.90 127
A.38 Dust-Atm Temperature Profile,
Light Dust Load, LMST 18.00 128
A.39 Dust-Atm Temperature Profile,
Light Dust Load, LMST 20.00 129
A.40 Dust-Atm Temperature Profile,
Light Dust Load, LMST 24.00 130
A.41 Dust Temperature Profile,
Moderate Dust Load, LMST 00.00 133
A.42 Dust Temperature Profile,
Moderate Dust Load, LMST 04.00 134
A.43 Dust Temperature Profile,
Moderate Dust Load, LMST 06.00 135
A.44 Dust Temperature Profile,
Moderate Dust Load, LMST 08.00 136
A.45 Dust Temperature Profile,
Moderate Dust Load, LMST 10.00 137
A.46 Dust Temperature Profile,
Moderate Dust Load, LMST 12.00 138
A.47 Dust Temperature Profile,
Moderate Dust Load, LMST 13.90 139
A.48 Dust Temperature Profile,
Moderate Dust Load, LMST 15.90 140

A.49 Dust Temperature Profile,
Moderate Dust Load, LMST 18.00 141
A.50 Dust Temperature Profile,
Moderate Dust Load, LMST 20.00 142
A.51 Dust Temperature Profile,
Moderate Dust Load, LMST 24.00 143
A.52 Dust-Atm Temperature Profile,
Moderate Dust Load, LMST 00.00 145
A.53 Dust-Atm Temperature Profile,
Moderate Dust Load, LMST 04.00 146
A.54 Dust-Atm Temperature Profile,
Moderate Dust Load, LMST 06.00 147
A.55 Dust-Atm Temperature Profile,
Moderate Dust Load, LMST 08.00 148
A.56 Dust-Atm Temperature Profile,
Moderate Dust Load, LMST 10.00 149
A.57 Dust-Atm Temperature Profile,
Moderate Dust Load, LMST 12.00 150
A.58 Dust-Atm Temperature Profile,
Moderate Dust Load, LMST 13.90 151
A.59 Dust-Atm Temperature Profile,
Moderate Dust Load, LMST 15.90 152
A.60 Dust-Atm Temperature Profile,
Moderate Dust Load, LMST 18.00 153
A.61 Dust-Atm Temperature Profile,
Moderate Dust Load, LMST 20.00 154

A.62 Dust-Atm Temperature Profile,
Moderate Dust Load, LMST 24.00 155
A.63 Atmospheric Temperature Profile,
Heavy Dust Load, LMST 00.00 158
A.64 Atmospheric Temperature Profile,
Heavy Dust Load, LMST 04.00 159
A.65 Atmospheric Temperature Profile,
Heavy Dust Load, LMST 06.00 160
A.66 Atmospheric Temperature Profile,
Heavy Dust Load, LMST 08.00 161
A.67 Atmospheric Temperature Profile,
Heavy Dust Load, LMST 10.00 162
A.68 Atmospheric Temperature Profile,
Heavy Dust Load, LMST 12.00 163
A.69 Atmospheric Temperature Profile,
Heavy Dust Load, LMST 13.90 164
A.70 Atmospheric Temperature Profile,
Heavy Dust Load, LMST 15.90 165
A.71 Atmospheric Temperature Profile,
Heavy Dust Load, LMST 18.00 166
A.72 Atmospheric Temperature Profile,
Heavy Dust Load, LMST 20.00 167
A.73 Atmospheric Temperature Profile,
Heavy Dust Load, LMST 24.00 168
A.74 Dust Temperature Profile,
Heavy Dust Load, LMST 00.00 170

A.75 Dust Temperature Profile,
Heavy Dust Load, LMST 04.00 171
A.76 Dust Temperature Profile,
Heavy Dust Load, LMST 06.00 172
A.77 Dust Temperature Profile,
Heavy Dust Load, LMST 08.00 173
A.78 Dust Temperature Profile,
Heavy Dust Load, LMST 10.00 174
A.79 Dust Temperature Profile,
Heavy Dust Load, LMST 12.00 175
A.80 Dust Temperature Profile,
Heavy Dust Load, LMST 13.90 176
A.81 Dust Temperature Profile,
Heavy Dust Load, LMST 15.90 177
A.82 Dust Temperature Profile,
Heavy Dust Load, LMST 18.00 178
A.83 Dust Temperature Profile,
Heavy Dust Load, LMST 20.00 179
A.84 Dust Temperature Profile,
Heavy Dust Load, LMST 24.00 180
A.85 Dust-Atm Temperature Profile,
Heavy Dust Load, LMST 00.00 182
A.86 Dust-Atm Temperature Profile,
Heavy Dust Load, LMST 04.00 183
A.87 Dust-Atm Temperature Profile,
Heavy Dust Load, LMST 06.00 184

A.88 Dust-Atm Temperature Profile,
Heavy Dust Load, LMST 08.00 185
A.89 Dust-Atm Temperature Profile,
Heavy Dust Load, LMST 10.00 186
A.90 Dust-Atm Temperature Profile,
Heavy Dust Load, LMST 12.00 187
A.91 Dust-Atm Temperature Profile,
Heavy Dust Load, LMST 13.90 188
A.92 Dust-Atm Temperature Profile,
Heavy Dust Load, LMST 15.90 189
A.93 Dust-Atm Temperature Profile,
Heavy Dust Load, LMST 18.00 190
A.94 Dust-Atm Temperature Profile,
Heavy Dust Load, LMST 20.00 191
A.95 Dust-Atm Temperature Profile,
Heavy Dust Load, LMST 24.00 192

TABLE PAGE

Table 1. Program parameters;
No Dust Load 85
Table 2. Program parameters;
DUSTAMP=1.2 x 10^{-7} cm^{-1} 94
Table 3. Program parameters;
DUSTAMP=3.0 x 10^{-7} cm^{-1} 131
Table 4. Program parameters;
DUSTAMP=6.0 x 10^{-7} cm^{-1} 156

1. INTRODUCTION

1.1 Overview

Certain properties of gas-particle mixes in dust-laden atmospheres would seem to be uniformly applicable over a wide range of combinations. The terrestrial and Martian atmospheres show some similarities in the character of their respective gas-aerosol interactions, despite the obviously different conditions on the two planets. The primary effects of atmospheric aerosol loadings are radiative in nature, and this thesis examines the manner in which aerosols can modify the propagation of radiation in model atmospheres.

Atmospheric radiative transfer is also an essential element in planetary heat distribution. The processes of emission, absorption, and scattering of radiant energy are different for the gaseous (molecular) and nongaseous (aerosol) components of an atmosphere, and continuing research concentrates on how these two regimes interact. Since radiative transfer is the stuff of which climate is made, this approach can lead to very broad conclusions despite its limited focus.

1.2 Statement of the Problem

Knowing the size distribution and material composition of an aerosol leads to extinction and scattering functions for these particles via classical Mie theory, whereas knowing the molecular concentration of the gases involved allows development of analogous functions for these gases using Rayleigh theory. Quantification of local and global radiative transfer is achieved by combining these functions with multiple scattering effects, surface albedo, and ground emission characteristics.

Radiative fluxes can then be inferred and enthalpy (internal energy) balance applied to describe the spatial and temporal distribution of temperature by conductive, convective, radiative, and phase change heating/cooling processes. Because the various atmospheric components have different specific heat capacities, deduced heating rates for these components will generally not be the same. Enthalpy rate disparities arising from the differential heating of the aerosol and gas act to promote a significant temperature difference between these constituents.

Research has shown that particle-gas temperature differences can approach values over 100 K in the Earth's mesosphere (Fiocco et al., 1975). Mars, having an atmosphere that is very radiatively active (95% CO2), may exhibit temperature differentials quite distinct from the terrestrial case, especially since its aerosol is persistent and, during global dust storms, attains much higher optical depths than are typical on Earth (Thorpe, 1981; Zurek, 1981, 1982).

1.3 Thesis Objectives

As a logical extension of the preceding discussion, the topical objective of this study was to determine the distinction between gas and dust temperature, as a function of time and altitude, for the Martian atmosphere in the mature, steady-state, global dust storm phase.

The methodological objective of the thesis was to construct an algorithm, based on sound physical principles, to compute dust temperatures from output fluxes produced by the MARSTEMP model of Pallmann (1976, 1977, 1983). MARSTEMP calculated solar and planetary fluxes as a function of time (over the diurnal cycle) and vertical coordinate

(within a 51-layer plane-parallel atmosphere of 50 km thickness and a 30-layer ground structure of 60 cm thickness).

Given the setting of a tenuous but nearly chemically homogeneous, radiatively active atmosphere, justifiable simplifications to the dust temperature algorithm were made possible. Direct observations of the Martian surface and atmosphere provided by the Viking and Mariner spacecraft permitted reasonable quantification of the optical properties of the dust aerosol using Mie theory. The highly refined and extensive databases of atmospheric spectroscopic line parameters compiled by McClatchey and Rothman provided accurate input for the simulation.

An additional objective of this investigation was the validation of model findings with respect to Viking observations. Model output agrees rather well with conclusions drawn in the late 1970's by various principal investigators immediately following the Viking mission, and is within the numerical range of actually observed or reasonably extrapolated values. Validation of the model was also achieved by several independent methods, including the comparison of dust free with "dusty" outputs, which were mutually consistent. As a

consequence of the validated results of the simulation, the thesis objectives were considered accomplished.

2. MODELING CONCEPTUALIZATION BASED ON REVIEW OF THE PERTINENT LITERATURE

2.1 Overview

Modeling radiative transfer for a vertically inhomogeneous planetary atmosphere requires knowledge of the radiative output of the parent star (or stars), as well as any other major energy sources or sinks that may be operating; the chemical, physical, and spectroscopic properties of the planetary atmosphere-ground subsystems; and the orbital and rotational characteristics of the planet. The effects of aerosols, variable atmospheric and surface albedo, volcanic outgassing, clouds, trace gases, precipitation and phase changes, loss of atmospheric gas to space or the gain of extraplanetary material by the atmosphere, and so on, need to be accounted for whenever applicable. A comprehensive model would involve a multidisciplinary effort in physics, chemistry, astronomy, astrophysics, geology, geophysics, meteorology, etc., as well as a host of related specialties and subfields. Such a model remains a goal as yet unattained.

Any meaningful analysis requires integration of accurate data with sound concepts and theory.

The physical scale of the phenomena is vast; even the most recent advances in technology have only made it possible to obtain in situ observations for our nearest planetary neighbors, and the Moon alone has received human explorers. Acquisition of data for planets beyond our solar system is, at best, far in the future.

However, given the chemical and physical nature of the surface (and potential surface-derived aerosols) of any planet, the scattering, absorption, and surface albedo characteristics of such material can be ascertained and quantified by current theory to a reasonable degree of accuracy. Identification of the constituent gases and their abundance by volume permits the determination of a mean molecular weight for the atmosphere, which can be used with the equation of state to calculate the thermodynamic variables; these values of pressure, density, and temperature indicate directly the local effects of radiative transfer, and also give a basis for constraining the model to a particular regime of spectroscopic interest (strong-line, weak-line, or intermediate-line? Lorentz profile, Doppler profile, or Voigt profile?) for atmospheric absorption or transmission. Spatial gradients of the pressure, density, and temperature fields can also be derived, shedding light on the fluid flow

dynamics that create global circulation and climate patterns that ultimately interact with radiative transfer processes in a nonlinear feedback mode.

This interaction between radiative energy and the planetary atmosphere-ground subsystems must be a paramount consideration; it should be included in any comprehensive model, either through an approximation or parameterization of the feedback effects.

2.2 The Solar-Planetary System

The sun experiences both short-term variations (as evidenced by the 11\22 year sunspot cycle) and *long-term* variations (as evidenced by the well-known Maunder Minimum, from 1645 to 1715, as well as other similar occurrences, such as the Spörer Minimum) in its luminosity and energy output. These variations are not well understood, yet the solar output is generally considered constant at 3.827×10^{26} W (Pasachoff, 1979).

The sun's electromagnetic radiative energy is approximately distributed by wavelength λ as follows: 50% in the infrared, $\lambda > 0.7$ μm; 40% in the visible spectrum, 0.4 μm$< \lambda < 0.7$ μm; and 10% in the ultraviolet, $\lambda < 0.4$ μm (Liou, 1979). In these wavelength regions, the sun exhibits differing

equivalent blackbody temperatures, but the effective blackbody temperature is taken to be approximately 5800 K. Since the sun is considered here mainly as an energy source, its size, mass, and other physical characteristics will not be discussed in this study.

Mars has a mean distance of about 228 million km from the sun, with a revolution period (year) of approximately 687 terrestrial days. Its mean equatorial radius is about 3397 km, its density about 3.9×10^3 kg/m^3, and its mass about 11% of Earth's. The planet has an oblateness value of 0.009, almost three times the value for Earth (0.0034). One Martian day, referred to as a "sol", consists of 24 hours 37 minutes or 88 775 seconds (terrestrial units) (Leovy and Zurek, 1979). The planetary surface temperatures range from about 140 K at the poles to probably over 275 K at the equator (Viking measurements at the surface for 47° N latitude indicated maximum temperatures over 240 K, and for 22° N, maxima near 260 K; AGU, 1977).

The obliquity (inclination of the Martian equator to the Martian orbital plane) is 23°59', very close to Earth's value of 23°27'. The orbit of Mars is inclined 1°51' to the ecliptic. The eccentricity of the orbit (the ratio of the distance between the foci of the elliptical orbit

and the major axis of the ellipse) is 0.0934, more than five times the value for Earth (0.0167) (Pasachoff, 1979). The obliquity varies by 13^{o} around its mean value over time scales on the order of 10^{5} years, while the eccentricity varies from near zero (almost circular orbit) to about 0.14 (highly elliptical orbit) over time scales on the order of 10^{6} years. Precession of the Martian axis occurs at a frequency nearly in resonance with the frequencies of several of the planetary gravitational perturbations (mainly Jovian) responsible for driving the obliquity and eccentricity variations, thereby creating feedback effects accounting for the large magnitude of these variations. By comparison, the amplitudes of the obliquity and eccentricity variations for Earth's orbit are about 10 and 2.5 times smaller, respectively, than those of Mars (Liou, 1979; Pollack and Toon, 1982).

From these facts, it is apparent that the Martian orbit is far more irregular than Earth's, permitting greater extremes in insolation changes and seasonal variations. The present obliquity and eccentricity of the Martian orbit causes the southern hemispheric summer/ northern hemispheric winter to be shorter than the southern hemispheric winter/ northern hemispheric summer. Both the

northern hemispheric winter and southern hemispheric summer are warmer than the same seasons in the opposite hemisphere, since the former occur at perihelion while the latter occur at aphelion. Solar radiation influx is about 45% greater at perihelion than at aphelion (Pallmann, 1983).

The range of orbital deviations over 10^5 to 10^6 years allows such asymmetries to be even more pronounced for the appropriate combinations of obliquity and eccentricity extremes. (In this study, tectonic and structural changes that may occur over such time scales, intrinsic to the planet, and their effect on planetary radiative transfer characteristics, will not be considered.) Not only will the local net radiative input oscillate over a wide range under such circumstances (even apart from any intrinsic solar variations, which we have already neglected!), but these insolation changes in turn can alter the atmosphere-ground subsystems, which then may affect the net insolation in a complex feedback loop.

As a consequence of such irregular orbital behavior alone, radiative transfer on Mars is a highly variable and nonlinear process. In general, a fully time-dependent radiative transfer model for any planetary atmosphere covering characteristic time scales (even if inherent planetary structural

changes are ignored) is beyond the scope of present knowledge. Mars, in particular, will present a challenge for generations to come. On human time scales, however, these changes occur so slowly that we need not worry that our models are restricted to "present" or "constant" climatological conditions.

2.3 The Planetary Atmosphere-Ground Subsystems

The tenuous atmosphere of Mars is largely CO2 (95% by volume), with nitrogen (2.7%) and argon (1.6%) as minor constituents, and several trace gases in negligible amounts (totalling less than 1% by volume) (NASA/JPL, 1984; Hess, 1979). This composition leads to a value of about 43.62 g/mol for the mean molecular weight of "Martian air", and a value for the specific gas constant of about 1.9 x 10^2 J/(kg K). A surface atmospheric pressure of 7.7 hPa (7.7 mb) was measured by the Viking 1 lander at 22° north latitude, but at both Viking landing sites, the pressure was observed to vary seasonally by as much as 25%, due to the growth and shrinkage of the polar caps, which are effective CO2 reservoirs; an average surface pressure around 6.0 hPa is considered typical (NASA/JPL, 1984; Pollack and Toon, 1982). Both CO2 and H2O clouds have been observed on Mars (Hunt and James, 1985).

The northern ice cap (at a temperature near 140 K) contains a permanent water ice core which is the main source of atmospheric water vapor. This ice cap allows peak values of 50 to 100 precipitable μm's (column abundance) of water in the summer near its perimeter. A planetary average for water vapor abundance is taken to be 10 precipitable μm's; during summer, water vapor can account for as much as two to three percent of the atmosphere by volume (Pollack and Toon, 1982; NASA/JPL, 1984). With a high degree of accuracy, it is possible to restrict the study of the radiative character of the Martian atmosphere to the study of CO2, the most abundant and most radiatively active constituent.

Photographic evidence from orbit of the erosional action of liquid water supports the conclusion that the atmosphere was much denser on Mars sometime in the past (Cordell, 1986). Calculations indicate that the atmosphere has lost about 10 times as much nitrogen and about 20 times as much CO2 as is present today. The amount of water adsorbed within the regolith (weathered surface material or "soil") and existing below the surface as permafrost is unknown, but considering this and the permanent north polar cap of water ice, some infer that Mars, throughout its history,

may have produced enough water to cover the entire surface up to a 10 meter depth (NASA/JPL, 1984).

The surface of Mars has been photographed from orbit by several spacecraft, and in situ by the Viking landers, which also subjected soil samples to various physical and chemical tests. The reader is referred to the copious literature available on the Viking missions for detailed accounts of the results. Grossly oversimplified, the Martian surface consists of a highly fragmented layer, up to a kilometer thick, of boulders, rocks, dust, and fine particles, all probably derived from volcanic basalts (NASA/JPL, 1984; Pollack and Toon, 1982). Silicon and iron are the most abundant elements; the soil is about 45% SiO_2 and about 19% iron oxides. Sulfur is about 100 times more abundant in the Martian soil than in Earth soils, but potassium is at least five times less abundant (NASA/JPL, 1984). The finer dust particles are subject to aeolian saltation and lifting, and have been observed at heights over 40 kilometers in the atmosphere during the periodic global dust storms; these particles are on the order of a few μm's in radius and may be sufficiently rounded by aeolian erosion over planetary ("aeologic") time scales to be considered spherical (Pollmann, 1983), although Viking measurements indicate nonsphericity is more

the norm (Pollack et al., 1979; Chylek and Grams, 1978). The atmosphere, as photographed at the surface by Viking, has a reddish tinge, confirming that the haze particles responsible are indeed Mie scatterers (NSSDC, personal communication, 1986; NASA, 1978; NASA/JPL, 1984). Model simulations and direct observations of Martian dust seem to indicate montmorillonite 219B is the best candidate to approximate its mineralogical and optical properties (Egan et al., 1980; Pollack et al., 1979; Martin et al., 1979).

Periodic global dust storms have been observed on Mars, varying in severity from year to year. These storms originate preferentially in the southern hemisphere during the summer as local storms in Noachis and Solis Planum (Peterfreund and Kieffer, 1979; Pollack and Toon, 1982; Zurek, 1982). Gierasch and Goody (1973) postulated the "dusty hurricane" model to account for storm genesis at these tropical latitudes, where dust heating of the atmosphere played a role analogous to latent heating in terrestrial hurricanes (Pallmann, 1976); Viking photography has indicated local dust devils can attain heights of 6 km or more (Thomas and Gierasch, 1985). In a few weeks, these local storms can grow to global proportions, aided in this development by positive feedback

among the dust loading, the associated increased solar heating of the atmosphere, the subsequent strengthening of the storm winds and mean meridional circulation, and the associated thermal tides (Pollack and Toon, 1982). However, the extreme dust loadings that are ultimately achieved (extinction optical depths around 6 have been observed; Pollack et al., 1979) have a negative feedback effect on the global storm dynamics, and the storms quickly enter a plateau phase and slowly decay. The "e-folding" time for dust removal (the time required for a 63% reduction) from a 20 km atmospheric column of typical dust content has been calculated to be about 56 days (Haberle et al., 1982), implying that the average global dust storm has a lifetime of a few months (on the order of a hundred days or so). This agrees with observations, although the great dust storm of 1971-1972 observed by Mariner 9 was notable in its longevity. However, at altitudes above 20 km, dust has been observed to persist throughout the year, regardless of season.

Intricate layered terrain features at the polar caps, known as the laminae, so far have defied adequate explanation. They have been theorized to be dust covered mobile water-ice sheets, and thus may be intimately related to the global dust storms (Cordell, 1986). Dust from such

storms is preferentially deposited over the polar ice caps by general circulation patterns and through the scavenging action of CO2 condensation and precipitation from the atmosphere. Dust deposition has significant effects on the ice cap albedo, which again brings feedback effects into play as the clearing of the global dust storm accelerates (Pollack and Toon, 1982).

The complex relationship between insolation and global dust storms in the tenuous yet radiatively active atmosphere of Mars indicates how radiative forcing and planetary subsystems can interact to modify each other. Meaningful models of radiative transfer should account for such feedback, even if only in parameterizations.

2.4 Modeling Radiative Transfer

Radiative transfer processes involve the emission, absorption, scattering, and transmission of electromagnetic wave energy in a given medium. In this case, the modeling of radiative transfer on Mars can be restricted to an atmosphere of carbon dioxide with a variable optical depth caused by seasonal dust loadings. The compilation of CO2 spectroscopic absorption-line parameters by McClatchey et al. in 1973 and by Rothman et al. in

1980, Deirmendjian's 1969 derivation of size distributions and scattering parameters for spherical polydispersions, the radiative transfer equation evolved earlier by Chandrasekhar, van de Hulst, and others, and the well-known algorithms for single and multiple Mie scattering, are the basic tools used for quantifying radiative transfer in present models of the Martian atmosphere. Continual incorporation of new facts with these tools permits attunement of the models to observations.

Approximations and parameterizations can be used in the models to reduce computation time and effort, and may actually provide insight into the physical processes involved. The determination of directional scattering intensity in the atmosphere via phase functions that either require truncations of scattering in the forward direction (Hansen, 1969) or approximations using the delta-Eddington technique (Joseph et al., 1976; Zurek, 1978) has proved advantageous and has yielded excellent results. Indeed, Hansen (1969) concluded that optically thick atmospheres, to a high degree of accuracy, act as if their scattering actually is truncated in the forward direction, due to the cumulative effects of multiple scattering. However, the algorithms for multiple scattering, being

rather complex, need improvement with respect to describing the effects of the variable Martian dust loadings. Carbon dioxide absorption lines for the tenuous Martian atmosphere can be better quantified using the Voigt line-shape profile and the so-called "intermediate-line" approximation (rather than the strong- or weak-line exclusively) (Pallmann, 1976, 1983).

Extension of well-known terrestrial layer models (along with their parameterizations associated with turbulence, convection, conduction, scale height, etc.) to the Martian setting allows the vertical structure of the atmosphere to be more clearly defined, and in concert with thermodynamic equilibrium considerations, permits the construction of vertical temperature soundings for comparison with satellite observations (Pallmann, 1976, 1977, 1983; Egan et al., 1980). This is especially important when attempting to describe dust loading effects on radiative transfer. The principles of terrestrial Hadley cell dynamics and global circulation patterns (Haberle et al., 1982; Haberle, 1986), as well as those of katabatic winds (initiated by the significant meridional temperature gradient; W. Fernandez, Saint Louis University MS thesis, 1973) and dust hurricane formation (with dust heating playing a role

[illegible] Hansen and Hovenier, 1974), can be utilized in describing the growth and decay of global dust storms on Mars, and in so doing, increase understanding of the time- and space-dependent variation of optical depth and its subsequent effects on radiative transfer.

The description of the optical characteristics of spherical polydispersions as given by van de Hulst (1957, 1980), Deirmendjian (1969), and Deirmendjian (1969) can perhaps be expanded to include other shapes and particle compositions, but at present forms the core of understanding for particulate absorption and scattering. A better mineralogic match to Martian dust and a more detailed spectroscopic description for such dust would help elucidate the complexities of the radiative interaction between the carbon dioxide atmosphere and the seasonal dust injections.

The "scavenging" of dust from the Martian atmosphere by carbon dioxide precipitation requires a more detailed analysis, with emphasis on the phase change during deposition and the mechanics of CO_2 ice accretion on dust nuclei. The albedo changes of the polar caps caused by preferential dust deposition, too, also need further study, focusing attention on the absorption and scattering characteristics of "dirty" and "clean" ice mixtures

of CO_2 and H_2O, and the nature of the laminae. However, for the purposes of this study, the polar regions and their associated phase changes will be left to future study and the model applied only to mature dust storms near midlatitudes. Changes at midlatitudes in local surface albedo due to the redistribution of dust after the cessation of global storms should be investigated, since these variations could be significant enough to affect local thermal equilibrium and alter subsequent dust storm patterns and/or intensity (Wells et al., 1984); this issue, too, will be left for future consideration.

2.5 Modeling Convective Heat Transfer on Mars

Pallmann (1983) describes an atmospheric model for Mars in which an interim vertical temperature profile is calculated, then subjected to convective adjustment by determining which, if any, of the model's layers in this temperature profile possess a superadiabatic lapse rate. The enthalpy of these layers is redistributed within neighboring layers above and below until all such layers have a strictly adiabatic lapse rate. The layer next to the ground, however, is permitted to show steep superadiabatic lapse rates, in accordance with the

accepted concepts of Kraichnan's turbulent thermal convection theory, as well as Monin-Obukhov length and roughness length theory (Pollmann, 1981).

This dual approach to vertical convective heat exchange, consisting of turbulent thermal convection theory and the simulated redistribution of enthalpy, seems effective in modeling thermal stratification in the lower Martian atmosphere.

2.6 Optical Properties of Aerosols

To understand the effects of aerosols on radiative transfer in model atmospheres, two parameters are fundamental: the size distribution and the complex refractive index of the aerosol. The size distribution (along with the wavelength interval under investigation) determines the scattering regime to be modeled (Rayleigh or Mie), while the refractive index describes the absorption and scattering character of the aerosol (Cadle and Grams, 1975). In addition, the crystalline structure of the aerosol's constituent matter may be of consequence; in a lithospheric aerosol of silicates, for example, some of the incoming radiative energy can be distributed among phonons in the crystal lattice structure (the "reststrahlen" or residual ray effect), a

phenomenon quite distinct from true absorption. A silicate-type aerosol would seem to have a brightness temperature lower than expected because the energy of the phonons would be unavailable for emission. This effect is apparent for terrestrial desert sands, and must be taken into account when attempting to derive brightness temperatures of desert surfaces. Collisional shock effects experienced by the parent bodies of crystalline aerosols, as in cratering episodes, could affect the lattice structure and the phonon resonance energies involved, but this will be considered of minor consequence for our purposes.

For the case where the wavelength of the radiation under study is sufficiently small compared to the radius of the particle, classical Mie theory describes the processes of scattering and absorption, as formulated by van de Hulst, Sekera, and Deirmendjian. Otherwise, Rayleigh theory applies. The sizes of the lithospheric aerosols considered in this study fall into the Mie regime, as previously discussed. The determination of the size distribution itself depends critically on accurate sampling techniques for the aerosol particles. However, the remotely measured characteristics of a given particle population, such as optical extinction, albedo, absorption,

etc., can be compared to the same attributes of well studied and directly measured terrestrial aerosol size distributions. This permits us to apply what is known about terrestrial aerosols to the cases of aerosols in planetary atmospheres in general. In the case of Mars, Viking lander imaging allowed estimates of the size distribution function to be made, and the spectral similarity of montmorillonite 219B to the dust constrains the dust's complex refractive index to a narrow range.

The real part of the complex refractive index accounts for scattering effects, while the imaginary part describes absorption. These values are typically functions of the wavelength of radiation under consideration, and published values for a given substance are usually statistically averaged over a given wavelength or frequency interval.

Aerosol particles in general are irregularly shaped, and this departure from sphericity decreases the backscattered radiation (Liou and Sasamori, 1975). Inhomogeneities in the aerosol particles would also be expected to cause variations in scattering and absorption. Models using homogeneous spherical particles, incorporating the well-known Mie scattering theory, thus give upper bound values for backscattering and

absorption (Liou and Sasamori, 1975; Cadle and Grams, 1975).

2.7 Aerosols on Earth and Mars

For the lithospheric aerosols of Earth and Mars, erosion of the particles by saltation and other wind-generated collisions makes the assumption of sphericity and the application of classical Mie theory quite reasonable, although Pollack et al. (1979) supported the view that smooth platelike particles (typical of clays) give a better fit to the Viking extinction data. The assumption of sphericity may still be only a small source of error if one considers the random orientations of an ensemble of such particles. Cadle and Grams (1975) found that for the terrestrial aerosol, the number of particles tended to increase rapidly with decreasing particle size for particles of less than 1 μm radius. This could imply that on Earth, the smallest aerosol particles are the most important radiatively because of their sheer numbers. However, increasing particle radius gives a rapidly increasing optical cross-section, so even the less numerous large particles could still dominate the aerosol optical effects, due to

their increased scattering and absorption capabilities.

Cadle and Grams (1975) also determined that for terrestrial aerosol size distributions, the greatest contributions to scattering and absorption are made by particles with radii between 0.1 and 2.0 μm. Size distributions of Martian aerosols seem roughly similar to Earth's, so these conclusions could apply on that planet also, although our model's dust temperature algorithm assumes that within the highly radiative and tenuous atmosphere of Mars, particle size effects are rather negligible. Pollack et al. calculated an "effective" particle radius for Martian aerosols of 2.5 μm from Viking data, in agreement with earlier conclusions made by Toon et al. in 1977 from Mariner 9 IRIS data (Pollack et al., 1979). However, this "effective" radius is the result of an analysis of a broader size distribution, including submicrometer sizes, with a modal radius of 0.4 μm. Many other authors have derived effective radii closer to 0.5 μm. As a compromise, a radius of 1 μm will be assumed in this study.

The real and imaginary parts of the refractive index determined by Lin et al. in 1973 for terrestrial soil particles (Liou and Sasamori, 1975) are 1.525 and 0.05, respectively, with a

wavelength around 0.5 μm. On the other hand, Ivlev and Popova (1973) calculated "effective" real and imaginary values of 1.65 and 0.02, respectively, in a sophisticated model of the terrestrial aerosol, over a wavelength range of 0.4 to 15 μm, assuming dry conditions and incorporating a wide range of molecular species in the aerosol. A perfect match for Martian dust has yet to be developed, but the results obtained by using montmorillonite 219B have proved adequate. The results of investigations by Singer (1985) indicate that a certain class of Hawaiian palagonite soils are the best spectral match to Martian soils yet known. Palagonite is an amorphous hydrated ferric-iron/silica gel formed by the alteration and secondary weathering of volcanic glasses under semi-arid conditions, and may be described as an extremely poorly crystalline clay. Singer does not claim palagonite as the universal Martian soil, however, and stresses that more crystalline ferric oxides may exist in great abundance locally. Indeed, Viking Orbiter data indicate that surface regions exist better described as hematite-like material. It is hoped that the Mars Geosciences/Climatology Orbiter mission scheduled for the latter part of this decade will shed some light on this issue.

The existence of the terrestrial stratospheric aerosol layer has been known since its discovery by Junge et al. in 1961 using balloon-borne impactors (McCormick et al., 1982) but only in the last decade have satellite-borne experiments been used for its investigation. Satellite observations have shown that meridional circulation patterns carry aerosols poleward from their high concentrations at the tropopause in the equatorial regions and preferentially deposit them near the poles. Aerosols can act as nuclei for Polar Stratospheric Clouds (PSC's) if the polar stratospheric temperature is low enough and there is adsorbed or otherwise intermixed water in the aerosols (McCormick et al., 1982). This is especially true over Antarctica, with its strong subsidence cell and extremely low temperatures. This polar deposition of aerosol particulates because of Hadley cell dynamics and cold air mass subsidence is not unique to Earth. Mars also exhibits such scavenging of atmospheric dust particles and the formation of high altitude clouds over its poles. This is accentuated by carbon dioxide deposition on the dust caused by the extreme cold of the Martian polar atmosphere, ultimately leading to removal of the dust by precipitation, as well as subsidence. It is possible that any planet with a moderate

inclination to the ecliptic, an adequate rotation rate, and a sufficient meridional temperature gradient would experience a similar poleward flow pattern for aerosol circulation.

Dust storms on Mars have been observed from orbit and from the planet surface by the Mariner and Viking missions. Heating of the atmosphere in the vertical by dust is thought to be an important factor in the evolution and maintenance of Martian storms. The presence of a thick dust aerosol modifies the vertical temperature profile during the day, increasing static stability near the surface and the topmost dust layers (Pallmann, 1976), as well as enhancing the optical extinction, low-level atmospheric heating, and surface warming. Martin and Kieffer (1979) noted that the dust load of the 1977 storms created optical depths in the range 1.5 to 2.0, compared to a median value of 0.3 of the "clear" pre-storm atmosphere. From the orbital observations of the Viking Infrared Thermal Mapper (IRTM) at the 15 μm wavelength, Martin and Kieffer deduced that polar warmings of over 80 K at about 25 km altitude can be caused by the presence of the dust aerosol. This was inferred through inversion of the measured 15 μm radiance, assuming an ensemble gray body emissivity near 0.2 for the dust cloud (this is not individual particle

emissivity!). They pointed out that this polar warming bears striking resemblances to the sudden stratospheric warmings (SSW's) on Earth, although the causative factors are undoubtedly different.

2.8 Radiative Transfer in Aerosol Atmospheres

Radiative transfer in an atmosphere-ground system involves successive absorption and re-radiation at various levels. Atmospheric "counter radiation" is the downward re-emission of absorbed upwelling planetary emission, which in turn is dependent on the amount of incoming solar radiation absorbed at the planetary surface. This primary absorption is affected by the surface reflectivity, or albedo.

Liou and Sasamori (1975) determined that surface and aerosol albedos interact to yield a "local albedo", and resultant values between 0.3 and 0.4 constitute a transition regime for the effective atmospheric heating rates caused by aerosol haze. For local albedo values below 0.3, hazy and clear atmospheres show approximately the same degree of warming. As the local albedo increases, however, and even more dramatically as the value exceeds 0.4, absorption across the solar spectrum increases in a hazy atmosphere as opposed

to the clear case. Thus the hazy atmosphere gives rise to greater total atmospheric warming, although it can promote cooling near the surface. Liou and Sasamori, as well as other investigators, have also clearly established that absorption, and thus total warming, increases with increasing solar zenith angle. It should be apparent that local warming effects are critically dependent on seasonal and geographical factors, as well as the previously discussed microphysical and optical parameters.

In planetary climate studies, the absorption and scattering characteristics of the atmosphere-ground system in the near IR wavelengths (about 1 to 10 μm) are of primary importance. Generally, the atmosphere contributes most strongly to the absorption of these wavelengths while the lithosphere, and aerosols derived from it, dominate the scattering processes. The "equivalence theorem" of van de Hulst (1980) states that we can simplify the problem of describing a gas-aerosol mix by ascribing the scattering capabilities of the gas to the particulates and the absorption characteristics of the aerosol to the gas. This amounts to modeling the system as an "equivalent" mixture of an absorbing nonscattering gas with a scattering nonabsorbing aerosol (van de Hulst, 1980; Davies et al., 1983). This technique is highly effective in

reducing the complexity of the mathematical models used.

Models of atmospheres with high optical depths, caused by cloudiness or high aerosol loadings, should properly consider multiple scattering effects to fully describe the radiative transfer processes, and this can complicate the mathematics considerably. Parameterizations such as the delta-Eddington technique (Wiscombe, 1977[a], 1977[b]), however, seem to handle this problem quite well, without any significant loss of accuracy. Also, because atmospheric absorption exhibits a pressure dependence, the Curtis-Goodson approximation can be applied to simplify the mathematical treatment of vertical inhomogeneity, allowing models to take the vertical variation of pressure into account by substituting multiple layers of homogeneous stratification for the actual pressure profile (Liou and Sasamori, 1975; Pallmann, 1976).

2.8 Modeling the Radiation and Heat Budgets

The temperature of aerosol particles in a planetary atmosphere depends upon the energy exchanges occuring. These include the radiative processes of emission and absorption for the

particles, collisional exchanges with the ambient gas (convectively mixed wherever superadiabatic lapse rates occur), and the exchanges possible due to phase transitions of the ambient gas or of other volatiles within the atmosphere (Stephens, 1983; Mugnai et al., 1978). This study avoids the case of phase change effects on Mars. For the terrestrial case, Ficcco et al. (1975, 1976) calculated that the particle temperature can exceed the ambient gas temperature by as much as 100 K in the mesosphere, and this temperature differential varies significantly with season, altitude, and time of day. The rate of change of the particle temperature defines the rate of enthalpy change for the particle, which is equal to the net divergence of all the thermal fluxes mentioned above, namely, phase change, emission, absorption, and collisional fluxes (including turbulent convection).

The temperature of the ambient gas is similarly dependent on its phase changes, collisional exchanges, and the emission and absorption character of its constituent molecules. Because of the extreme density differences between the subsystems of particles and ambient gas, the states of local thermodynamic equilibrium (LTE) achieved by each separate subsystem are not equivalent, except at higher pressures where

collisional processes dominate. Obviously, as long as thermal fluxes (and thus enthalpy exchanges) exist between the two subsystems, there is a distinct lack of a local equilibrium between them. For Mars and Earth at most latitudes (regions of extended polar night or polar day excluded), planetary diurnal variations in insolation occur over such (relatively) short time scales that local thermodynamic equilibrium between the two subsystems is probably never fully achieved, and thus some sort of temperature differential between the aerosol particles and the gas is to be expected almost always. This would imply, at least on Earth, that the aerosol acts as a heat source during daylight hours and a heat sink at night. Generally, above a certain threshold altitude where collisional processes become negligible, aerosols are a heat source even at night. However, the most efficient daytime radiators for the terrestrial case tend to be smaller than the most efficient nighttime radiators (Blocco et al., 1976). Interestingly enough, our current model indicates that even at night, the longwave emissions of the atmosphere and surface of Mars act to keep the dust warmer than the ambient air.

Fiocco et al. (1975) found for Earth that the temperature differential tended to increase with altitude and decreasing pressure, then diminished slightly before it attained a constant limiting value where energy exchanges between gas and dust were negligible, a characteristic of the radiative equilibrium of interstellar dust (as calculated by van de Hulst in 1946 and 1949).

The black body radiation laws are implicit to any model of radiative transfer and related energy budgets. To apply the modification of a gray body assumption to these basic black body laws for the aerosols in a dust cloud, a value of the bulk or ensemble emissivity is needed, a much different situation from determining the emissivity of individual particles. This can be a significant stumbling block, especially for nonhomogeneous aerosols with poorly known refractive indices. Also, as was noted earlier, phenomena such as the residual ray effect can invalidate black or gray body assumptions by modifying the energy transfers that occur. If black body theory cannot be applied, modeling radiative transfer becomes virtually impossible.

Obviously, great care must be taken when drawing conclusions from satellite observations of radiative processes. The emissions of dust aloft,

as discussed previously, could yield an inverted brightness temperature totally different from that of the ambient gas, and this discrepancy would become even more severe if the data corresponded to aerosols at increasingly higher altitudes. If the aerosol was highly crystalline in nature, the residual ray effect could put even the inverted brightness temperature of the dust itself in doubt. The use of an inaccurate bulk or individual particle emissivity, as mentioned above, would cause similar problems. At depth, below the dust layer, the thicker atmosphere can be warmed by the dust emissions, and the fact that the aerosol is not present in great quantities in a particular layer should not lead to the conclusion that the layer is free of the aerosol's influence. This effect is more pronounced for a radiatively active atmospheric constituent such as carbon dioxide, because of its enhanced absorption capability in the infrared. A moderate dust layer at medium or low altitude can affect the lapse rate profile of a much thicker atmospheric layer above it, and modify the static stability as well. The implications for convection and other dynamic effects are profound.

3. METHODOLOGY

3.1 Overview

For an aerosol atmosphere, disparities in gas temperature, T_g, and particle temperature, T_p, may materialize over the diurnal cycle. A radiative-conductive-convective heat transfer simulation of the Martian dusty atmosphere was developed to obtain data on such gas-aerosol interactions. This thesis proposed to quantify the temporal and spatial character of the temperature differential (T_p-T_g), and then to analyze and interpret the result and its ramifications on the atmospheric thermal structure of Mars.

The use of well-known radiative transfer algorithms within the simulation established some familiarity with meteorological computer modeling as well as emphasized the physics involved in planetary thermal behavior. These algorithms were chosen on the basis of their proven efficacy, sound theoretical foundations, and basic compatibility with available computing equipment in terms of financial and time constraints.

Such algorithms, modified as needed, were utilized to construct a practical computer program to produce thermal energy fluxes in the temporal

and vertical domains in a model of the Martian atmosphere. Temperature and opacity data from Mariner and Viking space probes were used, along with orbital and physical constants given by Souders (1970) and Mechtly (1973), to provide model input and set the boundary and initial conditions for the simulation. Temperature fields within the atmosphere were inferred from flux fields by means of enthalpy rate principles, while the radiation laws of Kirchhoff and Planck were applied to the flux fields to determine aerosol temperatures.

3.2 Description of the Model

The MARSTEMP program of Pallmann et al., developed from 1974 to 1976 under NASA Grant NGR 26-006-042-2, was the nucleus of the current model, MARSDUST. The reader is referred to the works of this author listed in the Bibliography if an explicit description of the program is desired. Since MARSTEMP was written in FORTRAN-H and subsequent modifications were not entirely documented, significant effort was expended in updating and debugging the program to run under the FORTRAN 77 compiler now in use on the department's MASSCOMP computer. Many difficulties also had to be overcome before the lengthy but necessary HITRAN

database was in a format easily usable. Most of this work preceded the development of the algorithm to compute dust temperatures.

MARSTEMP utilized input files derived from a database of atmospheric spectroscopic parameters compiled by McClatchey et al. at the Air Force Cambridge Research Laboratory (AFCRL) in 1973 for use in the their LOWTRAN code. MARSDUST similarly requires data for CO2 extracted from the updated database named HITRAN, developed by Rothman et al. (1983) of the renamed Air Force Geophysics Laboratory (AFGL) and subject to periodic revision. The 1986 HITRAN version used in this effort was kindly provided by Dr. Laurence S. Rothman of the Infrared Physics Branch at AFGL to the Department of Earth and Atmospheric Sciences at Saint Louis University.

A random band transmission model, based on that of Goody (1964), was developed for MARSTEMP utilizing a combined Lorentz-Doppler line shape profile in a treatment of intermediate line intensities, to better account for the spectral gappiness in the absorption spectrum of the tenuous atmosphere of Mars; a more sophisticated approach using the Voigt profile from AFGL's FASCODE, as described by Clough et al. (1981), proved beyond the scope of this study. The transmission model

used parameters extracted from the McClatchey database, namely, line intensity, lower state energy, and collision half-width; MARSDUST also uses the same quantities, although taken from the Rothman HITRAN compilation. An algorithm for effective absorption by an assumed height-dependent polydisperse silicate aerosol was installed in the program to account for dust effects on radiative transfer. MARSTEMP used data for silicate polydispersions calculated by Deirmendjian (1969) in its treatment of dust effects; MARSDUST incorporates data derived by Viking investigators wherever possible to improve on MARSTEMP's parameterization of the aerosol. A sophisticated model for multiple scattering was beyond the scope of available computing facilities; a decoupled and modular algorithm, as described by Isaacs et al. (1986) for use in AFGL's FASCODE and LOWTRAN routines (Clough et al., 1981), would be a desirable improvement to the parameterized treatment given multiple scattering in the MARSTEMP and MARSDUST programs. Such an algorithm would seem ideally suited for accomodation in a multitude of radiative transfer problems, assuming one possessed equipment with the computing power to handle the considerable number of iterations required by the program.

MARSTEMP was attuned by Pallmann et al. to the McClatchey input by using data obtained during the period November 1971 to February 1972 by the Infrared Interferometric Spectrometer instrument (IRIS) on the Mariner 9 spacecraft, as well as the IR radiometric and S-band occultation experiments. Since similar IRIS data was not available from the Viking mission, attunement of MARSDUST to the revised Rothman database was achieved by constraining the model to cyclical diurnal balance under the condition of no dust loading, such that temperatures at all levels at 24 hour intervals were approximately unchanged. The new attunement, although opposite in sense, is comparable in magnitude to the prior adjustment, and seems quite reasonable in light of the distinct differences between the two databases used. The Rothman compilation has nearly double the number of absorption lines in the spectrum as the McClatchey listing, necessitating the opposing trend of the current attunement process. The MARSTEMP adjustment, in essence, was a calibration implying a wider "effective" line half-width and an increased "effective" absorber amount due to the relatively coarse resolution of the McClatchey database. This attunement had to be negated and,

indeed, reversed, in accordance with the improved spectral resolution of the new HITRAN database.

3.3 Governing Equations and Boundary Conditions

The governing equations for MARSTEMP and MARSDUST are the Equation of Transfer (Liou, 1978; Siegel and Howell, 1971) and its derivatives, and the Enthalpy Rate Equation, along with the laws of black body radiation, spectroscopy, "perfect" gases, and thermodynamics. Within either model, enthalpic heating rates are equated to the negative divergence of the pertinent net fluxes of surface and atmospheric infrared radiative heating (amplified by a non-radiative term, the conductive heat flux) and of solar radiative heating. These radiative fluxes are obtained through the numerical integration of the Equation of Transfer over the wavelength range 0.2 μm to 50 μm, the altitude range 0 to 50 km, and the entire solid angle. The Enthalpy Rate Equation is solved numerically at 52 atmospheric levels between 0 and 50 km, and at 30 subsurface levels between 0 and 60 cm. Solutions to these equations are common in the scientific literature, and the reader is referred to Pallmann (1976; 1977) for a detailed treatment of the mathematics. It is important to note the nonlinear

character of the integro-differential equation describing radiative transfer. No analytical solutions exist; approximations are required and feedback effects are implicit.

The optical characteristics of polydisperse aerosols were tabulated by Deirmendjian in 1969, and the principal investigators of the Viking mission have used his modified gamma distribution to describe the size distribution of the Martian dust particles. Analysis of photographic data from the Viking Lander imaging cameras established reasonably accurate values for the necessary input parameters to the gamma distribution function, which allowed Mie theory to be applied toward the computation of values for the optical constants of the dust (Pollack et al., 1979). Other researchers used radiance data obtained from the Infrared Thermal Mapper (IRTM) on the Viking Orbiter as boundary conditions to define the optical properties of the planet as a whole under varying conditions. Kieffer et al. (1976), using the 20 μm band of the Viking Orbiter IRTM, implied a mean value of 0.285 for the surface albedo near the Viking 1 landing site (Pollack et al., 1979) and implied values between 0.90 and 1.0 for surface infrared emissivity. Pollack et al., using the Viking Lander imaging, derived explicitly a value

of 0.86 for the single scattering albedo of the dust averaged over the solar spectrum centered at 0.67 μm, which amounts to setting the average dust absorptivity at 0.14 in this spectral region. Hunt (1979) derived ensemble infrared emissivities between 0.4 and 0.7 for dust clouds under variable dust loadings and zenith angles, implying high infrared emissivity values, perhaps as high as 0.8 to 0.9, for individual dust particles. Thus, by analogy to terrestrial silicate sands, infrared emissivity values between 0.8 and 0.9 may be considered typical of individual Martian dust particles. These parameters were required by MARSDUST as a prerequisite to the establishment of an algorithm to calculate dust temperature. Conversion of the dust extinction coefficients used in the MARSDUST simulations to actual optical depth values is dependent on accurate figures for the integrated column density of the dust as well as the mean radius of the particles (Pallmann, 1976). In the abscence of agreement on these quantities, precise values of optical depth will not be quoted here; observations indicate that the dust extinction coefficients used in this study are well within the range of optical depths and dust distributions possible on Mars. In any case, trends in atmospheric thermal behavior can indeed be

ascertained from the data, and further analysis or refinement by others is welcome and encouraged.

3.4 Initial Atmospheric Conditions of the Model

An initial condition vertical temperature profile for MARSDUST was deduced from the Viking data of Seiff and Kirk (1977) and the initial profile used by Pallmann et al. in MARSTEMP. Temperatures above the 35 km level in the Seiff and Kirk profile disagree with the Pallmann profile based on Mariner 9 data, and in one review by Pollack et al. in 1979, no values above this level were quoted at all! MARSDUST output was very unstable at the upper altitudes when the Seiff and Kirk profile was used, which had the temperature at the 50 km level at an usually cold and physically suspect 148 K. This is very near the frost point of CO2, where the transition from the gaseous to the solid phase may occur; no such behavior was ever observed by Mariner or Viking spacecraft. In the upper layers of the Seiff and Kirk profile, diurnal balance proved unattainable and intense warming of these highest layers could not be eliminated in the model output. The Seiff and Kirk profile is perhaps more properly a trajectory profile rather than a vertical one; its uppermost temperatures seem to be

more characteristic of the polar region or at least the higher latitudes, which may indeed have been the region of entry for the deorbiting lander, but which is very far removed from the final landing site located at subtropical latitudes. Because of such practical concerns, the profile used in MARSDUST was a hybrid of the Seiff and Kirk data and the Mariner 9 data. The Mariner 9 profile implies upper layer temperatures warmer than Seiff and Kirk, including a 50 km value near 160 K; this profile was adopted by Pallmann for MARSTEMP. MARSDUST assumes the lowest level temperatures quoted by Seiff and Kirk are accurate but adopts the original values of Pallmann (1976) for the uppermost levels.

After initialization, the model requires that several hundred timesteps be run before numerical stability is attained by the output. Planetary fluxes in the model output increased slightly but steadily over the first few days of simulation, as did derived temperatures, but then temperatures were observed to oscillate mildly about median values after approximately three simulated days. It appears the model is more sensitive to variations in solar radiative input than planetary output; derived temperatures after three days varied typically by less than five percent from their

initial values, while planetary fluxes increased by about ten percent over the same time. These disparities were lessened by having no dust load and aggravated by increased dust loading, and are apparently a measure of the success of the applied attunement process described previously, as well as the affects of dust loads. In the discussion of results offered here, values quoted are for the fourth day of simulation or later, when model output is assumed to be more or less computationally stable.

3.5 The Dust Temperature Algorithm

MARSDUST includes an algorithm to calculate dust particle temperature, derived from principles set forth by J.R. Howell and R. Siegel (1969). An explicit formulation of the dust temperature module is given in Figure 1. The model consists of idealized concentric spheres, where the net influx of energy, Q_{in}, to the particle is the sum of the contributions of longwave and shortwave absorption, integrated over all incident zenith angles with azimuthal independence assumed. Because of the extreme minuteness of the particles, instantaneous thermal equilibrium can be considered a good approximation, such that $Q_{out} = -Q_{in}$. Absorptivity

of 0.14 for solar (shortwave) flux is assumed in accordance with Pollack et al. (1979). By invoking Kirchhoff's principle that a good emitter is a good absorber, the absorptivity is set equal to the emissivity for the planetary (longwave) spectrum. For all data presented here, an emissivity of 0.80 is assumed in analogy to terrestrial desert sands, and by considering the suppressing effect of the silicate lattice structure on emission (reststrahlen effect), which would tend to lower the emissivity value. As a sink mechanism, CO2 conductivity of heat away from the particle was assumed to follow a Gaussian distribution function (height-square logarithmic profile), as described by Pallmann (1983). Such a vertical dependence was justified by considering the nature of the eddy exchange processes and turbulent mixing responsible for carrying the dust aloft. It was assumed that the same physical processes that allow dust suspension permit the effective conduction of heat away from the particle by the atmosphere, such that smaller dust loadings at any level corresponded to less effective CO2 conductivity at that level, and vice versa. As a consequence, dust and atmospheric temperatures at the lowest levels are always equal, with any dust heat excess quickly being lost to the atmosphere.

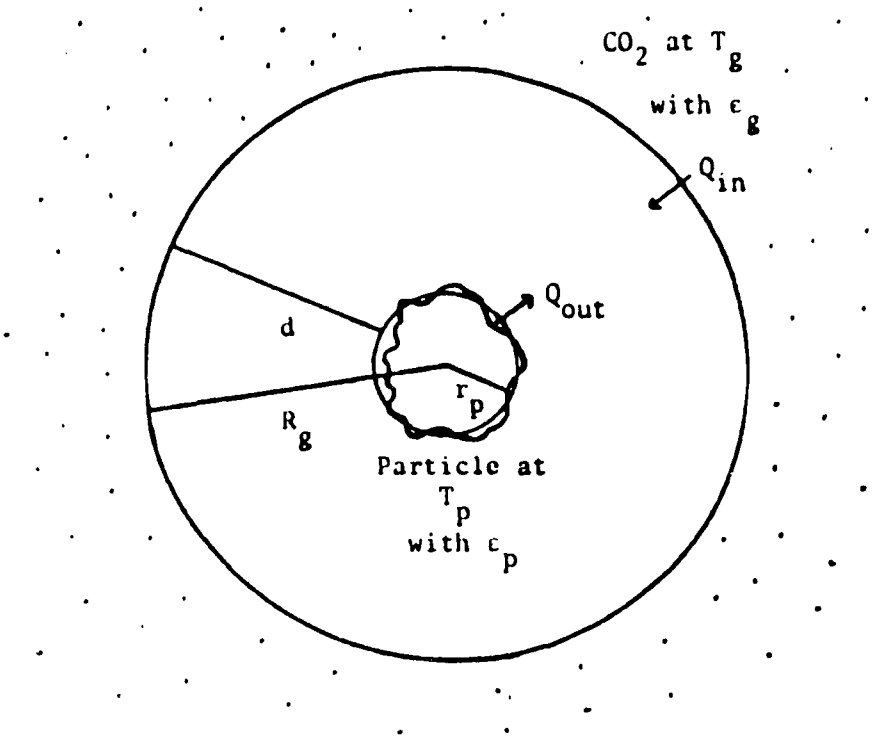

$$Q_{out} = -Q_{in}$$

R_g, r_p = Radii of Model Spheres
T_g = Gas (CO_2) Temperature
T_p = Particle Temperature
ϵ_g = Gas (CO_2) Emissivity
ϵ_p = Particle Emissivity
d = Molecular Mean Free Path

$$Q_{out} = \frac{A_p \sigma (T_p^4 - T_g^4)}{\frac{1}{\epsilon_p} + A_p/A_g (\frac{1}{\epsilon_g} - 1)}$$

A_g = Surface Area of Gaseous Shell
A_p = Surface Area of Particle
σ = Stefan-Boltzmann Constant

Figure 1. The Dust Temperature Algorithm

In the model, a dust particle with effective spherical radius r_p lies within a spherical gaseous shell of radius R_g. The value of R_g is physically limited to be never less than $r_p + d$, where d is on the order of the mean free path of a gas molecule. For the tenuous atmosphere of Mars, this strongly suppresses any direct thermal interaction between the gas and the particle, since R_g is nominally an order of magnitude larger than typical r_p's, even at the lowest altitudes. The algorithm does permit dust-gas feedback, such as that described by Fiocco et al. (1975), but only when R_g and r_p are of the same order of magnitude, or when the gas has a very low emissivity in the thermal infrared; for the Mars case, the surface area of the gaseous shell is always much larger than the surface area of the particle, and the term involving gas emissivity in the formula given in Figure 1 is negligible. It was therefore deemed appropriate to neglect this effect in the MARSDUST model, considering the assignment of a typical 1 μm radius, implicit within MARSTEMP, to the individual dust particle. (A flowchart of the MARSDUST program is presented in Figure 2 to assist the reader in visualizing the various modules and algorithms).

It is important to note that this assumption does not imply any lack of synergy between gas and dust in the model when one considers overall atmospheric warming. Indeed, this thesis supports the contention that dust contributes to warming of the atmosphere; but the effect is primarily the result of increased atmospheric absorption due to multiple scattering of radiation by the dust, not by the heated particles directly warming the gas by radiation or conduction.

Radiative heating of the gas by the dust can indeed occur, and may become significant for the higher dust concentrations, but this feedback effect is neglected in the current model. MARSDUST output indicates that particle fluxes are much smaller than solar fluxes and usually smaller than planetary fluxes, which are the two most important thermal forcing mechanisms. Flux errors introduced by this neglected effect are probably on the order of 10%, roughly the ratio between solar fluxes and atmospheric layer fluxes; errors in temperatures derived from the Stefan-Boltzmann Law would be even less because of their fourth-power relationship to fluxes. It is hoped, however, that future work will improve on the current algorithm in treating these nonlinear effects.

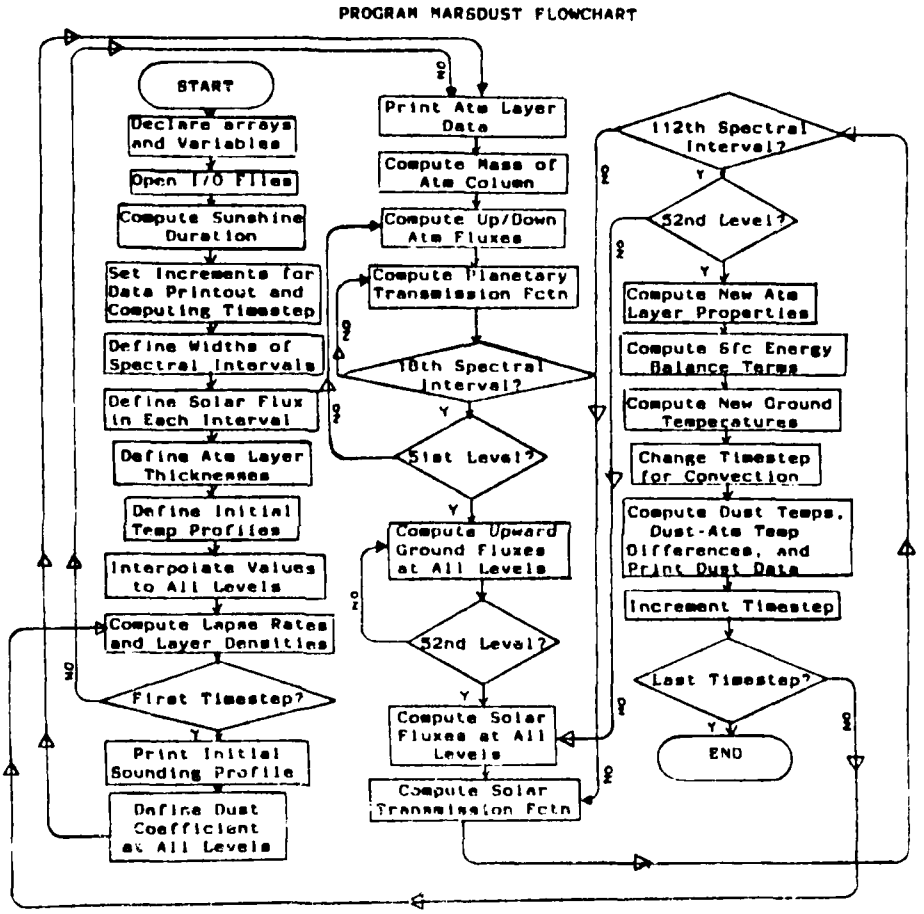

Figure 2. Program MARSDUST Flowchart

4. DISCUSSION OF RESULTS

4.1 Overview

The reader is referred to the Appendix for a comprehensive graphic presentation of the results of the MARSDUST simulations. Please note that LMST is an abbreviation for Local Martian Solar Time, while DUSTAMP is shorthand for Dust Amplitude, a measure of the atmospheric dust loading. LMST 0.000 indicates the beginning of a diurnal cycle, while LMST 24.000 signifies the end of the same 24 hour period. All plotted data for dust correspond to a dust emissivity of 0.80; output utilizing this emissivity differs by less than 3% from output using an emissivity of 0.90. A sensitivity study showed that derived dust temperatures were only a weak function of emissivity for values above 0.70 and strong dependence was seen only for highly unrealistic emissivities below 0.30. The values of emissivity referred to here are for the individual dust particle and are quite distinct from the bulk emissivity values quoted in the literature for an ensemble of particles in an optically thick cloud.

For a simulation without dust loading at all timesteps, atmospheric temperature soundings above 9 km showed the smooth exponential decline with

height characteristic of radiative cooling. The lowest 9 km were dominated by conductive and convective processes, as exhibited by persistent nearly adiabatic lapse rates (+5.2 K/km) and strong nightime inversions in this region (Figures 3 and 4). At night in the lowest 2 km, a temperature inversion is a constant feature because of the rapid cooling of the surface after sunset with respect to the overlying atmosphere. This inversion intensifies to lapse rates over -17 K/km just before dawn, and does not completely disappear until well into mid-morning, near 10.000 LMST. Without dust loading, maximum surface temperature is around 250 K just after local noon, while the minimum just before dawn approaches 185 K. The inversion in the lowest layers sets in very quickly after sunset.

Dusty atmosphere simulations were run with three extinction coefficients (representing three distinct dust loadings): 1.2 x 10^{-7} per cm, 3.0 x 10^{-7} per cm, and 6.0 x 10^{-7} per cm (Figure 5). These correspond to the moderate to heavy dust storms observed on Mars by the Mariner and Viking spacecraft. The dust load in each case was set to zero at an altitude of 42 km, in accordance with the observation that Martian dust loadings rarely exceed this level. This assumption creates an

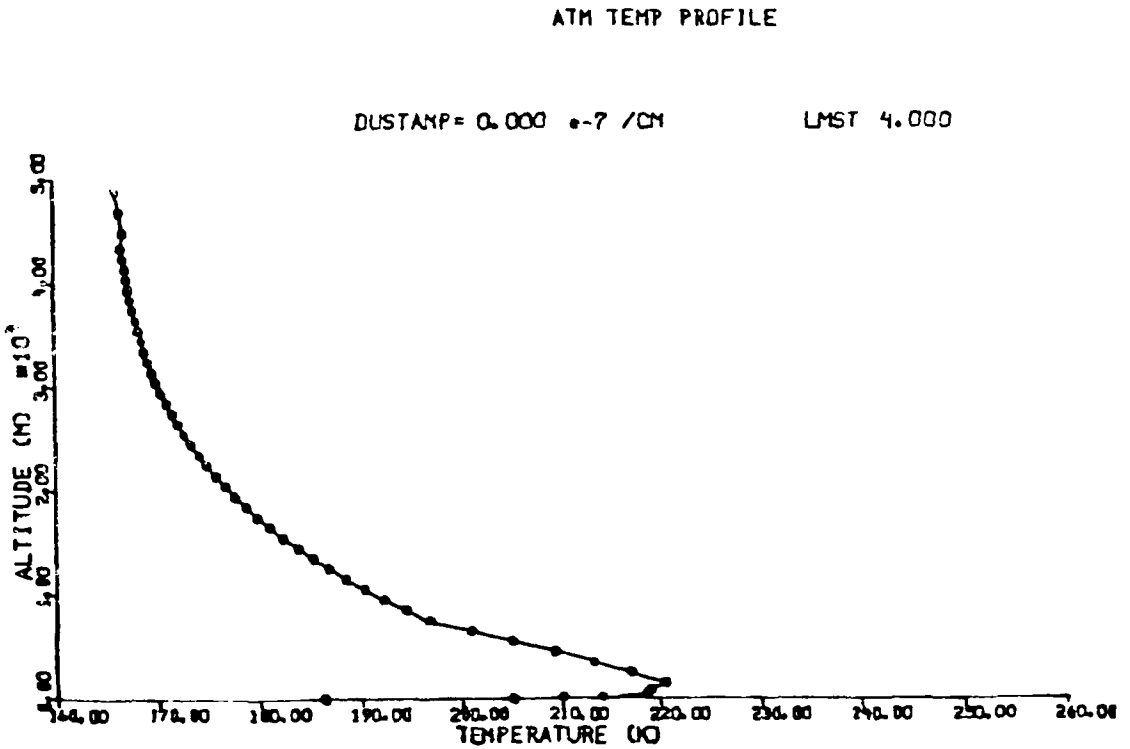

Fig. 3. Vertical Atmospheric Temperature Profile: No Dust Load, LMST 04.00
Y axis: 0 to 50 000 m, X axis: 160 to 260 K

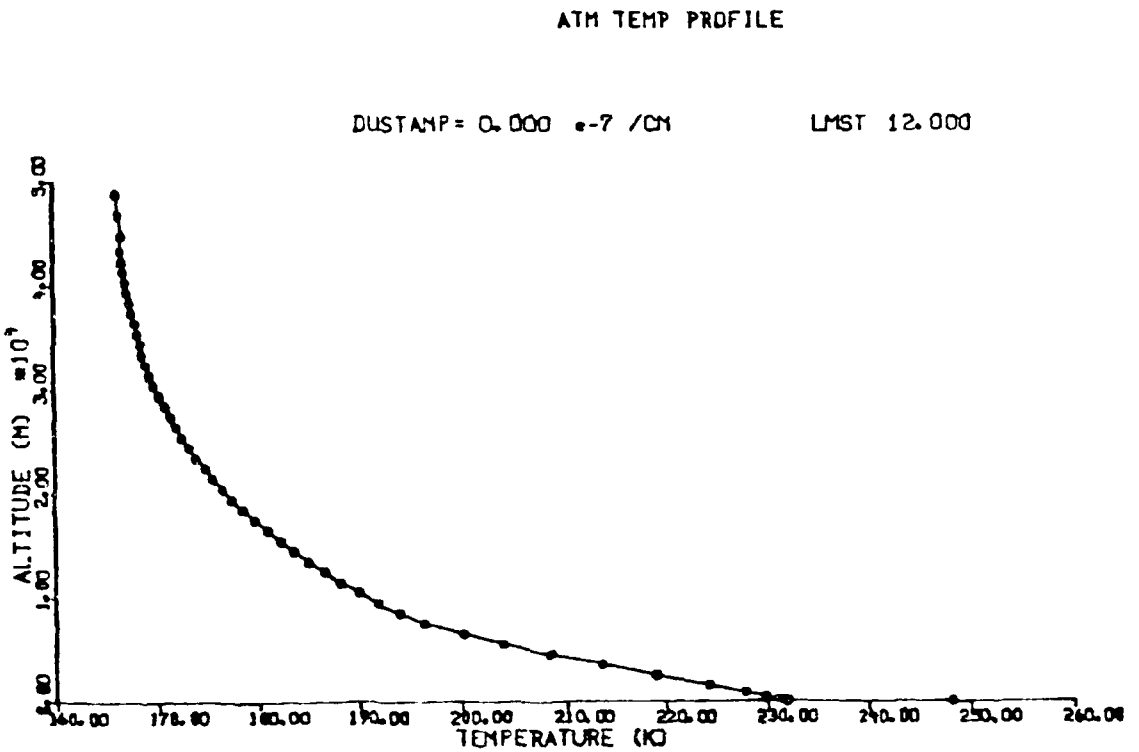

Fig. 4. Vertical Atmospheric Temperature Profile; No Dust Load, LMST 12.00
Y axis: 0 to 50 000 m, X axis: 160 to 260 K

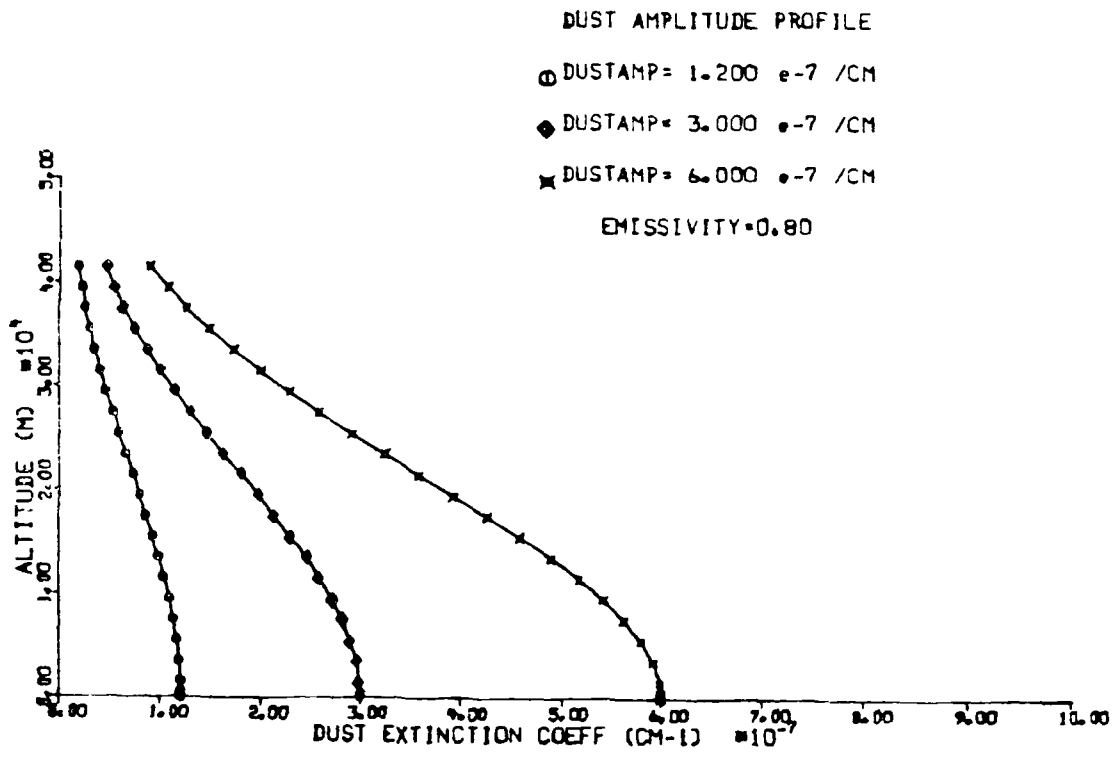

Fig. 5. Dust Amplitude Profiles; Dust Extinction Coefficient = (DUSTAMP) $\exp[(-1.11 \times 10^{-9})z^2]$, where z = altitude (m)

abrupt discontinuity in the atmospheric temperature profile at the 42 km altitude. The reader is cautioned that the temperature values in the uppermost layers of the dusty atmosphere soundings are only as realistic as the previously stated assumption. It does seem reasonable that such an abrupt change should occur at least somewhere in the upper atmosphere, since purely physical considerations imply a shallow transition region above which aerosols of a given effective radius cannot be kept aloft.

The shapes of the temperature soundings for the various dust loads are quite similar. However, with increasing dust load, layers above 25 km appear to be cooled, while the atmospheric layers below 25 km, and the surface itself, show a significant warming trend (Figures 6-9). A model sensitivity study indicated that surface cooling is achieved only after a drastic increase in dust concentration, corresponding to a DUSTAMP of 1.2 x 10^{-4} cm^{-1}. This is a thousand-fold increase in particle number density from our lowest previously stated DUSTAMP value, and represents a dust load of about 5000 particles per cubic centimeter, assuming an effective radius of one micrometer. Predawn minimum surface temperature for the lightest dust load is near 190 K, while for the heaviest dust

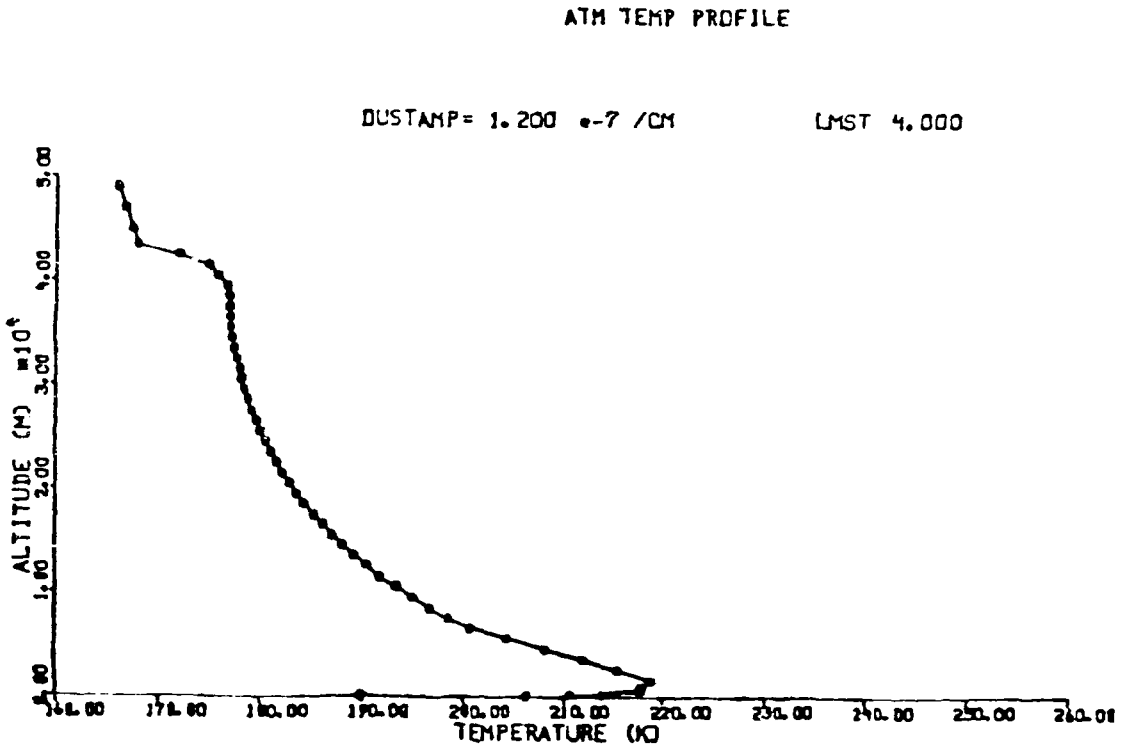

Fig. 6. Vertical Atmospheric Temperature Profile; Light Dust Load, LMST 04.00
Y axis: 0 to 50 000 m, X axis: 160 to 260 K

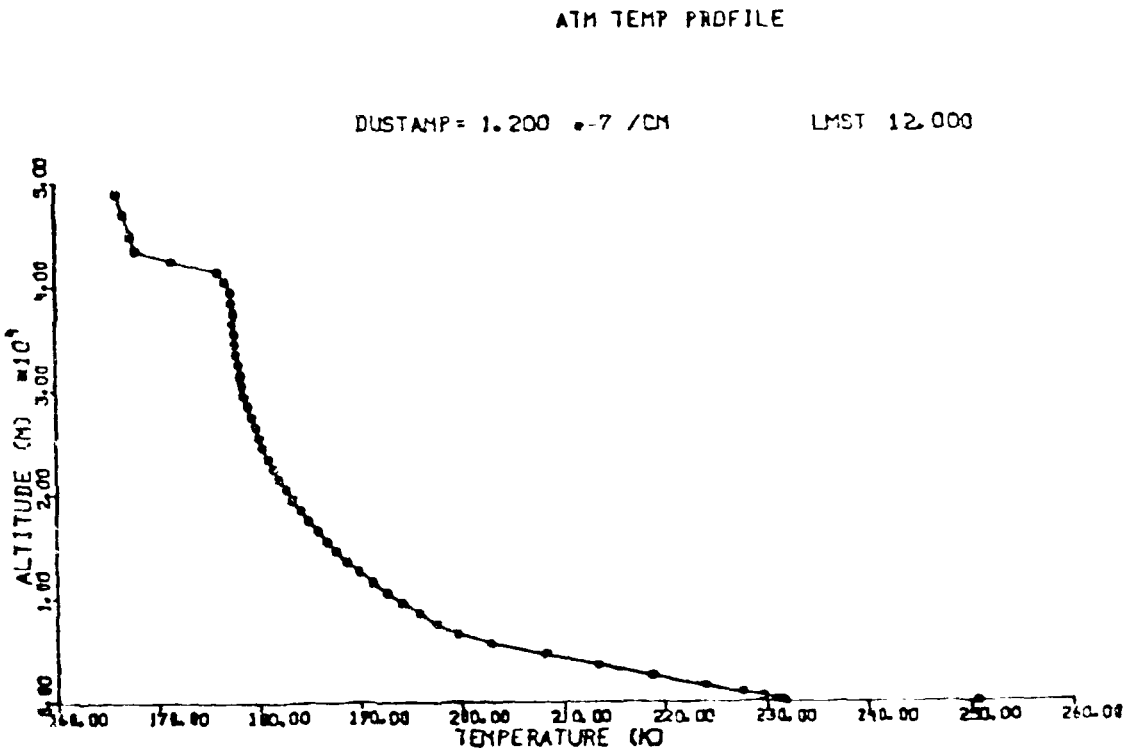

Fig. 7. Vertical Atmospheric Temperature Profile: Light Dust Load. LMST 12.00
Y axis: 0 to 50 000 m, X axis: 160 to 260 K

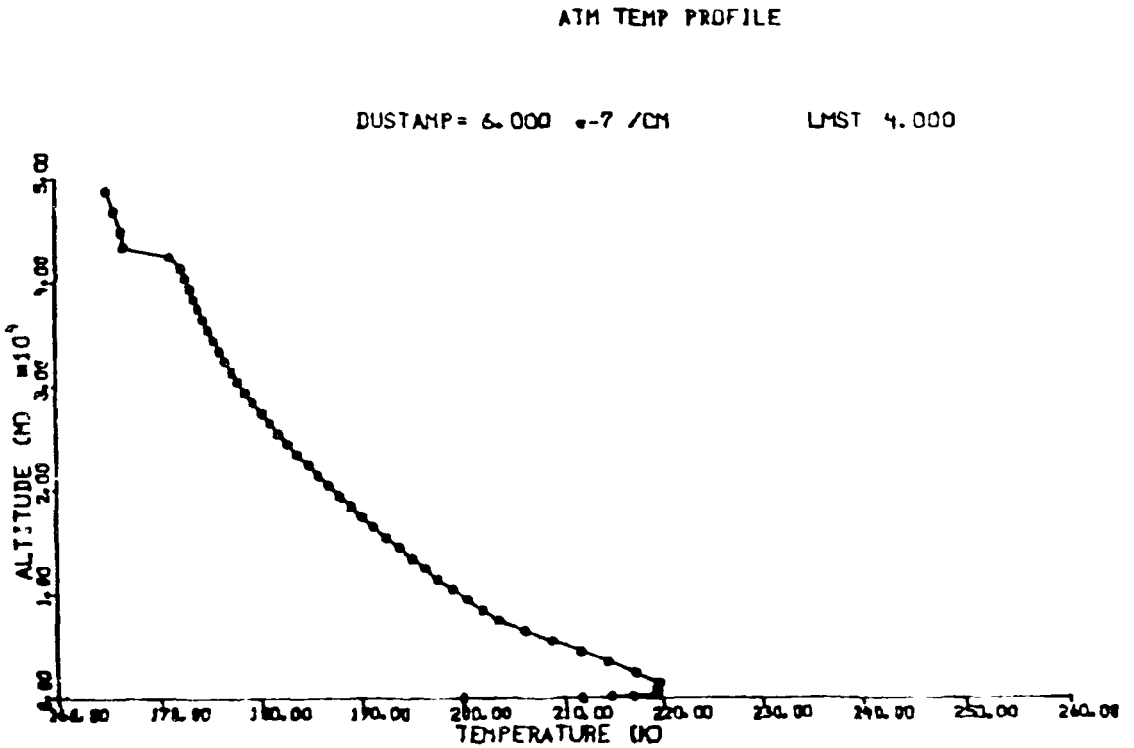

Fig. 8. Vertical Atmospheric Temperature Profile: Heavy Dust Load, LMST 04.00
Y axis: 0 to 60 000 m, X axis: 160 to 260 K

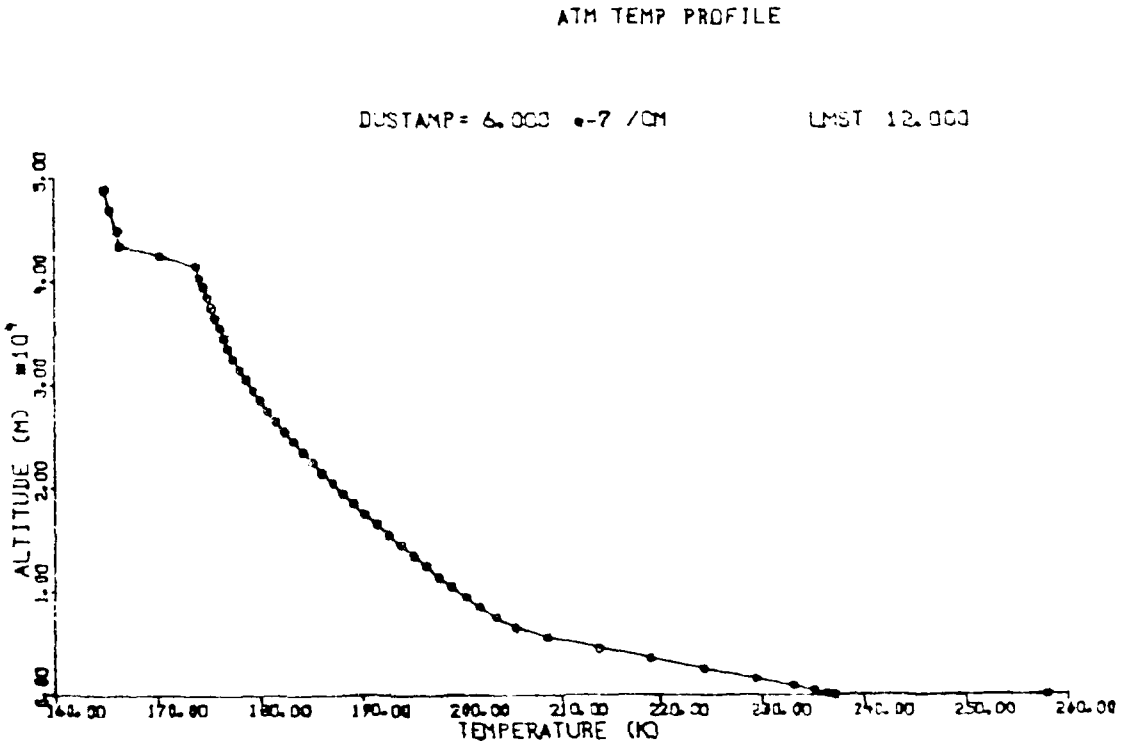

Fig. 9. Vertical Atmospheric Temperature Profile: Heavy Dust Load, LMST 12.00
Y axis: 0 to 50 000 m, X axis: 160 to 260 K

load, it is about 200 K. Predawn temperature at the 40 km level for the lightest dust load is about 176 K, while for the heaviest dust load it is closer to 172 K. At LMST 13.900, the maximum surface temperature for the lightest dust load is 253 K while it exceeds 260 K for the heaviest dust load. The effect of the thicker dust loading seems to be mainly felt near the surface, where the dust contributes to strong warming but also promotes cooling aloft by inhibiting escape of planetary emissions to higher altitudes. The increased multiple scattering induced by the higher dust load enhances absorption by carbon dioxide in the lowest levels at the expense of the upper atmosphere. By adding to the atmospheric counter radiation in the lower layers, the thicker dust loads can help warm the surface throughout the diurnal cycle.

Even a cursory inspection of the dust temperature profiles (Figures 10 and 11) shows the swift response of dust temperature to the influx of solar radiation, regardless of dust loading. Similarly, the surface temperature experiences drastic shifts between nighttime and daytime conditions. The response of the atmosphere as a whole to solar input, whether or not dust is present, is far more sluggish. This difference in response indicates the disparity between the

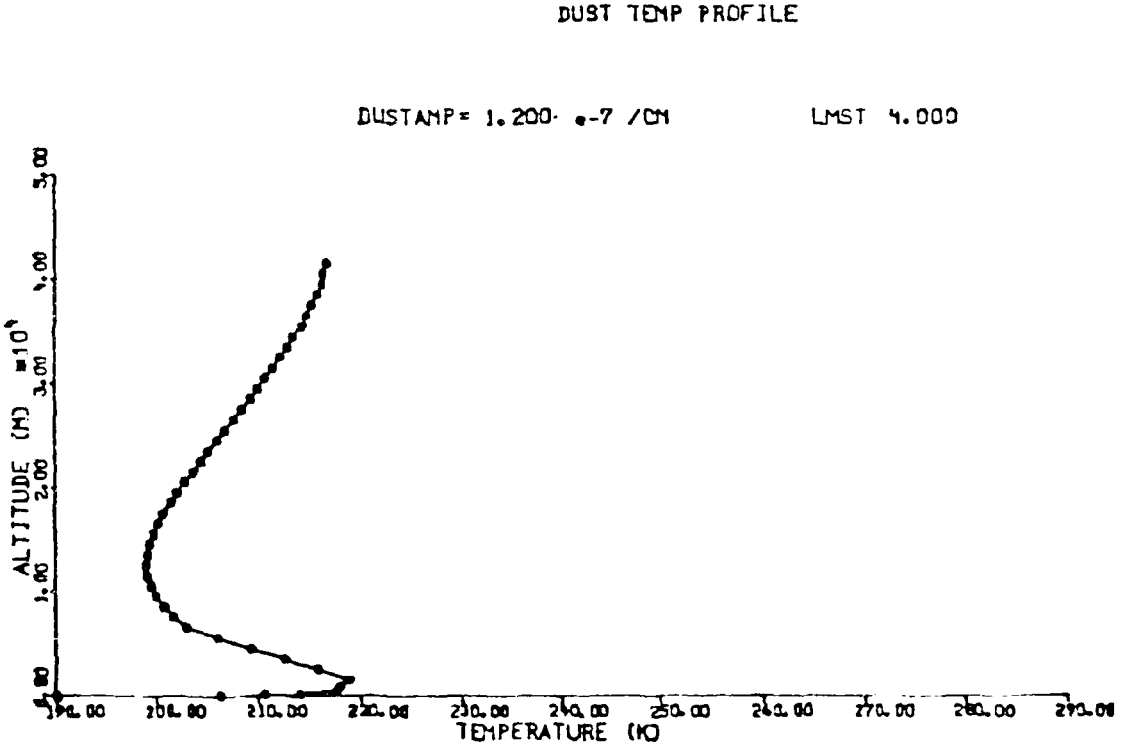

Fig. 10. Vertical Dust Temperature Profile; Light Dust Load, LMST 04.00
Y axis: 0 to 60 000 m, X axis: 190 to 290 K

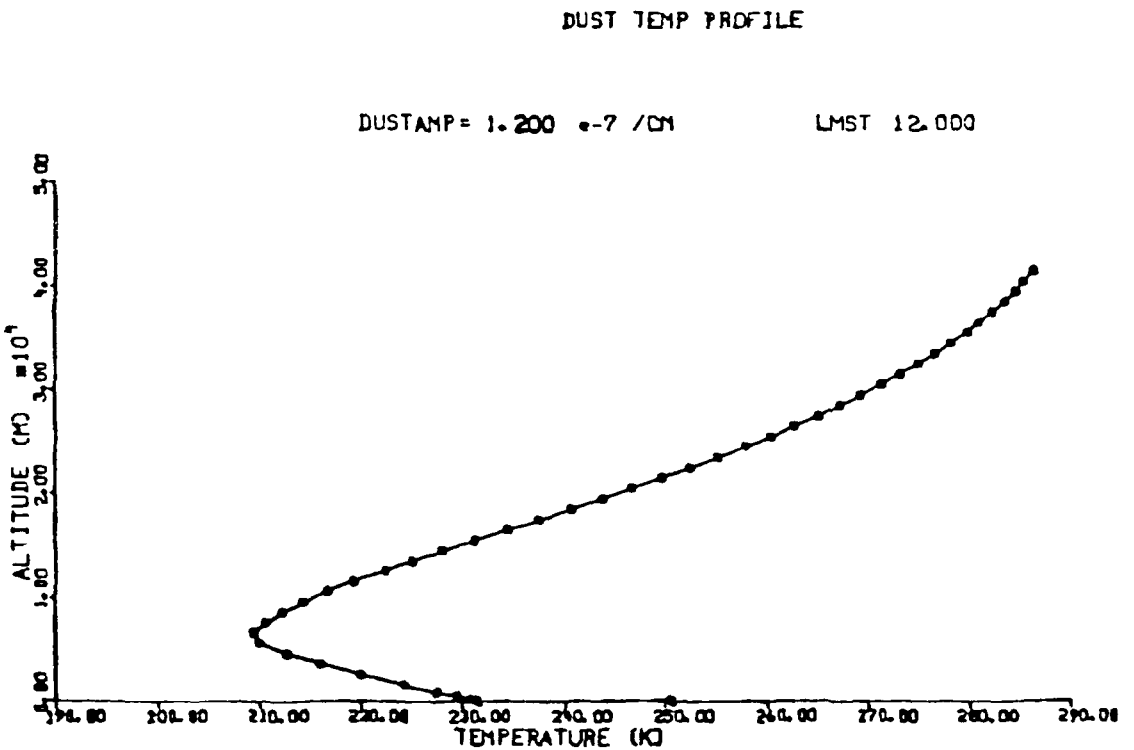

Fig. 11. Vertical Dust Temperature Profile; Light Dust Load, LMST 12.00
Y axis: 0 to 50 000 m, X axis: 190 to 290 K

specific heat capacities and thermal inertias of the solid and gaseous components of the planetary ground-atmosphere system.

With increasing dust load, dust temperatures attain lower maximum and higher minimum values, and the magnitude of the dust-atmosphere temperature differential decreases. The higher dust content also aids in burning off the morning inversion more quickly. Higher dust amplitudes tend to lower the altitude of minimum dust temperature at night, and raise it during the day. This implies that the upper levels "feed" off the heat content of the very dusty lower levels throughout the diurnal cycle; this is more evident at night, of course, when the heat source is not replenished, while in the daytime, the heat content of the lowest layers steadily increases with continued insolation. While dust-free and light dust load conditions give very stable, almost isothermal, lapse rates at the topmost levels, increased dust loading yields increasingly stable lapse rates at nearly all other levels higher than 9 km or so, throughout the diurnal cycle. The lapse rates in the lowest 9 km do not seem to be a strong function of dust concentration; the increasing heat content of the lowest levels appears to be quickly transferred to the mid-levels. This agrees with previous modeling

by various researchers who determined that the Martian dust storms carry the seeds of their own destruction; increasing the static stability of the lower atmosphere by warming middle layers inhibits the dynamic mechanisms required for dust lifting, and the storm is gradually extinguished from below.

Because of the tendency of high dust loads to decrease the amount of planetary flux reaching the uppermost layers, the maximum dust temperatures and dust-gas temperature differentials which occur at the highest levels are lower for the thicker dust loads. Maximum dust temperatures for all three simulated dust loadings exceeded 280 K with an assumed dust emissivity of 0.80, while maximum dust-atmosphere temperature differences exceeded 105 K at the 42 km level in each case during daylight hours. At night, the minimum temperature differentials at the 42 km level were over 41 K in each case, and perceptible dust-atmosphere temperature differences occured at lower levels than in the daytime.

The plotted atmospheric temperature profiles indicate that at least five distinct atmospheric layers exist whenever dust is present. These include a surface boundary layer of about 1 km thickness exhibiting conduction/convection dynamics and experiencing diurnal temperature shifts of

about 50 K; a well-mixed region, 8 to 9 km thick, of adiabatic lapse rates, just above the boundary layer, where turbulence, eddy mixing, convection, and dust influences dominate; a 30 km thick layer topping the adiabatic region, characterized by radiative heating/cooling processes with diurnal temperature changes of less than 5 K, and whose static stability increases with increasing dust load; a shallow (2-3 km thick) layer of near-adiabatic to adiabatic lapse rates overlying the topmost dust level, indicative of turbulent mixing; and finally, a region which returns to radiative heating/cooling processes. In the dust-free state, only three regimes are evident, namely the surface boundary layer, the well-mixed adiabatic layer above it, and the radiatively active layer overlying them both and extending to space. It is apparent that dust loading can cause significant changes in atmospheric stratification and static stability; detailed discussion of the attendant implications for the pertinent meteorological dynamics (e.g., storm genesis and decay) is left for future study. It is important to note, however, that on Mars, the characteristic relaxation times for thermal perturbations caused by radiation, with spatial scales on the order of several hundred meters, are comparable to the relaxation times for

thermal perturbations on similar spatial scales due to mild turbulent convection (Danneviek and Pallmann, 1974; Belton and Goody, 1967); this is very different from the terrestrial situation, and suggests that the character of dynamical processes on the two planets can be quite dissimilar. Consideration of the tenuity of the Martian atmosphere also supports this conclusion.

Model output indicates that reflected solar flux at any level is about 50% to 75% of the upwelling ground flux, while direct incoming solar flux is typically more than 1.5 to 2.5 times as great as the ground flux, depending on altitude. Atmospheric layer fluxes are about 20% of ground fluxes at a given level. This implies that solar fluxes are nominally at least an order of magnitude larger than atmospheric fluxes. Solar flux is greatest at the highest levels, of course, while the opposite is true of the planetary fluxes. Fluxes due to particles alone depend on altitude and dust loading, but range from about one third to twice as great as atmospheric layer fluxes. It is apparent that particle flux can be significant when compared with the atmospheric flux, but since ground emissions dominate the amount of energy radiated to space (output) and solar energy is the primary forcing function (input) for the system,

only unusually heavy dust concentrations are capable of perturbing the overall planetary thermal balance.

4.2 Validation of Model Output

Volume 84 of the Journal of Geophysical Research (JGR), dated June 10, 1979 and published as the "Mars Volatiles Issue", presented contributions from many of the principal investigators of the Viking mission, including several articles directly pertaining to the thermal infrared properties of the Martian atmosphere. Dust aerosols were also discussed in some detail, and derived particle parameters were incorporated into the model. The analyses offered in the Mars Volatiles Issue of JGR will be used here as one benchmark in determining the validity of the MARSDUST model, since they represent the best understanding of the Martian atmosphere yet available.

The previously discussed attunement of the model to cyclical balance is also a kind of validation. Obviously, if the model were incapable of such balance, it would not even be internally consistent, much less a valid simulation of reality. In addition, a necessary validation

procedure is to compare the fluxes computed for the dust free case with fluxes computed for the various dust loads, to determine if the "dusty" atmospheric fluxes are approximately equal to dust free atmospheric fluxes plus dust particle fluxes alone. This approach is more susceptible to error because of the lack of accurate estimates of dust concentration, which are needed to calculate dust particle fluxes, but it is hoped that even a rough order of magnitude agreement will provide increased confidence in the model.

In this regard, upward and downward fluxes computed for the atmospheric source layers by the model were compared for the dust free and dust laden cases. Then fluxes due to dust particles alone were computed manually, using the vertically integrated column number density derived by Conrath et al. (1973) from Mariner 9 data. This number density, corresponding to the MARSDUST amplitude of 1.2×10^{-7} cm^{-1}, was determined to be about 1.2×10^{7} for a radius of 1 μm. Assuming an atmospheric column of about 40 km maximum height, the Conrath et al. value yields a mean number density of $3/cm^3$. This is not in agreement with calculations made later by Pollack et al. (1977), who derived a value closer to $30/cm^3$; however, Pollack et al. assumed a radius almost an order of magnitude smaller, which

probably accounts for the discrepancy. It is important to note that these derived number densities apply only to the particle radii quoted, and are not meant to describe the entire size distribution. The Conrath et al. figure, being the result of a vertical integration, must be thought of as an average, implying smaller values at high altitudes and greater values near the surface. For the sake of this analysis, a value of $5/cm^3$ was assumed near the surface for a DUSTAMP (extinction coefficient) of 1.2×10^{-7} cm^{-1}; similarly, DUSTAMP values of 3.0 and 6.0×10^{-7} cm^{-1} correspond to near-surface number densities of about $12/cm^3$ and $25/cm^3$, respectively.

In a rectangular column with a base area of one square centimeter and height one kilometer (a typical source layer thickness in the model), the total number of particles would be about 500 000, 1 200 000, and 2 500 000 for the three DUSTAMPs. Since the particles are vastly smaller than the volume they occupy, even these numbers are considered to include a negligible amount of overlap in cross section, so that the particles are assumed not to obscure or "shadow" each other. Thus, the principle of linear superposition can be applied to compute the net upward and downward fluxes from such an ensemble of particles. Using

the Stefan-Boltzmann Law for gray bodies and an assumed emissivity of 0.80, flux densities for individual particles at a given temperature can be computed. Knowing their total surface area permits direct calculation of the total flux due to the particle ensemble.

Using a median temperature value of 230 K for a 1 km thick source layer centered at 1.5 km altitude at local noon (12 LMST), the sum of the total upward and total downward particle fluxes, based on the Stefan-Boltzman Law, is about 8000 erg/sec for the $5/cm^3$ dust load, 19 000 erg/sec for the $12/cm^3$ concentration, and 38 000 erg/sec for the $25/cm^3$ concentration. For this same layer in the dust free state, the sum of the upward and downward fluxes is about 19 000 erg/sec. For the three DUSTAMPs, in increasing order, the amount of flux in excess of this baseline figure for the given layer is 10 000, 24 000, and 43 000 erg/sec. These values differ from the dust fluxes stated above by about 25%, 21%, and 12%, respectively. In light of the crude assumptions made, this agreement is surprisingly close and permits a reasonable level of confidence in the validity of the model.

Martin et al. (1979) gave temperatures for the surface and dusty atmosphere, based on the inversion of Viking IRTM radiance data at various

wavelengths, which are in agreement with MARSDUST output. They conclude that surface temperatures are much greater than atmospheric temperatures typically between the hours of 9 and 16 LMST, a feature captured rather well by MARSDUST. According to Martin et al., the inversion of 20 μm radiance data gives an estimate of minimum surface temperatures while inverting the 7 μm data yields maximum surface temperatures. If so, their dust-free maximum around 253 K and minimum near 181 K is in good agreement with the model. Their dusty atmosphere data was mainly for the southern hemisphere, where summer temperatures are warmer than in northern summer, but even so, their figures of about 273 K and 210 K, corresponding roughly to the same time of season as the MARSDUST simulation, are very close to model outputs for the heavier dust loads. Peterfreund and Kieffer (1979) determined mean dust cloud temperatures near 237 K and cloud top heights between 8 and 17 km. A derivation of dust cloud height by Martin et al. from 9 μm radiance data implied an altitude of 11 km, which is remarkably close to the level for minimum dust temperature given by the model for the various dust loads. For model output below this altitude, adiabatic lapse rates are the rule, while above it, slower cooling of the atmosphere with

height gives increasing stability and a diminished capacity to raise dust. Indeed, Thomas and Gierasch (1985) report that local "dust devils" rarely exceed a height of 7 km. Thus the level of minimum dust temperature can indeed be considered the top of a dust cloud deck, and the Viking results support this interpretation. The amplitude of diurnal surface temperature changes was observed by the Viking IRTM to be within a range of about 50 to 100 K, while typical model data gives amplitudes on the order of 60 to 80 K.

These many comparisons are offered as a validation of the model; in no respect does the MARSDUST output grossly deviate from the norms set by Viking observations. These checks of internal consistency and similitude of output to actual measurements and known phenomena support the contention that the model is indeed a reasonable match to reality on Mars.

5. CONCLUSIONS

To adequately describe the effects of aerosols on radiative-convective heat transfer on Mars, the size distribution and optical properties of the aerosol must be known accurately. The shape and microphysical structure of the constituent particles should be considered; the residual ray effect could be extremely important for lithospheric aerosols derived from highly crystalline materials, such as silicates.

Aerosols generally contribute to an overall warming of the atmosphere, but interact with the surface to produce a "local albedo" (Liou and Sasamori; 1975) and can enhance cooling near the surface if the particle concentration is high enough. Maximum cooling rates, for a polydisperse aerosol characterized by an effective radius of [illegible], the [illegible] concentration to [illegible] cooling on Mars is about [illegible] particles [illegible].

Except at the lowest pressure levels, where collisional [illegible], the aerosol and the ambient gas will [illegible] a significant temperature difference with the aerosol usually [illegible] warmer than the ambient

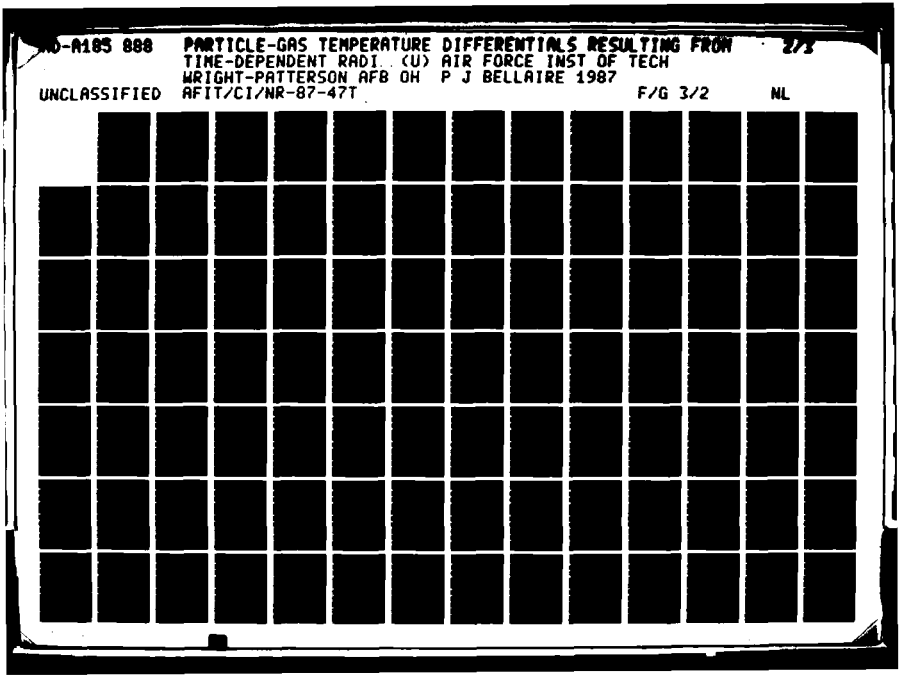
AD-A185 888
PARTICLE-GAS TEMPERATURE DIFFERENTIALS RESULTING FROM
TIME-DEPENDENT RADI (U) AIR FORCE INST OF TECH
WRIGHT-PATTERSON AFB OH P J BELLAIRE 1987
UNCLASSIFIED
AFIT/CI/NR-87-47T
F/G 3/2
NL

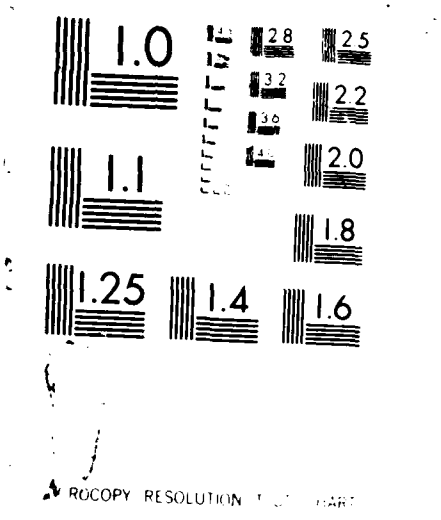
1.0
1.1
1.25
2.8
3.2
3.6
2.5
2.2
2.0
1.8
1.4
1.6
ROCOPY RESOLUTION

gas, even at night. For the Earth, 65 kilometers (corresponding to a pressure of 0.1 hPa or 0.1 mb) is the threshold altiude above which this difference becomes larger than 10 K, increasing to over 100 K near the 90 km or 0.001 hPa level (Fiocco et al., 1975). For Mars, the current model indicates that a 10 K difference can be achieved at a much lower altitude, closer to 15 km (1 hPa), while a surplus of 100 K is possible well below 50 km (indeed, MARSDUST restricts dust to altitudes below 42 km, or the 0.1 hPa level), depending on particle concentration. Because of the higher density, lower infrared emissivity, and more complicated chemistry of the terrestrial atmosphere compared to that of Mars, the dependence of dust temperature on particle radius and altitude is stronger and more complex for Earth than Mars. Our model neglects this weaker dependence of dust temperature on particle radius for Mars.

The atmospheric temperature profiles derived from MARSDUST output indicate that at least five distinct atmospheric layers are sustained when dust is present: a surface boundary layer of about 1 km thickness dominated by conduction/convection processes and experiencing diurnal temperature changes on the order of 50 K; a persistent region of adiabatic lapse rates, 8 to 9 km thick, just

above the boundary layer, where turbulent mixing, convection, and dust influences are maximized; a layer about 30 km thick above the adiabatic region, characterized by radiative heating/cooling processes with diurnal temperature changes on the order of 5 K, and whose static stability increases with increasing dust load; a shallow (2-3 km thick) layer of near-adiabatic to adiabatic lapse rates overlying the topmost dust level; and finally, a region charaterized by a return to radiative heating/cooling processes. Without dust, only three domains exist: the surface boundary layer, the adiabatic layer above it, and the region of radiative heating/cooling overlying them both and extending to space. On Mars at least, it appears that dust loading can cause significant changes in atmospheric stratification and static stability.

Atmospheric temperatures derived by inversion of radiance data obtained from orbit can become suspect when aerosols are present. Depending on the wavelength channel used by the orbiting radiometer, measured upwelling flux can be substantially increased by net particle emissions, which may be on the order of the atmospheric emission itself (or greater) for a given layer.

Viking Orbiter Infrared Thermal Mapper (IRTM) data of Mars indicate to some observers that sudden

warmings on the order of 80 K at the 25 km level near the poles are possible and are linked to atmospheric dust content (Martin and Kieffer, 1979). One may wonder if this is an exaggerated figure for actual warming of the atmosphere. In light of our model output, the increased IR emission detected by the Viking IRTM instrument could be due at least partially to the presence of dust at temperatures much higher than the ambient gas. It should be noted that for the tenuous atmosphere of Mars, heat exchange by conduction between the dust and gas is only significant near the surface.

The interpretation of this warming event depended on the confidence placed in the quite low bulk emissivities calculated for the dust cloud held responsible, yet the inversion technique that was used implied an altitude (25 km) indicative of a pressure level (0.6 hPa) that might have been inappropriate, since it was apparently based on a typical midlatitude vertical profile. This is almost certainly a source of some error if applied near the poles; consider the suspicious nature of the upper level temperatures of the Seiff and Kirk profile previously discussed.

At lower altiudes, warmer dust particles may be most significant as impediments to the

deposition and precipitation of CO2 in the cold polar atmosphere, and a reduction in the dust cloud's effective emissivity could be the result of its photon energy being lost to slowing the phase change process. At an altitude of 25 km, dust concentration (one or two particles of 1 μm mean radius per cm^3) and/or atmospheric density (1.5×10^{-6} g/cm^3) would be sufficiently low to cast doubt on the conclusion that the dust is directly responsible for any significant warming of the atmosphere at that level. However, an unusually thick but necessarily transient cloud of limited vertical extent carried poleward by Hadley cell dynamics (both Earth and Mars possess atmospheric circulation patterns which tend to preferentially deliver aerosol particles to the poles) could be the source of significant IR emission before it inevitably succumbs to gravitational settling and polar subsidence. Inverted temperatures based on radiance data under such circumstances should be viewed with a highly critical eye. Our model output indicates that even moderate dust loads may greatly distort the nominal flux fields one would expect to observe.

Research utilizing satellite radiometer data should therefore be discharged with great care, since the evidence suggests that many of the bias

body assumptions made during the inverting of radiance data can be invalidated by the presence of particulates, especially at the higher altitudes, where dust-gas temperature disparities are at their extreme. The black body radiation laws are the cornerstones of radiative transfer theory, and care must be taken that the underlying assumptions of the theory are not violated in the haste to arrive at dramatic conclusions.

A fully time-dependent planetary radiative-convective heat transfer model is beyond present capabilities because the complexities of orbital variations and intrinsic planetary structural changes have not been understood or described for the necessary time scales (100 000 to 1 000 000 years). The most technically advanced models available, such as the Community Climate Models of the National Center for Atmospheric Research (NCAR), attempt to address these issues for the terrestrial case. However, restricting model output for Mars to more modest human time scales makes the problem more tractable, and does not unduly limit our understanding.

As in all studies, accurate data is a critical concern. The phenomenological setting for Mars extends us to the limits of our technology with respect to data acquisition at great distances.

This significant constraint should be borne in mind when considering experimental procedures and techniques in planetary studies. Much desirable information will remain unobtainable for a long time to come. Without actual dust, soil, or rock samples in hand, it will be difficult to improve our quantitative understanding of the spectroscopic properties of Martian dust, for example. The insufficiency of the observation network on Earth is still hotly debated; it is not hard to imagine how our understanding of any other planetary atmosphere is crippled by not having even a meager on-site observation capability there.

Despite the fact that disparate planetary atmospheres may experience similar radiative effects due to the presence of particulates, differences also abound; in the Martian midlatitude atmosphere, where phase changes and latent heating are negligible, atmospheric warming by dust particles can act to replace or emulate these processes. Meridional heat transport, storm genesis, and so on, do not seem to require the existence of volatile components within the Martian atmosphere, unlike the terrestrial case.

Yet the extrapolation of terrestrial-based theory to other planets will have to suffice for the immediate future; this approach can provide an

adequate foundation for further research, as long as the dissimilarities between differing atmospheres are kept in mind. Extensive modeling efforts, such as MARSTEMP (Pallmann et al.) and LOWTRAN/FASCODE (AFGL), have given us valuable insight into planetary radiative transfer. The McClatchey et al. and Rothman et al. compilations of carbon dioxide spectroscopic parameters are evidence of what Earth-bound research can provide to planetary studies, and it is a strong step in the right direction for Mars, in particular.

But for the Earth itself, we lack data on basic radiative transfer processes. For example, global circulation patterns, cloud effects, aerosol loadings, albedo variations (especially for ice), and the effects of radiatively active trace gases are all imperfectly understood even for our own planet--what can we hope to say about these processes on stranger, less familiar, and far more distant worlds?

APPENDIX

VERTICAL PROFILES OF ATMOSPHERIC TEMPERATURE, DUST AMPLITUDE, DUST TEMPERATURE, AND DUST TEMPERATURE MINUS ATMOSPHERIC TEMPERATURE

PLOTTED FROM SIMULATION OUTPUT

COMPUTED FOR VARIOUS DUST LOADINGS

BY THE MARSDUST PROGRAM

TABLE 1. PROGRAM PARAMETERS;

NO DUST LOAD

Initial Time: 16.000 LMST; Local Martian Solar Time

Number of Timesteps: 1710

Timestep Interval: 10 minutes (Martian)

[4 minutes (Martian) from LMST 13.500 to 16.500]

Surface Albedo: 0.284

Surface Emissivity: 0.900

Soil Density: 1.500 g/cm^3

Soil Heat Capacity: 1.01×10^6 $J/(m^3 K)$

Soil Conductivity: 0.230 J/(s m K)

CO2 Conductivity: 0.0133 J/(s m K)

Latitude: 22.50° N

Solar Declination: 24.60°

Ratio of Mean to Actual Solar Distance: 0.9222

(This data for Viking 1 Lander; 20 Jul 1976)

Surface Pressure: 7.6 hPa (mb)

Dust Extinction Coefficient: 0.0

One Martian Solar Day = 24 Martian Hours = 1440

Martian Minutes; One Martian Minute = 61.6625 s

MARTIAN DUSTY ATMOSPHERE RAD-COND-CONV HEAT

TRANSFER SIMULATION: MARSDUST

Figures A.1 - A.7

Vertical Profiles of

Atmospheric Temperature

With No Dust Loading

DUSTAMP = 0.0

Four hour intervals from LMST 0.000 to LMST 24.000.

Horizontal axis temperature range: 160 K to 260 K;

Vertical axis altitude range: 0 m to 50 000 m.

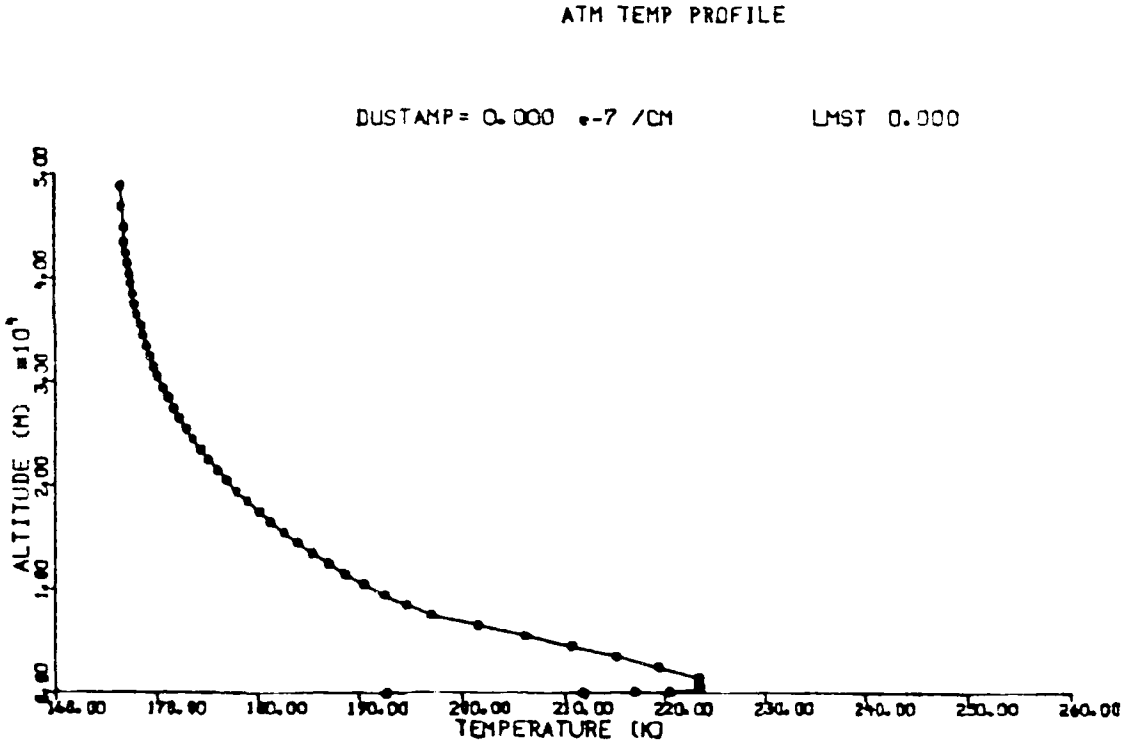

Fig. A.1 Atmospheric Temperature Profile: No Dust Load, LMST 00.00

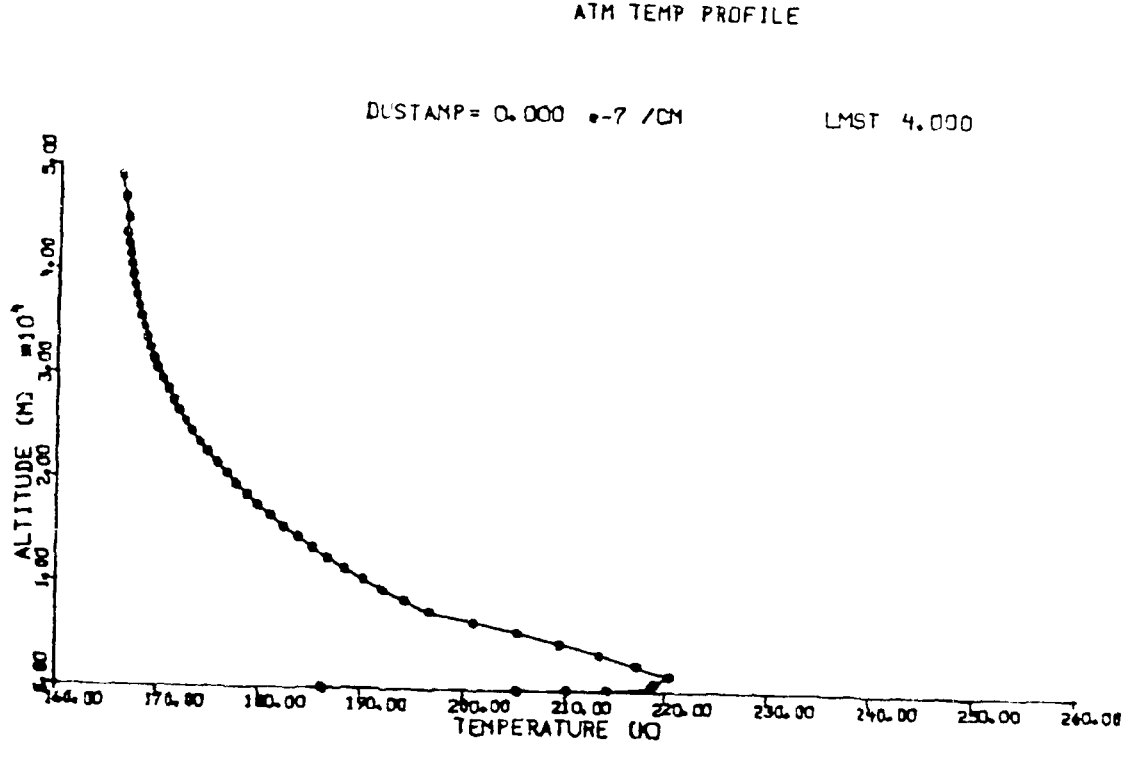

Fig. A.2 Atmospheric Temperature Profile: No Dust Load, LMST 04.00

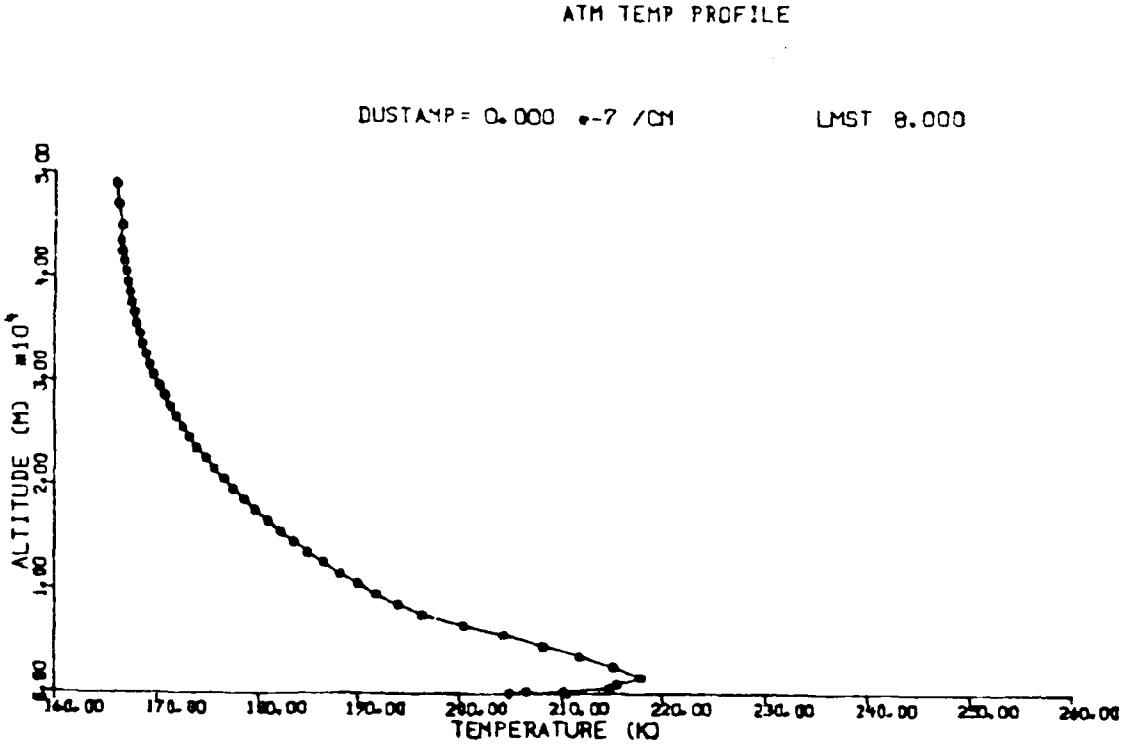

Fig. A.3 Atmospheric Temperature Profile: No Dust Load, LMST 08.00

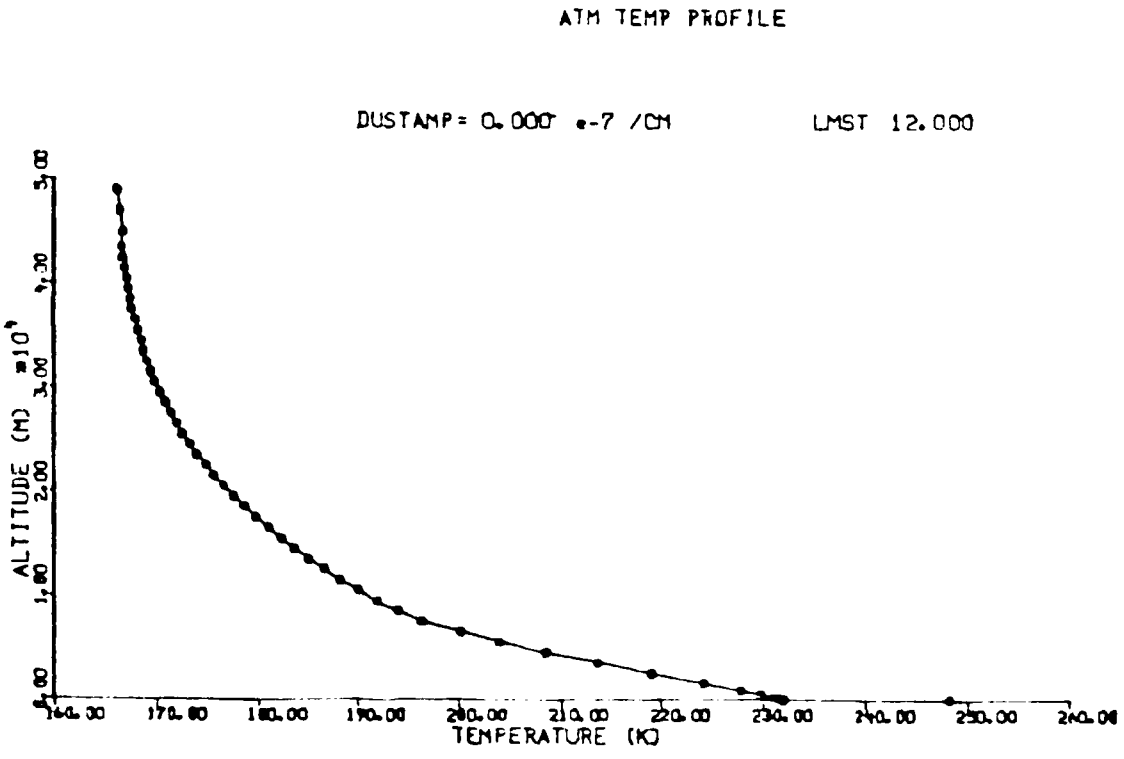

Fig. A.4 Atmospheric Temperature Profile; No Dust Load, LMST 12.00

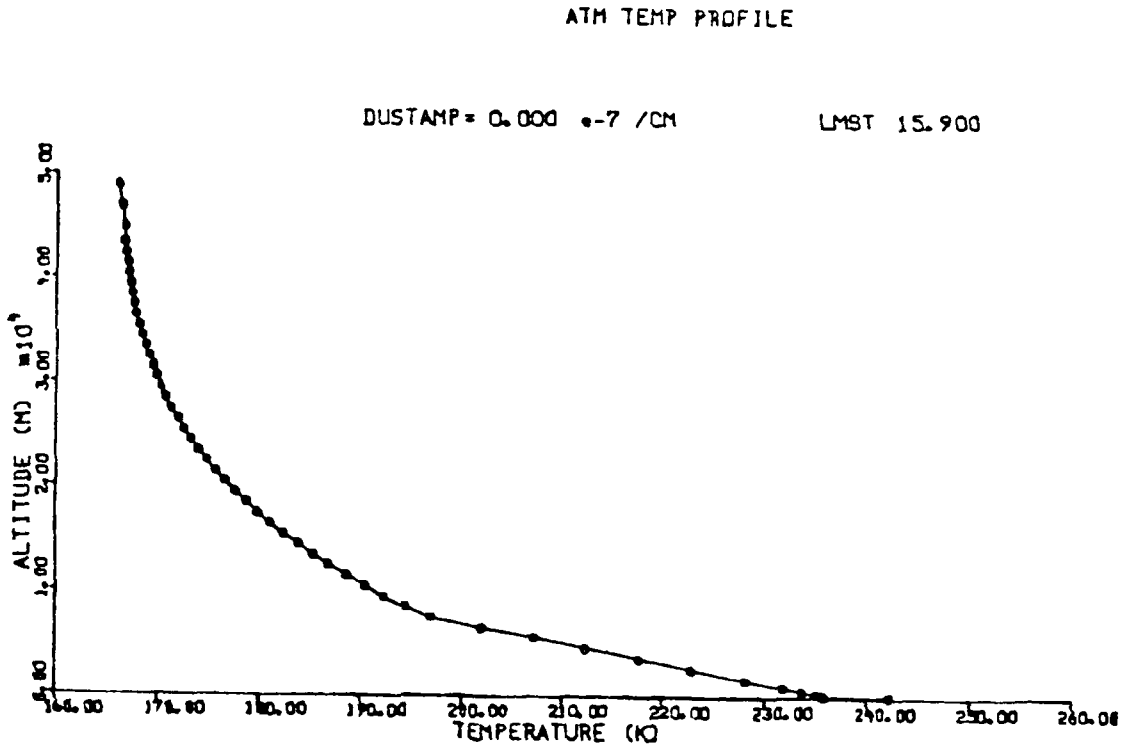

Fig. A.5 Atmospheric Temperature Profile; No Dust Load, LMST 15.90

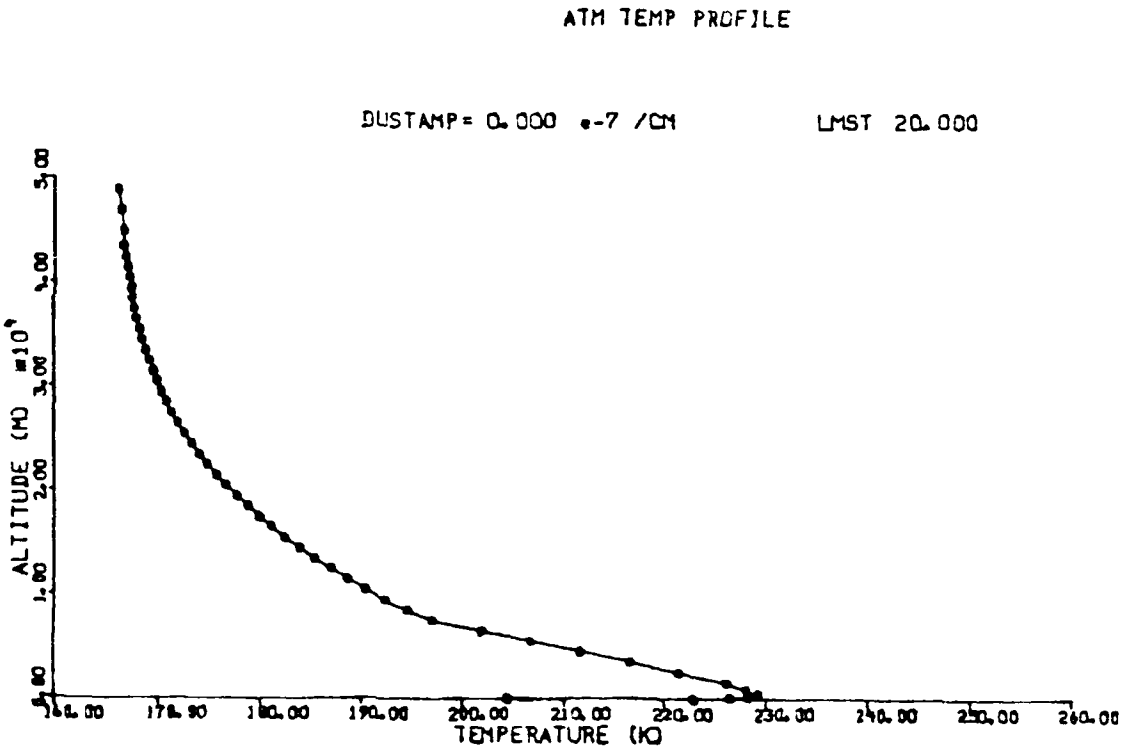

Fig. A.6 Atmospheric Temperature Profile; No Dust Load, LMST 20.00

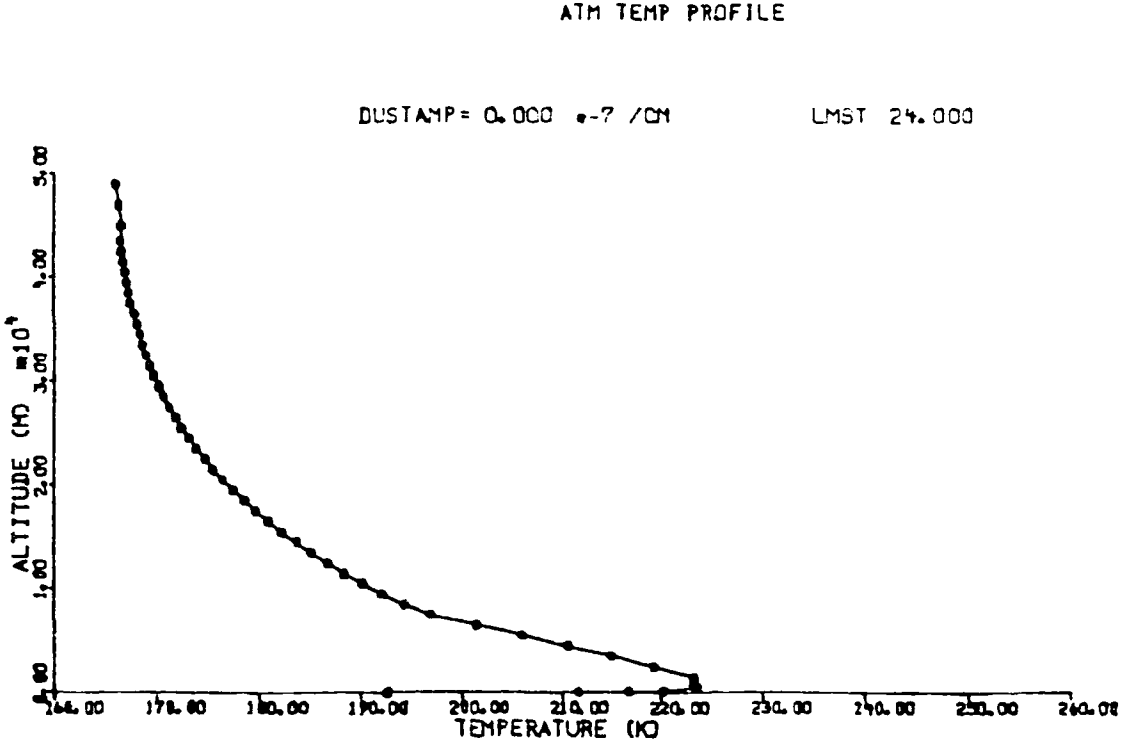

Fig. A.7 Atmospheric Temperature Profile; No Dust Load, LMST 24.00

TABLE 2. PROGRAM PARAMETERS:

DUSTAMP = 1.2×10^{-7} cm^{-1}

Initial Time: 16.000 LMST; Local Martian Solar Time

Number of Timesteps: 576

Timestep Interval: 10 minutes (Martian)

[4 minutes (Martian) from LMST 13.500 to 16.500]

Surface Albedo: 0.284

Surface Emissivity: 0.900

Soil Density: 1.500 g/cm^3

Soil Heat Capacity: 1.01×10^6 $J/(m^3 K)$

Soil Conductivity: 0.250 J/(s m K)

CO2 Conductivity: 0.0133 J/(s m K)

Latitude: 22.50° N

Solar Declination: 24.60°

Ratio of Mean to Actual Solar Distance: 0.9222

(This data for Viking 1 Lander; 20 Jul 1976)

Surface Pressure: 7.6 nPa (mb)

Dust Extinction Coefficient: 1.2×10^{-7} cm^{-1}

One Martian Solar Day = 24 Martian Hours = 1440

Martian Minutes; One Martian Minute = 61.6625 s

MARTIAN DUSTY ATMOSPHERE RAD-COND-CONV HEAT

TRANSFER SIMULATION: MARSDUST

Figures A.8 - A.18

Vertical Profiles of

Atmospheric Temperature

With Light Dust Loading

DUSTAMP = 1.2×10^{-7} cm^{-1}

Four hour intervals from LMST 20.000 to LMST 4.000;

two hour intervals otherwise.

Horizontal axis temperature range: 160 K to 260 K;

Vertical axis altitude range: 0 m to 50 000 m.

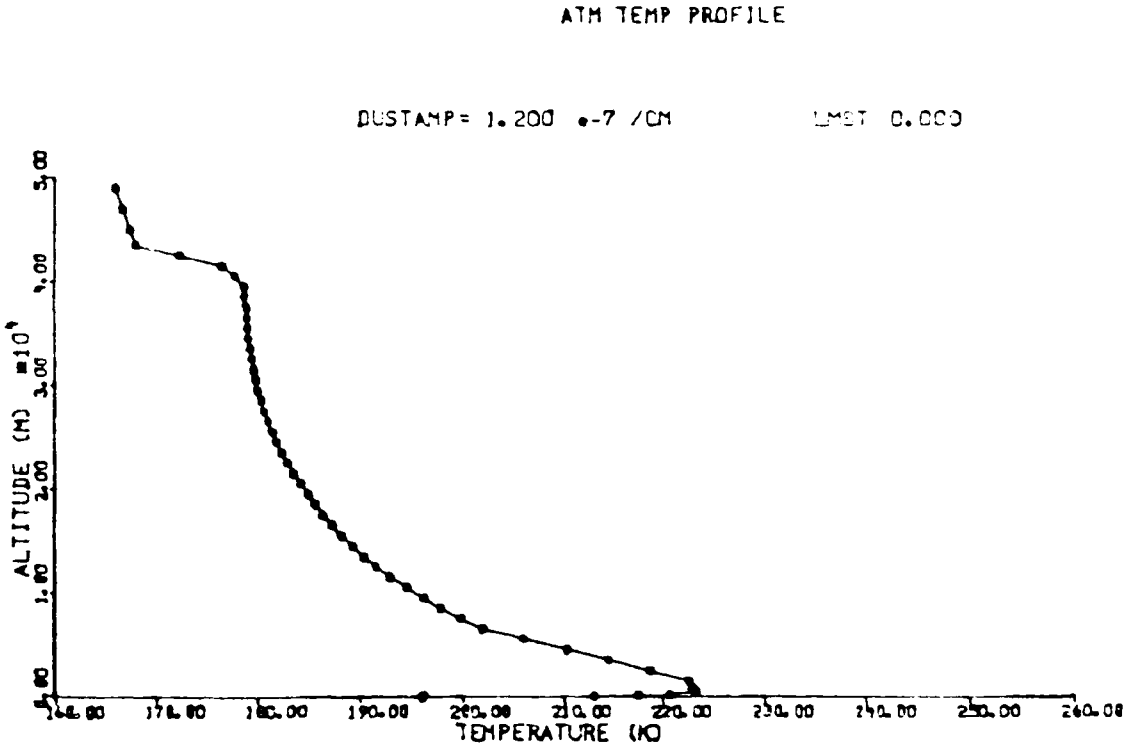

Fig. A.8 Atmospheric Temperature Profile; Light Dust Load, LMST 00.00

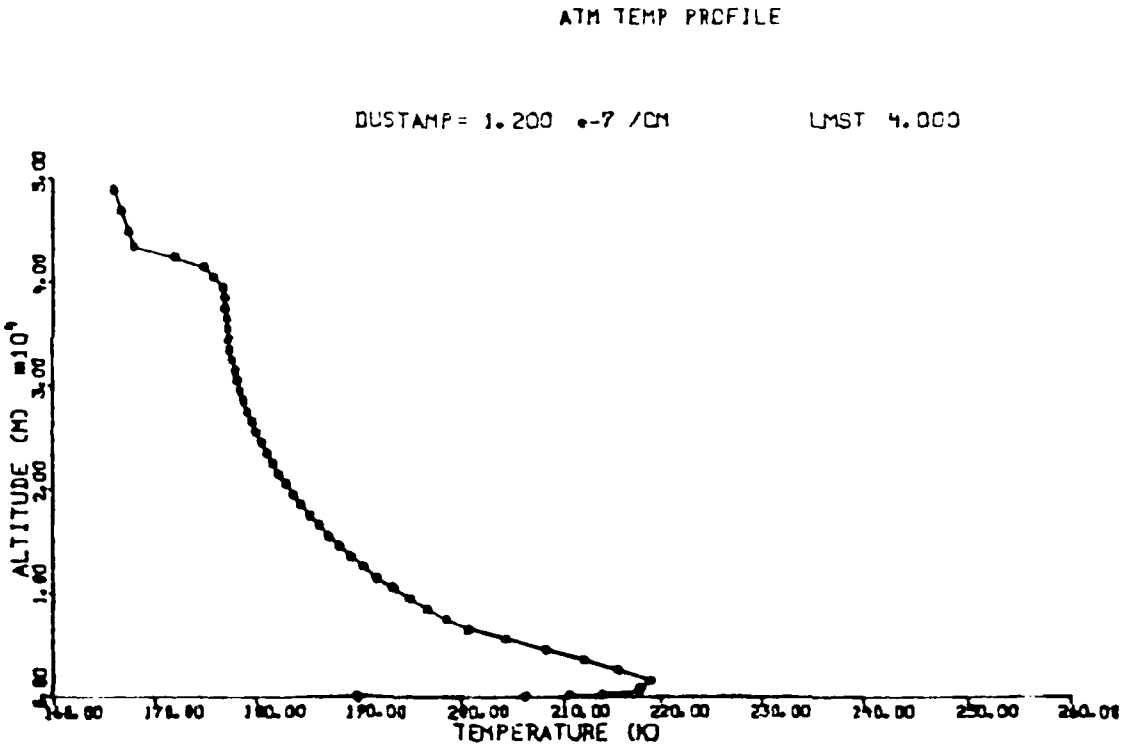

Fig. A.9 Atmospheric Temperature Profile; Light Dust Load, LMST 04.00

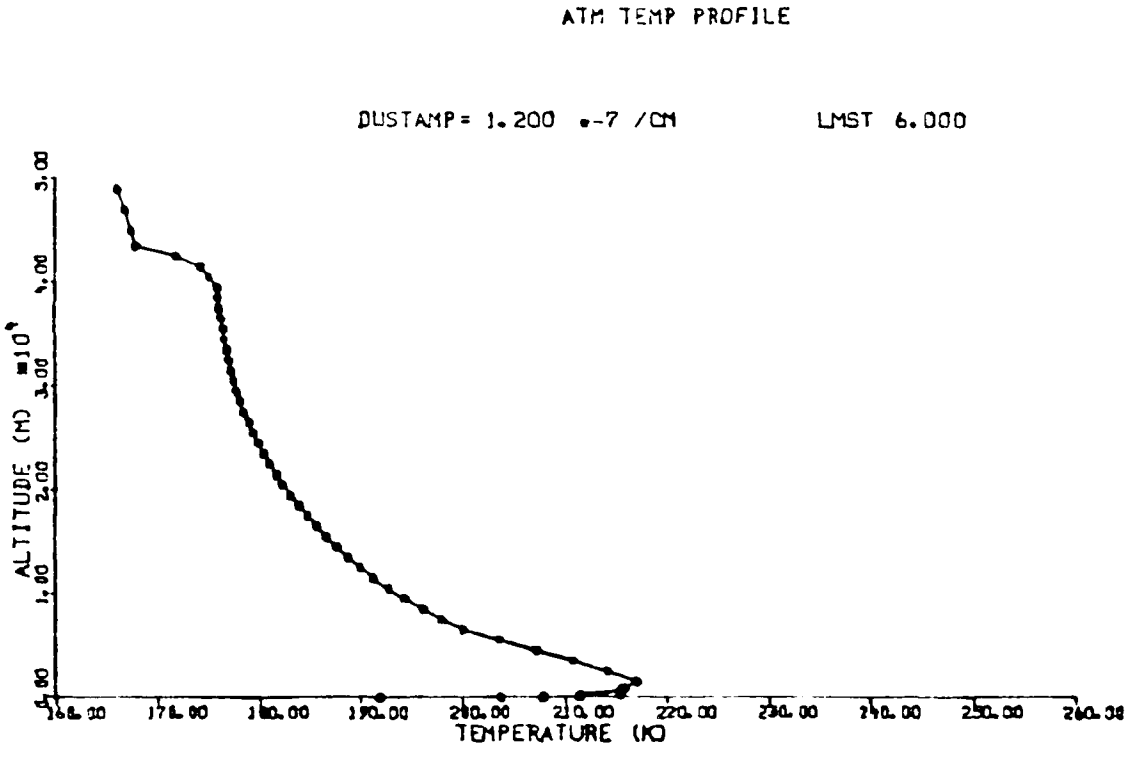

Fig. A.10 Atmospheric Temperature Profile; Light Dust Load, LMST 06.00

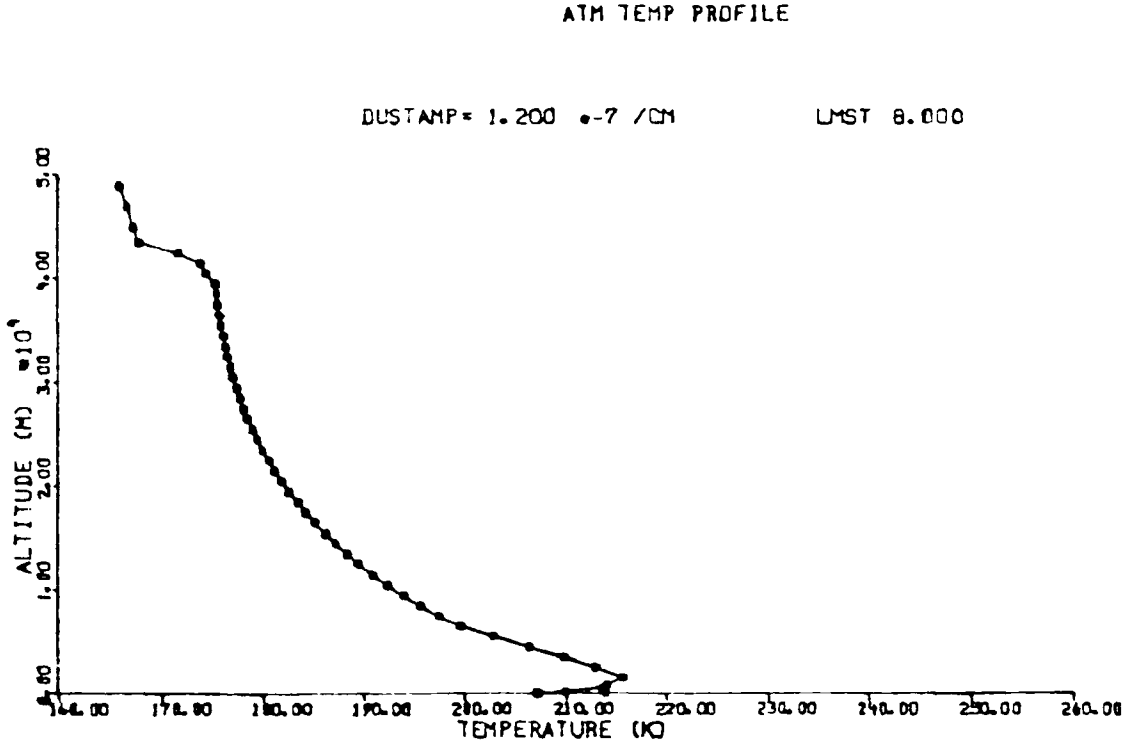

Fig. A.11 Atmospheric Temperature Profile; Light Dust Load, LMST 08.00

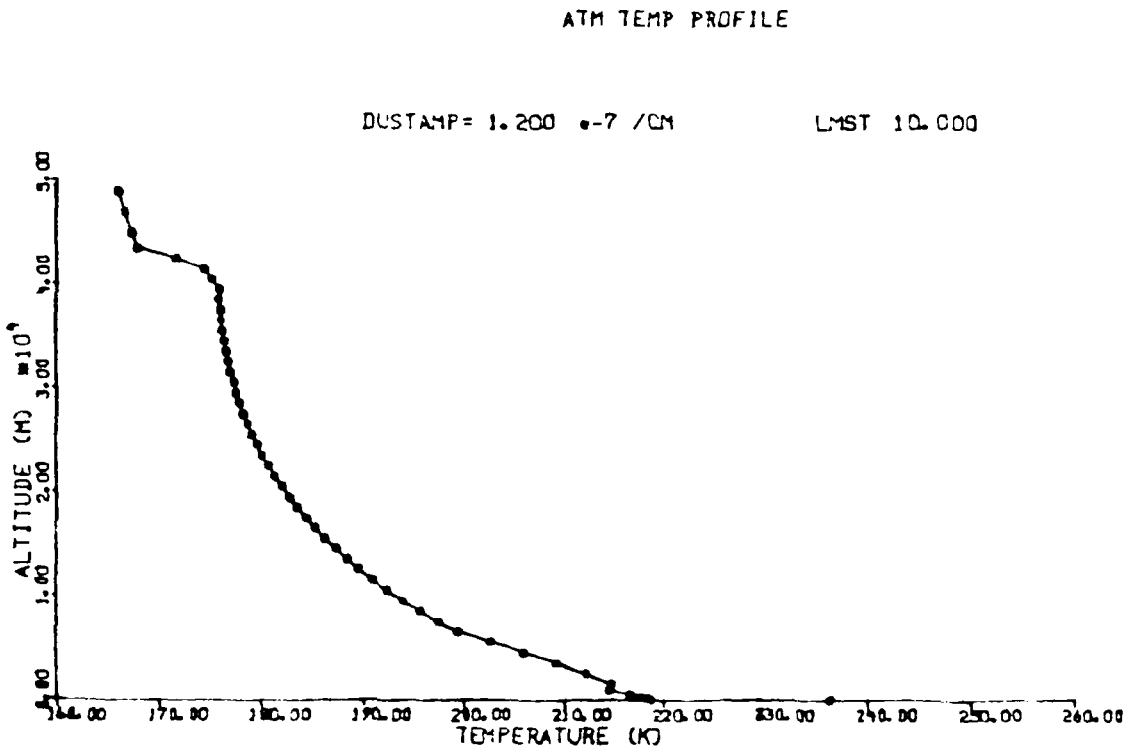

Fig. A.12 Atmospheric Temperature Profile; Light Dust Load, LMST 10.00

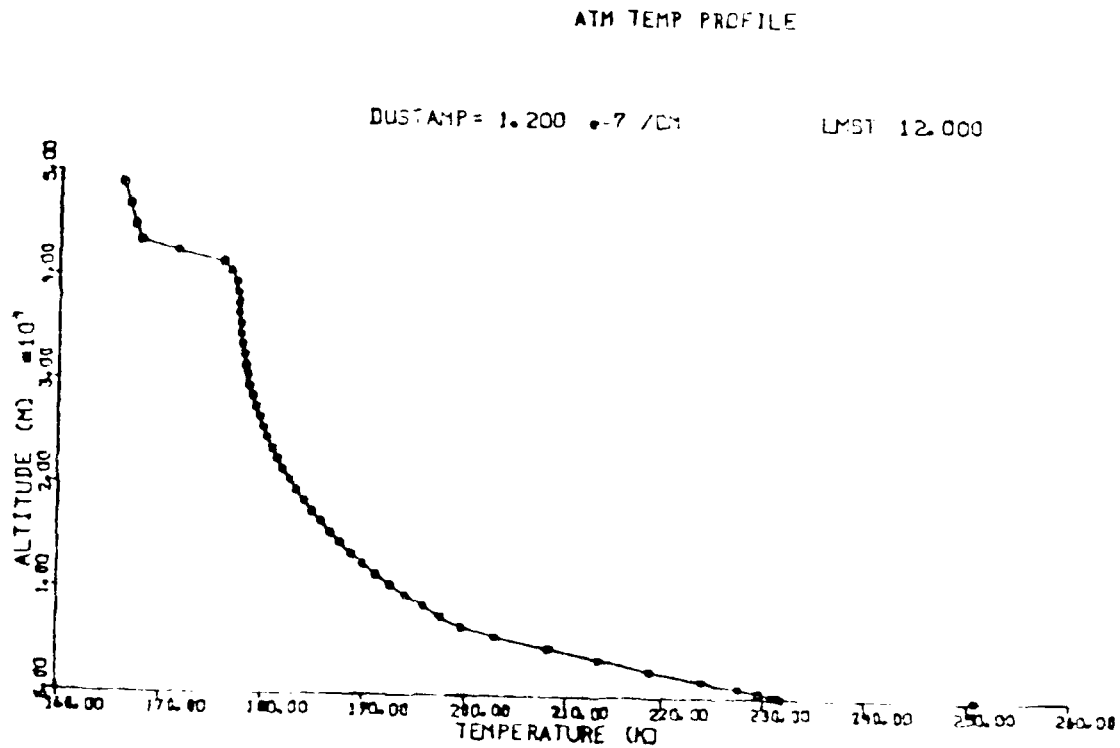

Fig. A.13 Atmospheric Temperature Profile: Light Dust Load, LMST 12.00

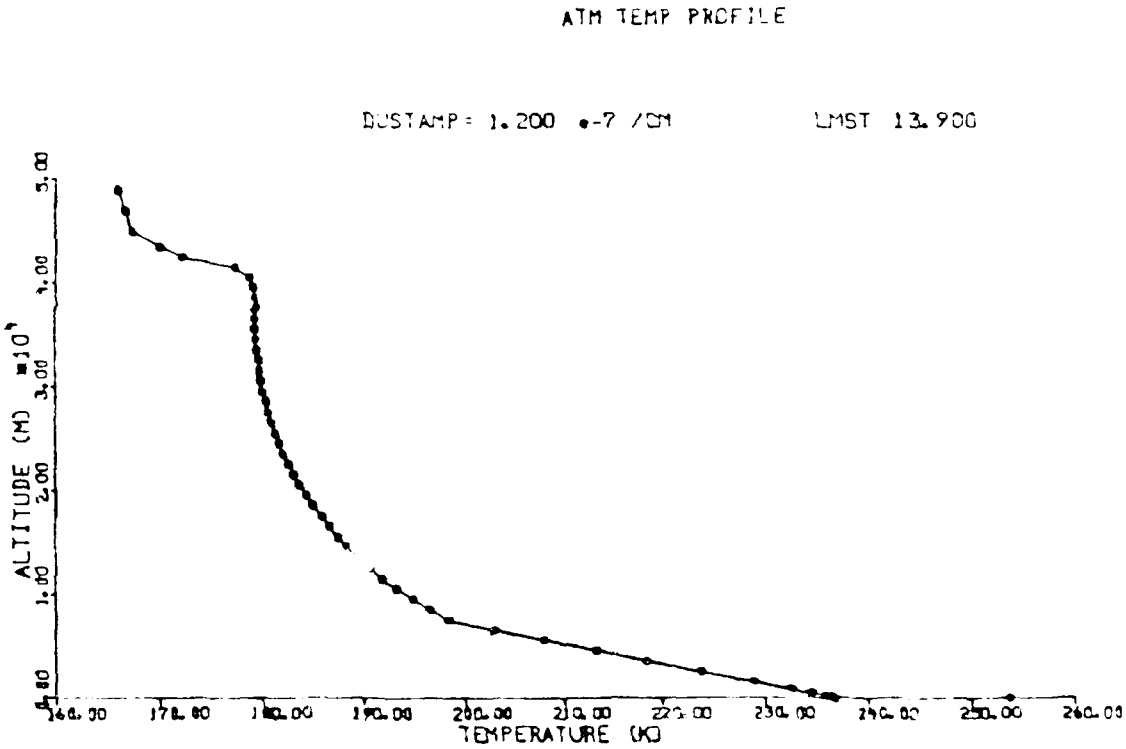

Fig. A.14 Atmospheric Temperature Profile: Light Dust Load, LMST 13.90

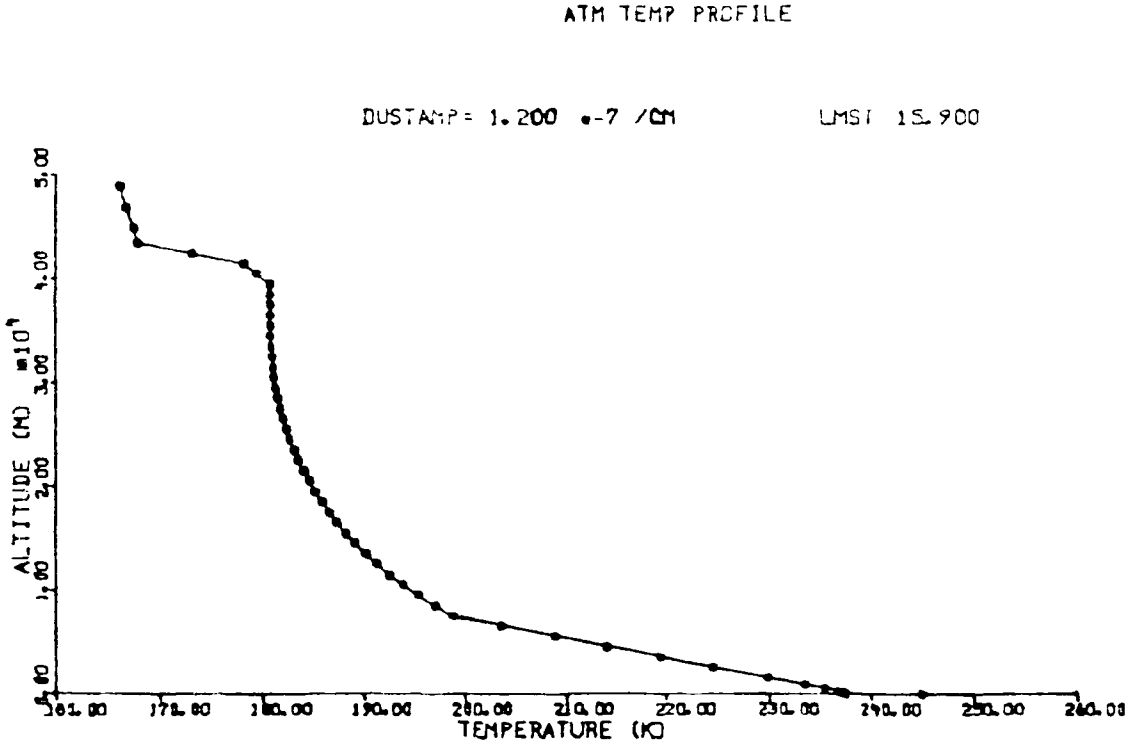

Fig. A.15 Atmospheric Temperature Profile: Light Dust Load, LMST 15.90

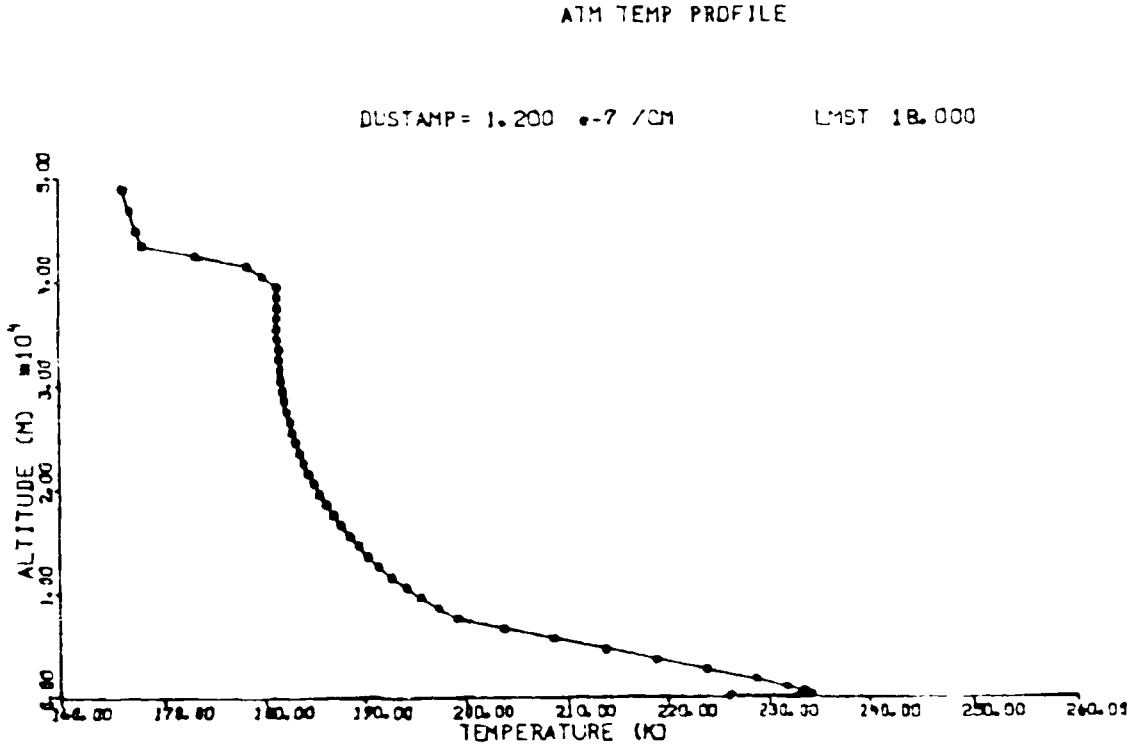

Fig. A.16 Atmospheric Temperature Profile: Light Dust Load, LMST 18.00

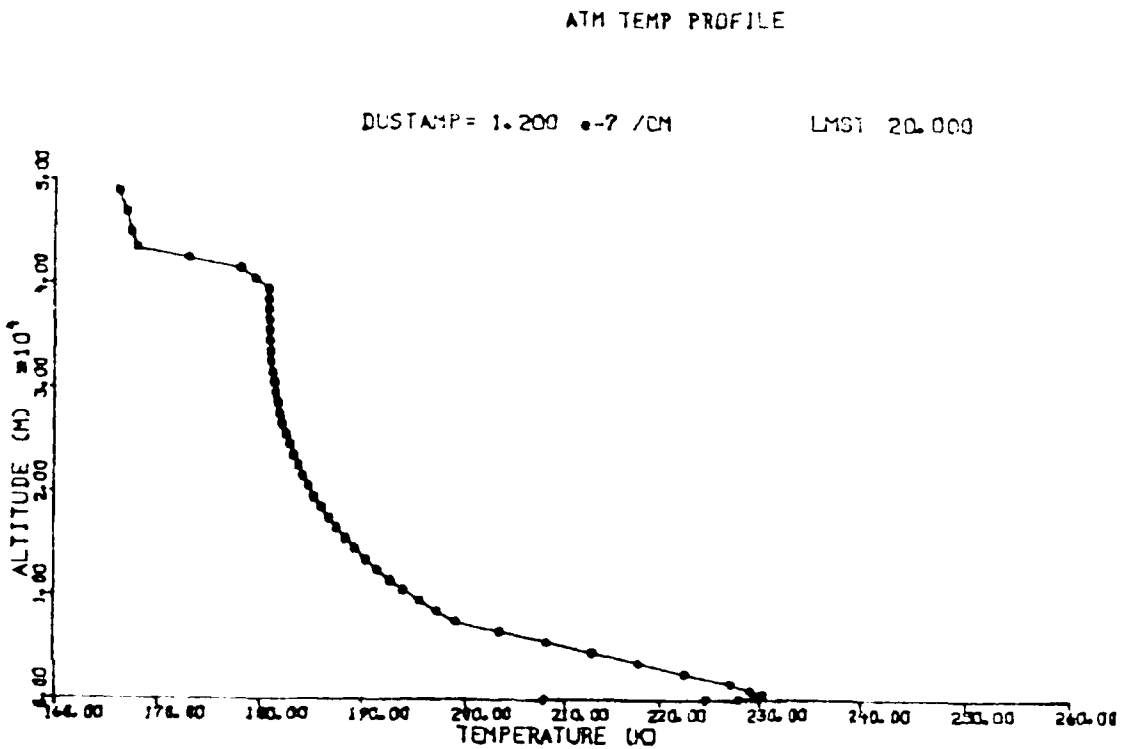

Fig. A.17 Atmospheric Temperature Profile; Light Dust Load, LMST 20.00

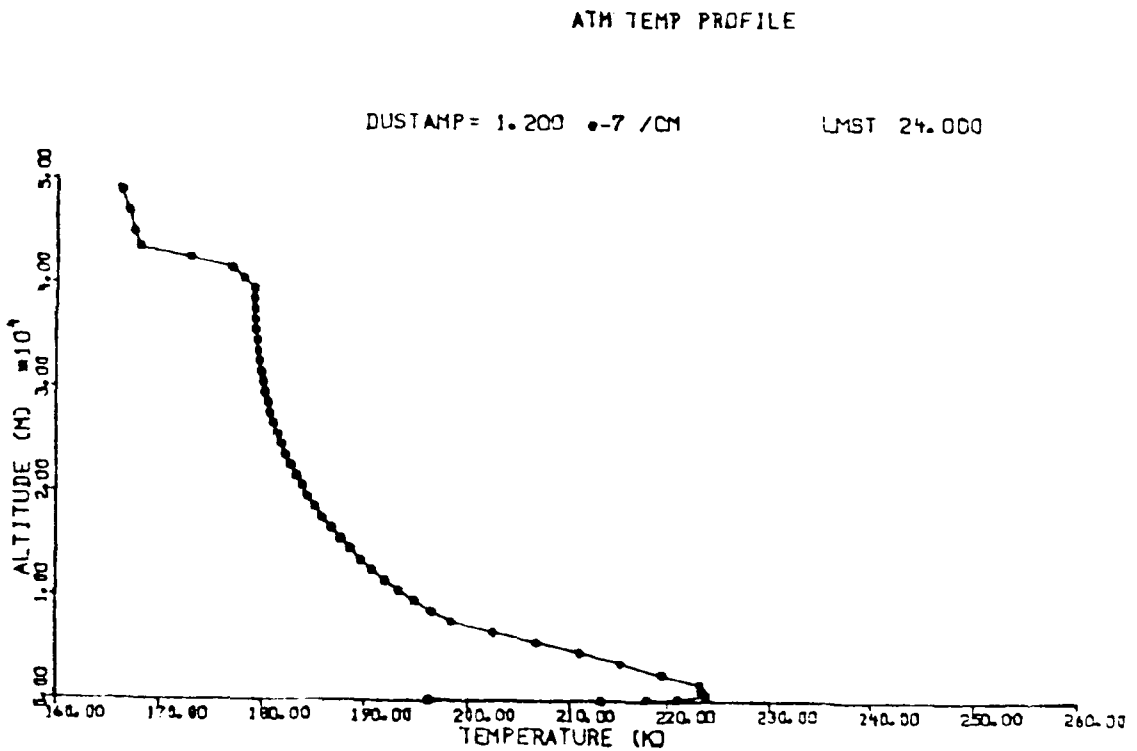

Fig. A.18 Atmospheric Temperature Profile: Light Dust Load, LMST 24.00

MARTIAN DUSTY ATMOSPHERE RAD-COND-CONV HEAT

TRANSFER SIMULATION: MARSDUST

Figures A.19 - A.29

Vertical Profiles of

Dust Temperature

With Light Dust Loading

DUSTAMP = 1.2×10^{-7} cm^{-1}

Four hour intervals from LMST 20.000 to LMST 4.000;

two hour intervals otherwise.

Horizontal axis temperature range: 190 K to 290 K;

Vertical axis altitude range: 0 m to 50 000 m.

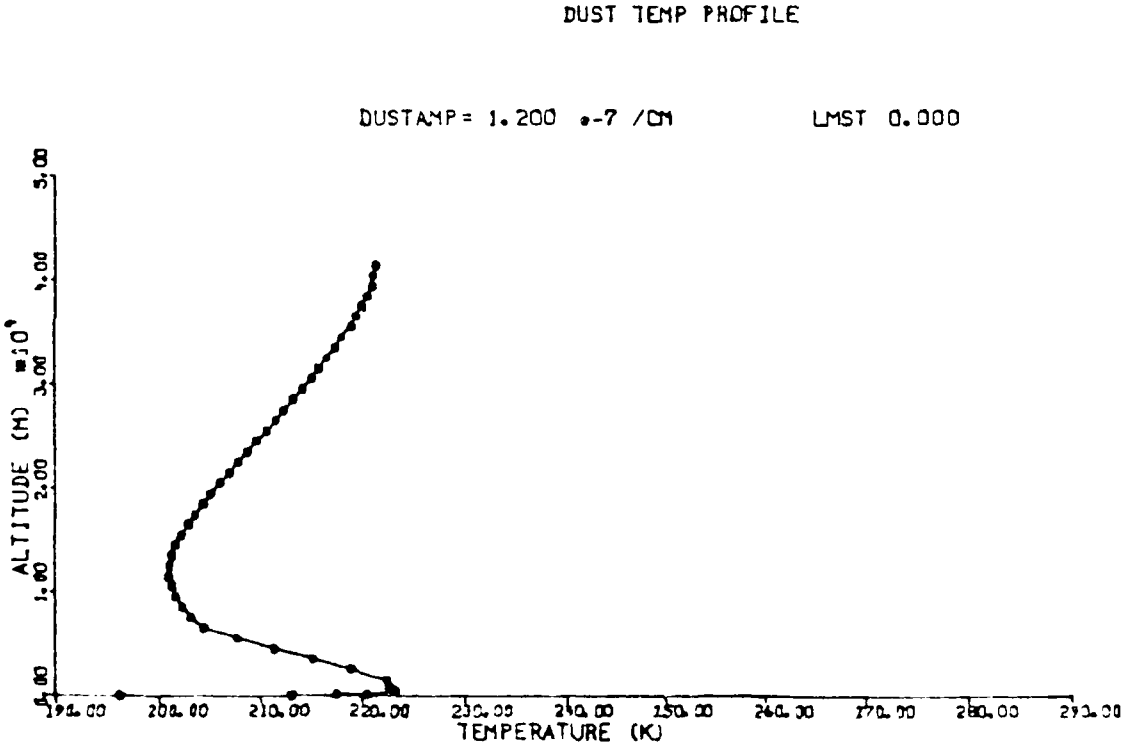

Fig. A.19 Dust Temperature Profile; Light Dust Load, LMST 00.00

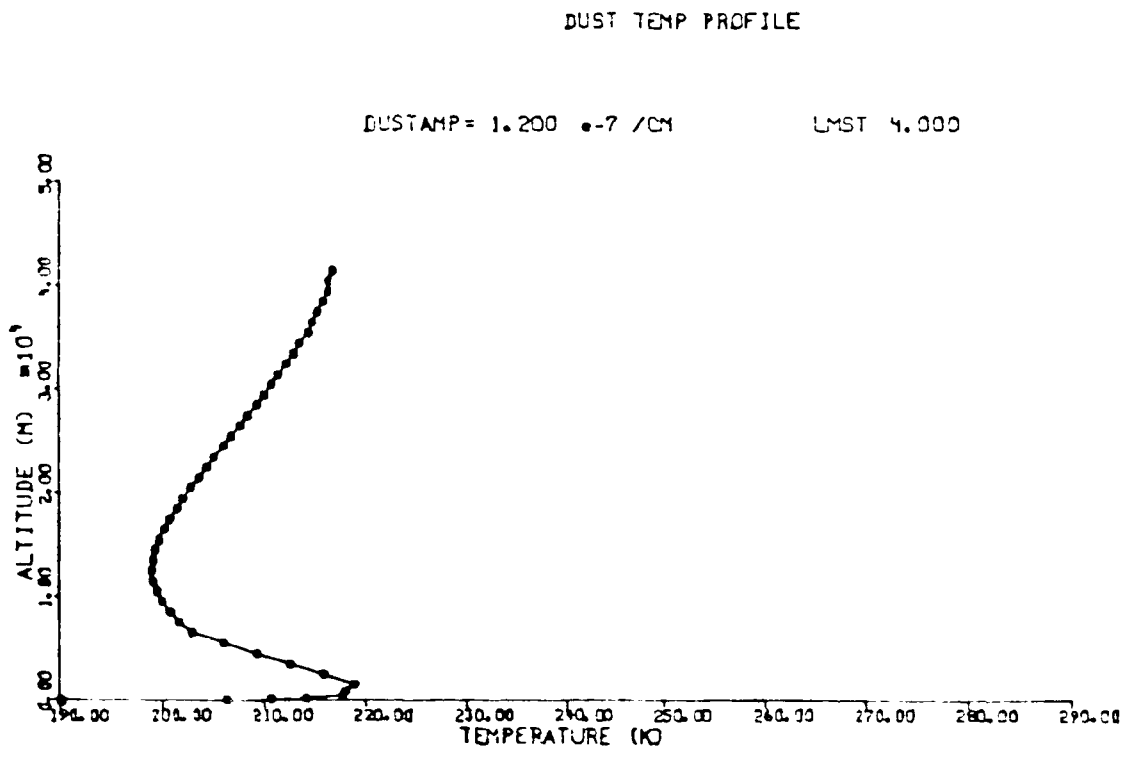

Fig. A.20 Dust Temperature Profile; Light Dust Load, LMST 04.00

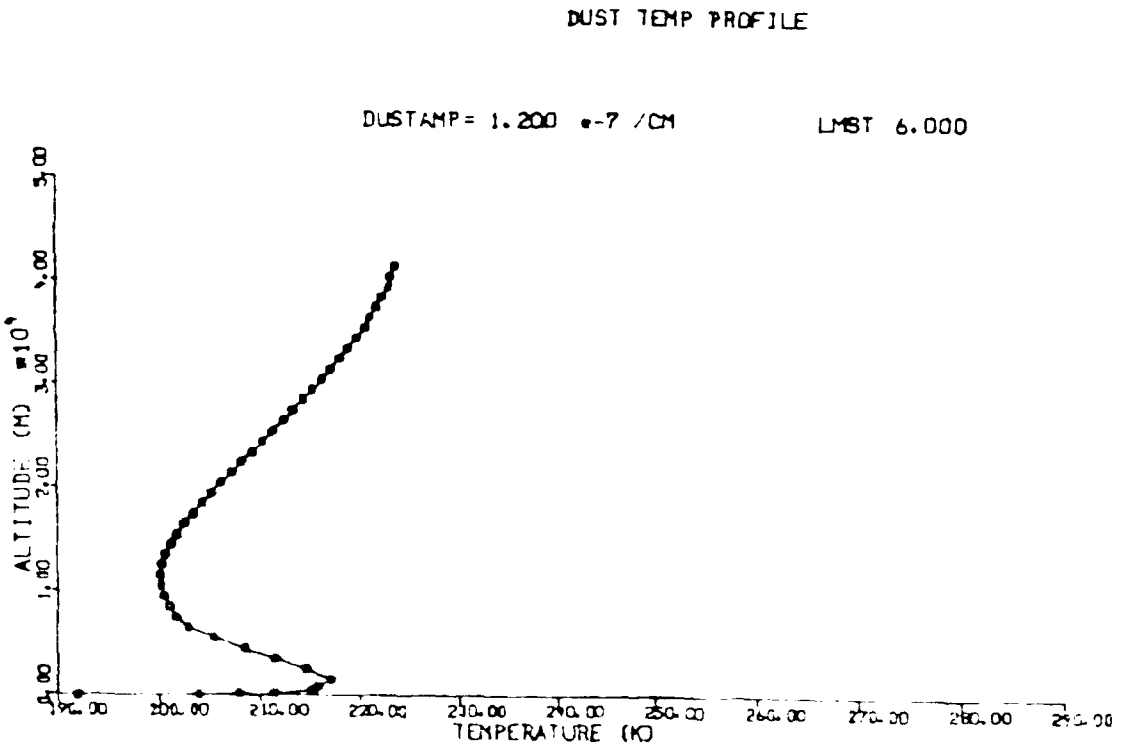

Fig A 21 Dust Temperature Profile: Light Dust Load, LMST 06 00

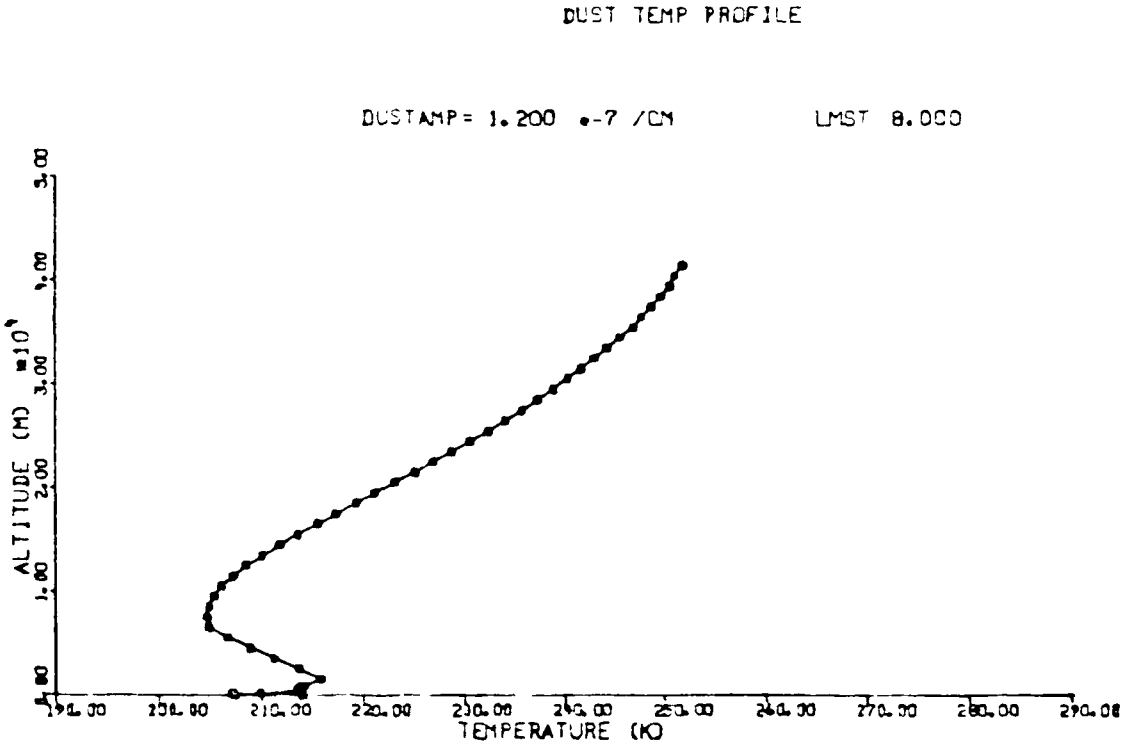

Fig A 22 Dust Temperature Profile; Light Dust Load, LMST 08.00

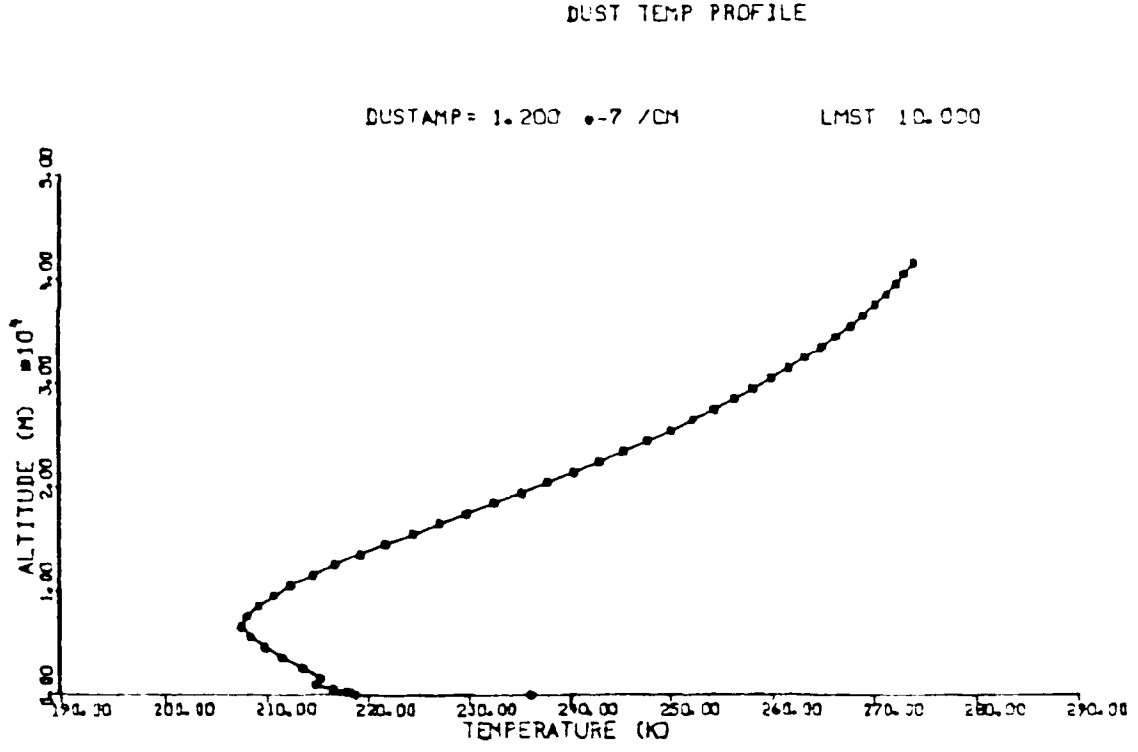

Fig. A.23 Dust Temperature Profile; Light Dust Load, LMST 10.00

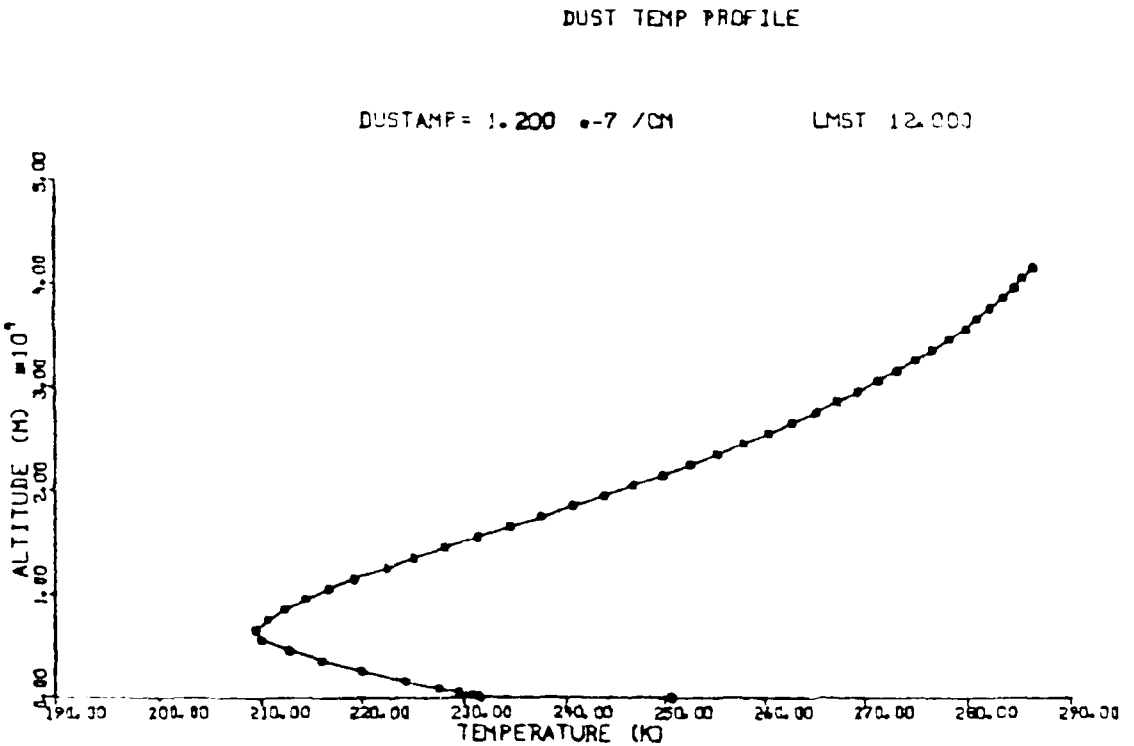

Fig. A.24 Dust Temperature Profile; Light Dust Load, LMST 12.00

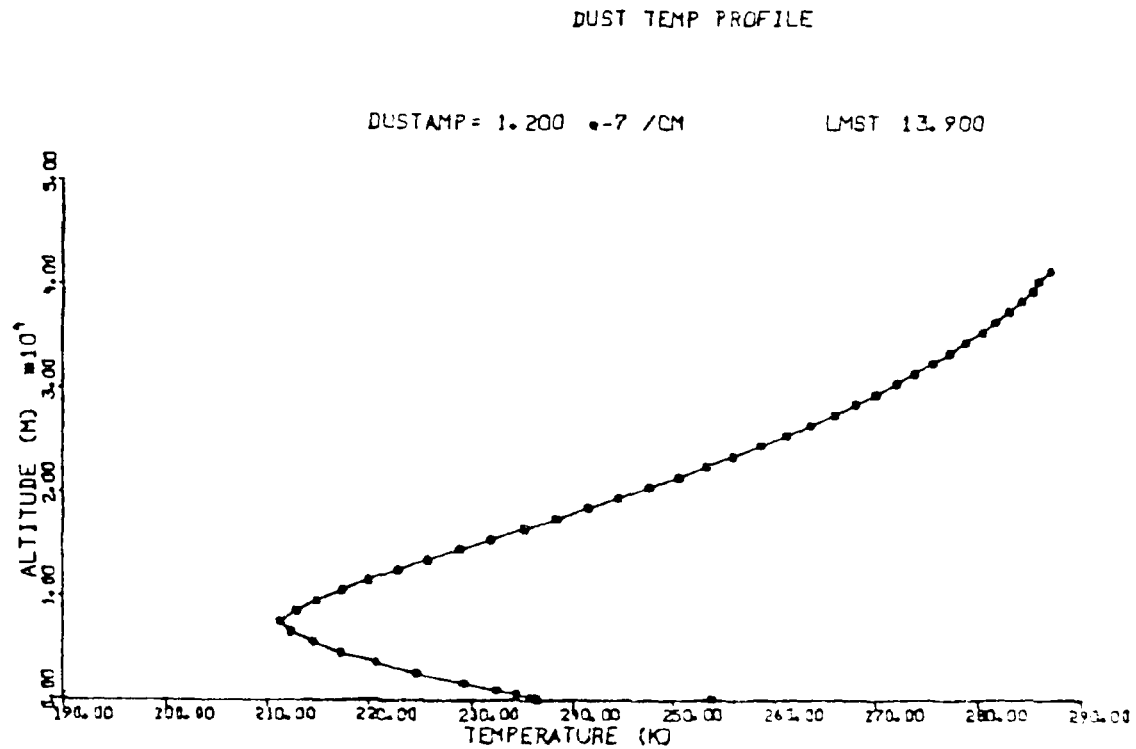

Fig. A.25 Dust Temperature Profile; Light Dust Load, LMST 13.90

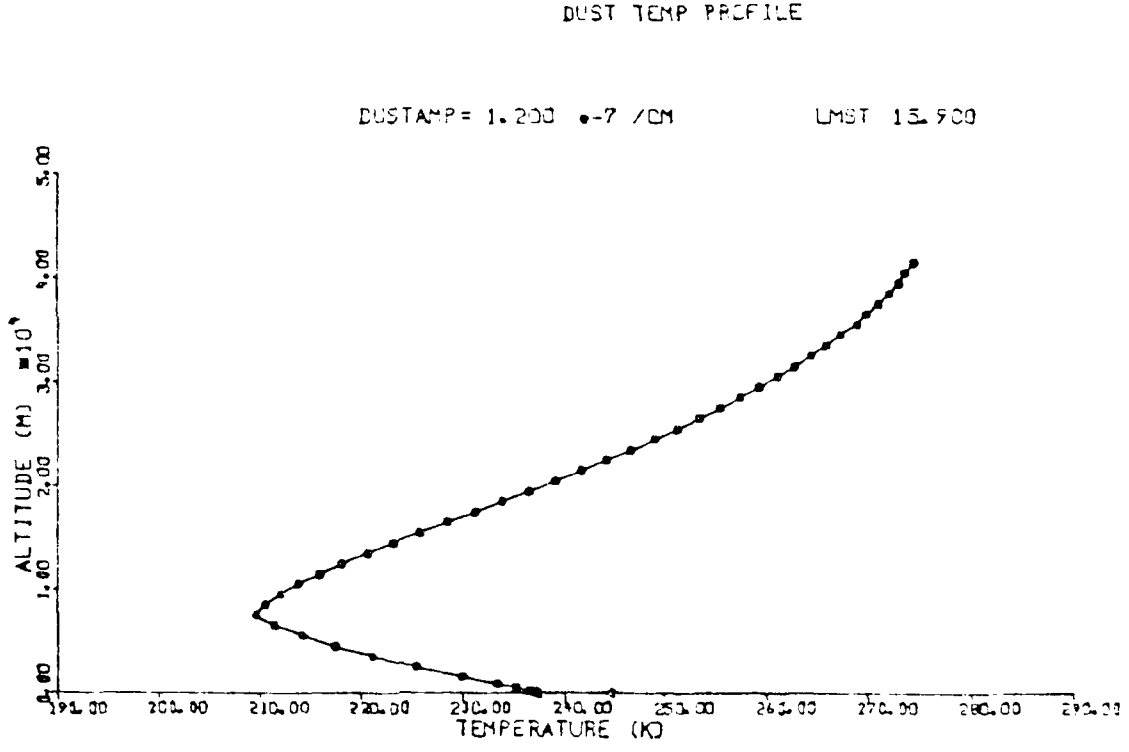

Fig. A.26 Dust Temperature Profile; Light Dust Load, LMST 15.90

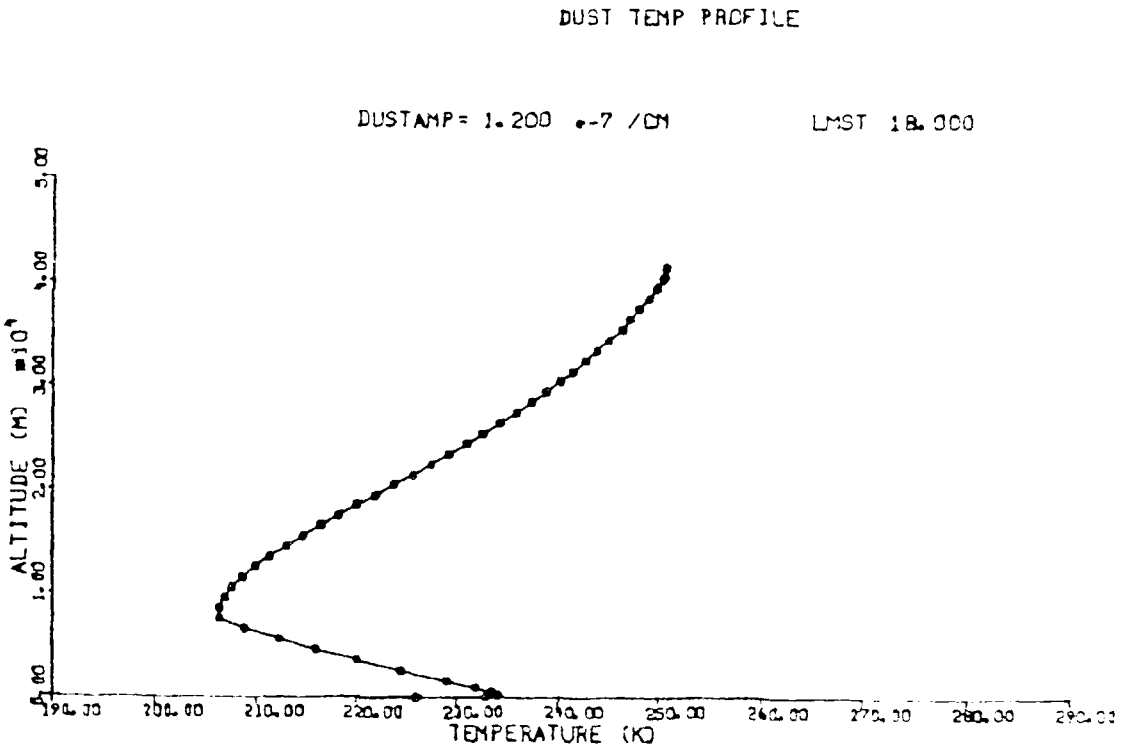

Fig. A.27 Dust Temperature Profile; Light Dust Load, LMST 18.00

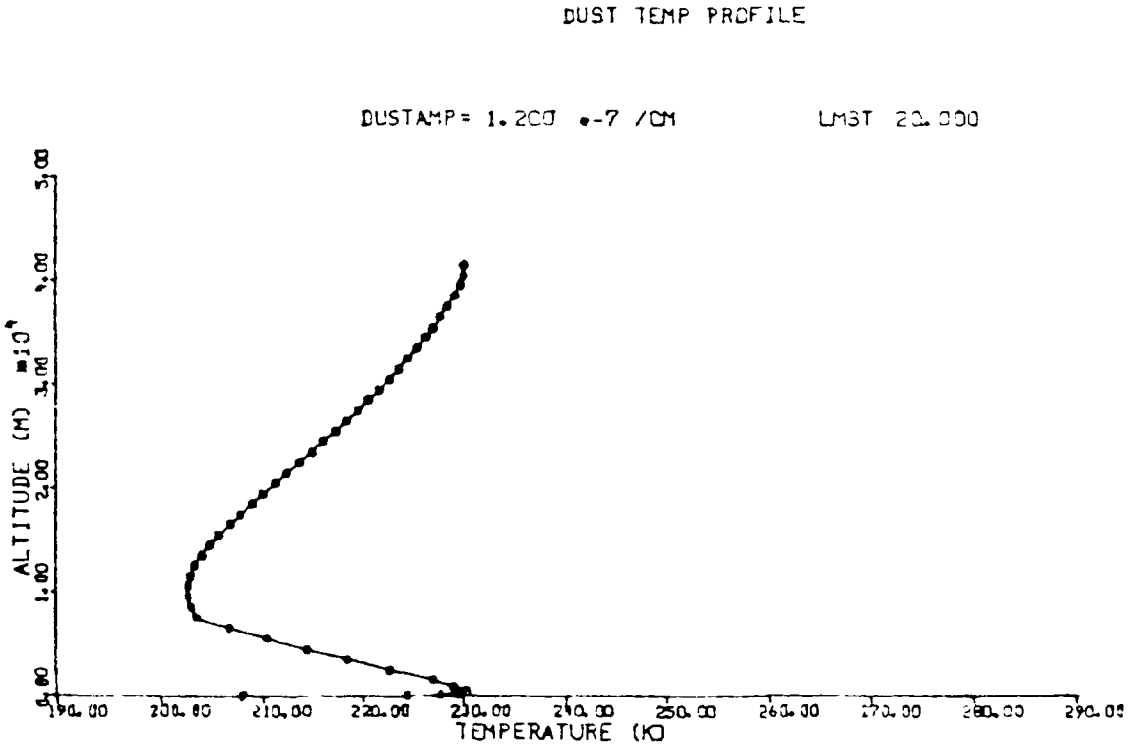

Fig. A.28 Dust Temperature Profile: Light Dust Load, LMST 20 00

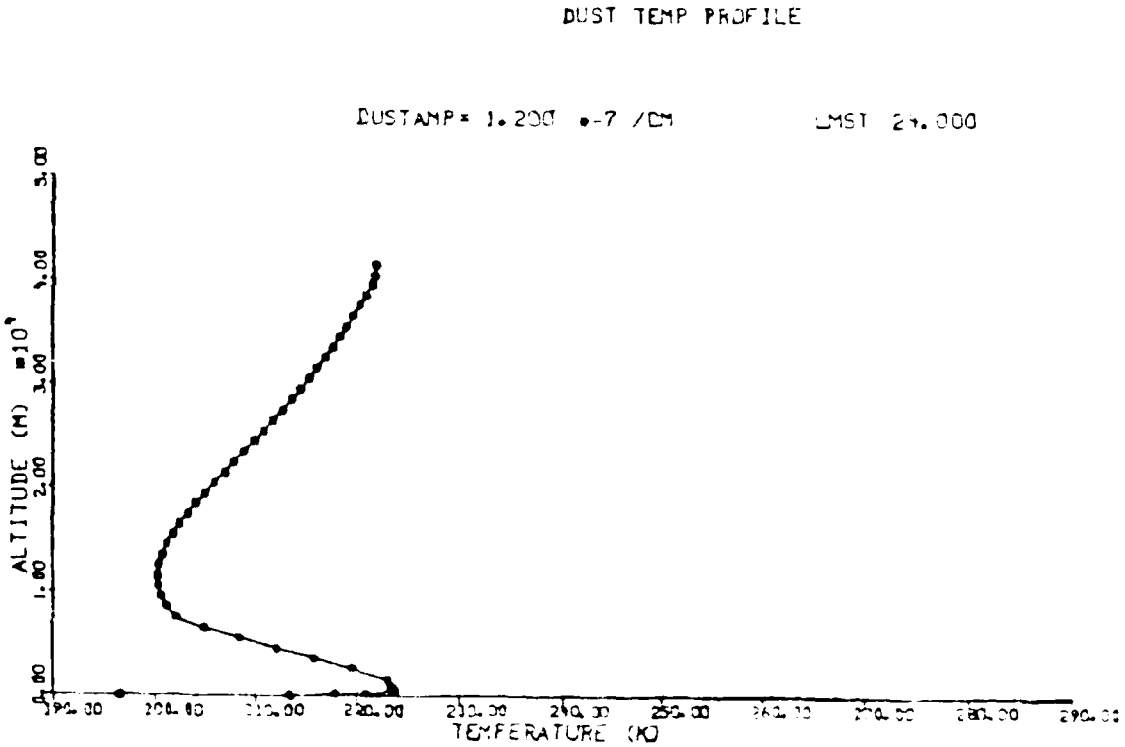

Fig A 29 Dust Temperature Profile: Light Dust Load, GMST 24.00

MARTIAN DUSTY ATMOSPHERE RAD-COND-CONV HEAT

TRANSFER SIMULATION: MARSDUST

Figures A.30 - A.40

Vertical Profiles of

Dust Temperature Minus Atmospheric Temperature

With Light Dust Loading

DUSTAMP = 1.2×10^{-7} cm^{-1}

Four hour intervals from LMST 20.000 to LMST 4.000;

two hour intervals otherwise.

Horizontal axis temperature difference range:

0 K to 150 K;

Vertical axis altitude range: 0 m to 50 000 m.

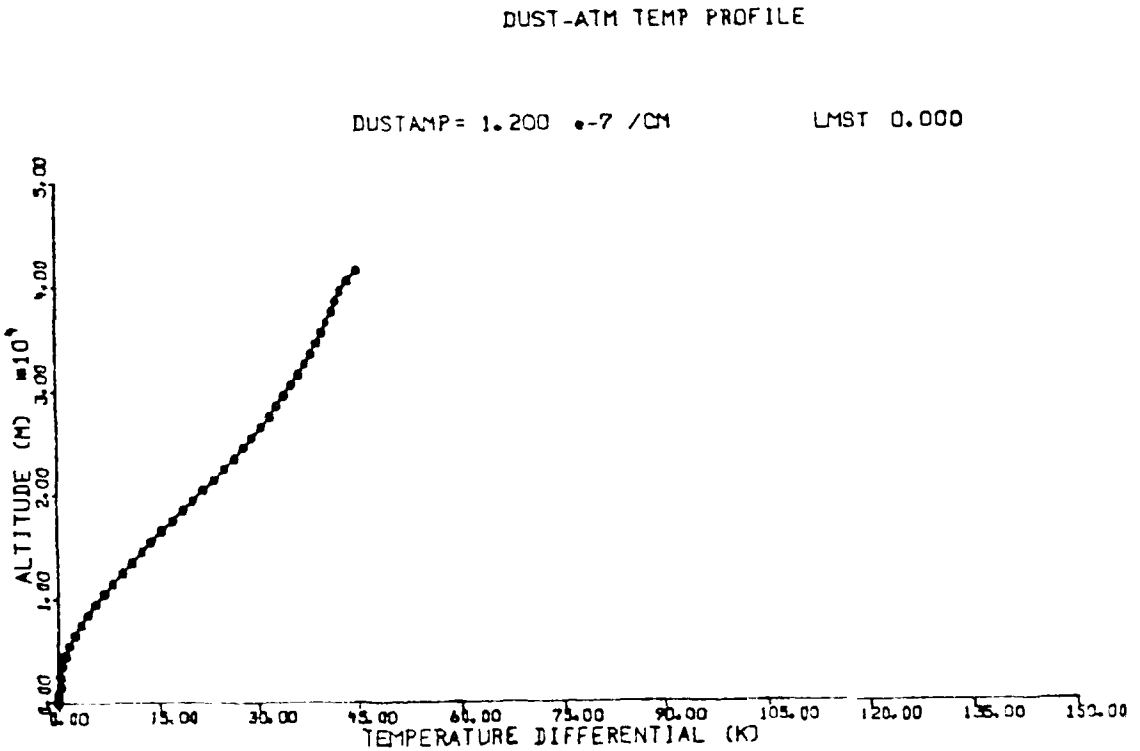

Fig. A.30 Dust-Atm Temperature Profile: Light Dust Load, LMST 00.00

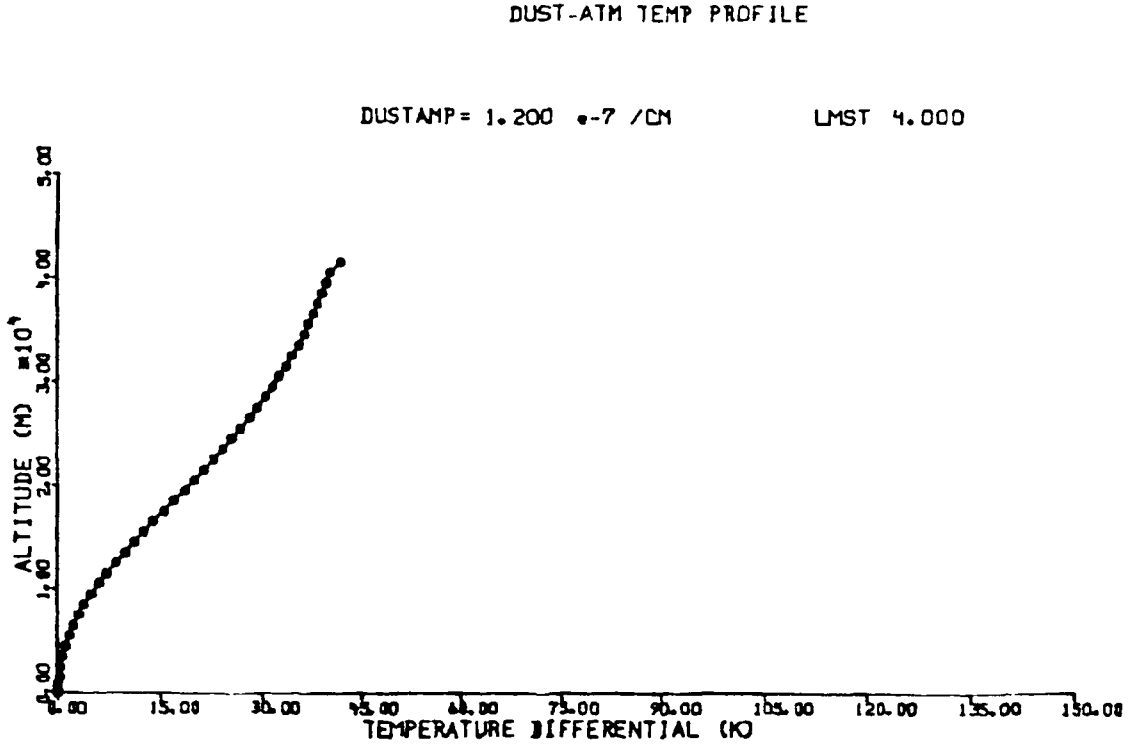

Fig. A.31 Dust-Atm Temperature Profile: Light Dust Load, LMST 04.00

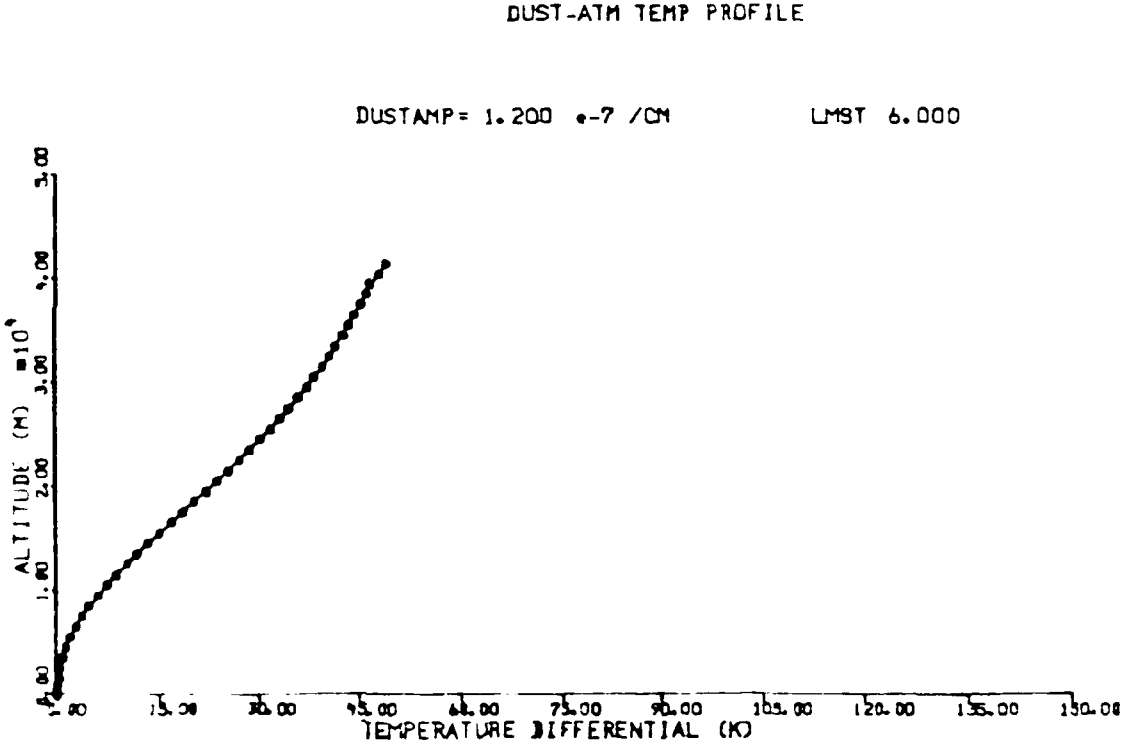

Dust Atm Temperature Profile: Light Dust Load, LMST 06.00

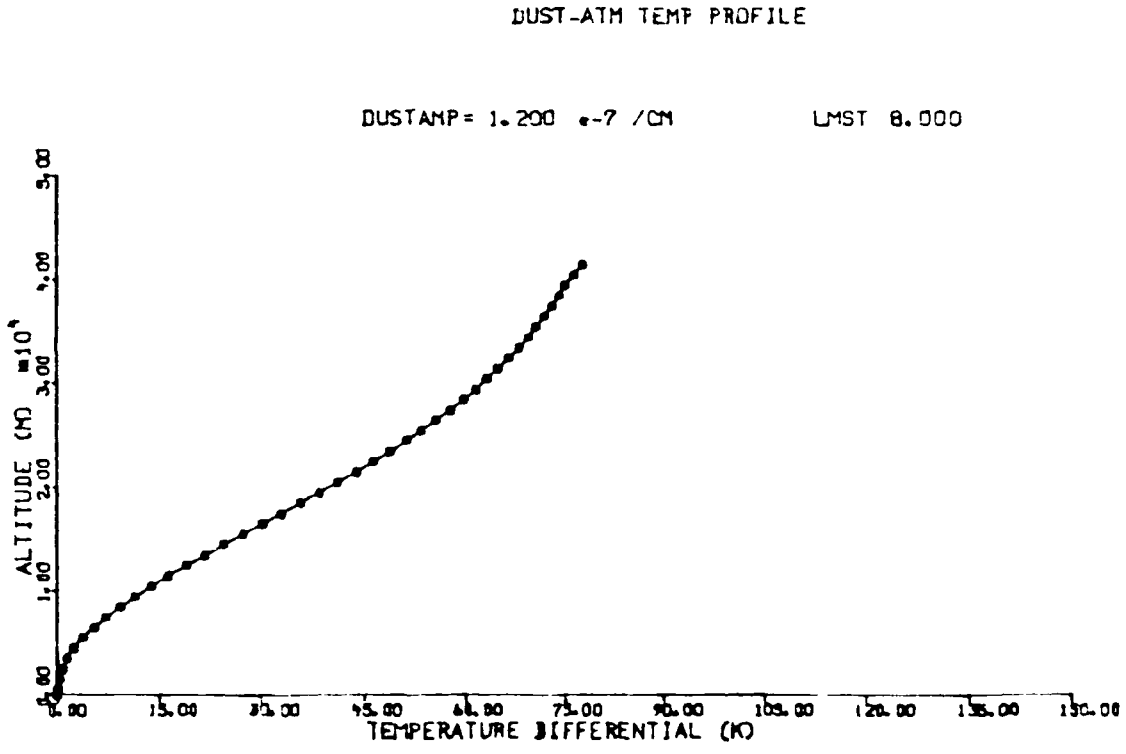

Fig. A.33 Dust-Atm Temperature Profile: Light Dust Load, LMST 08 00

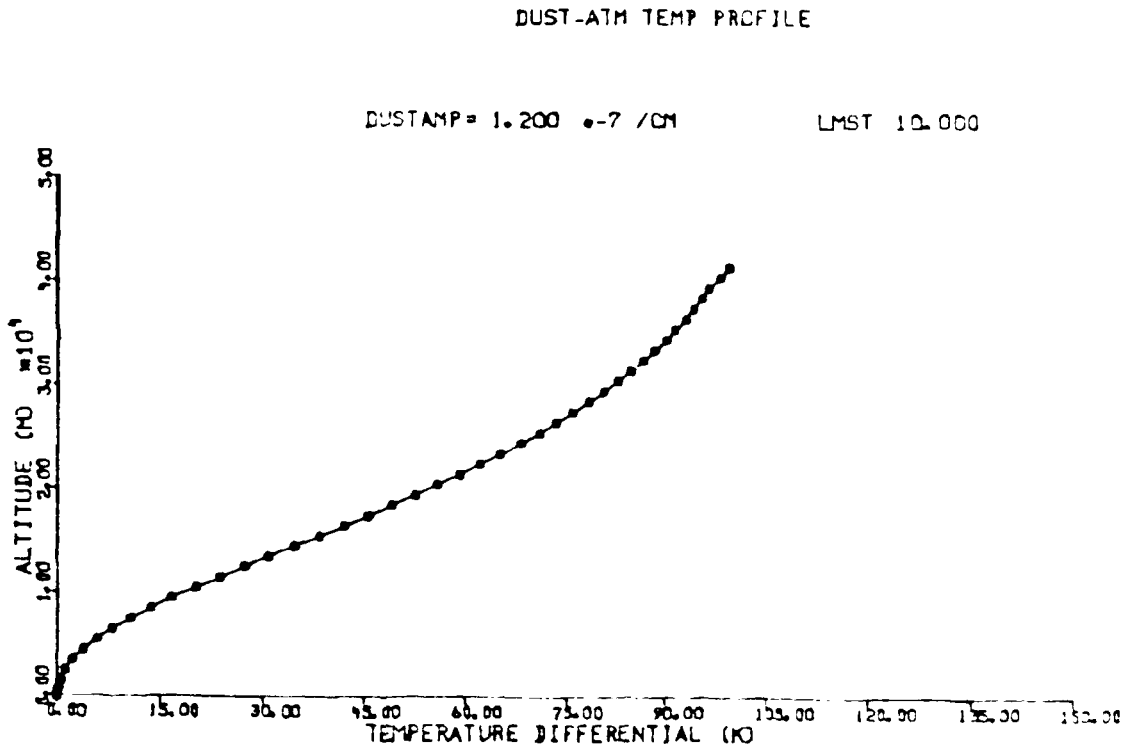

Fig. A.34 Dust-Atm Temperature Profile; Light Dust Load, LMST 10.00

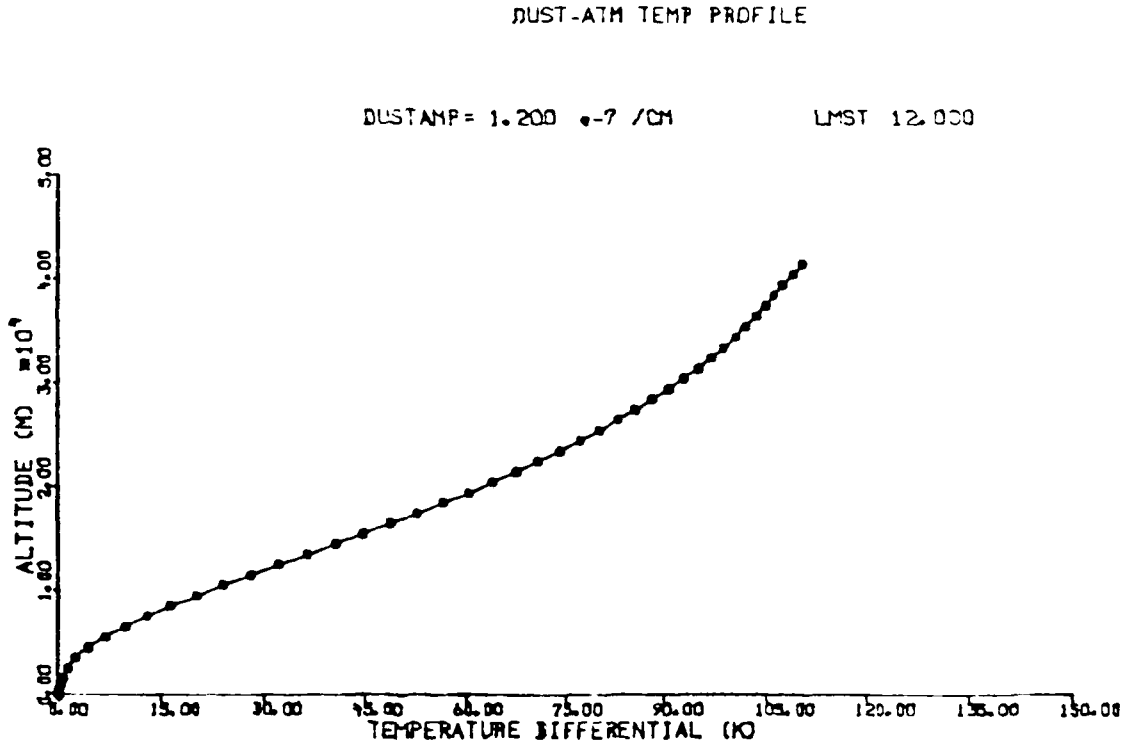

Fig. A.35 Dust-Atm Temperature Profile; Light Dust Load, LMST 12.00

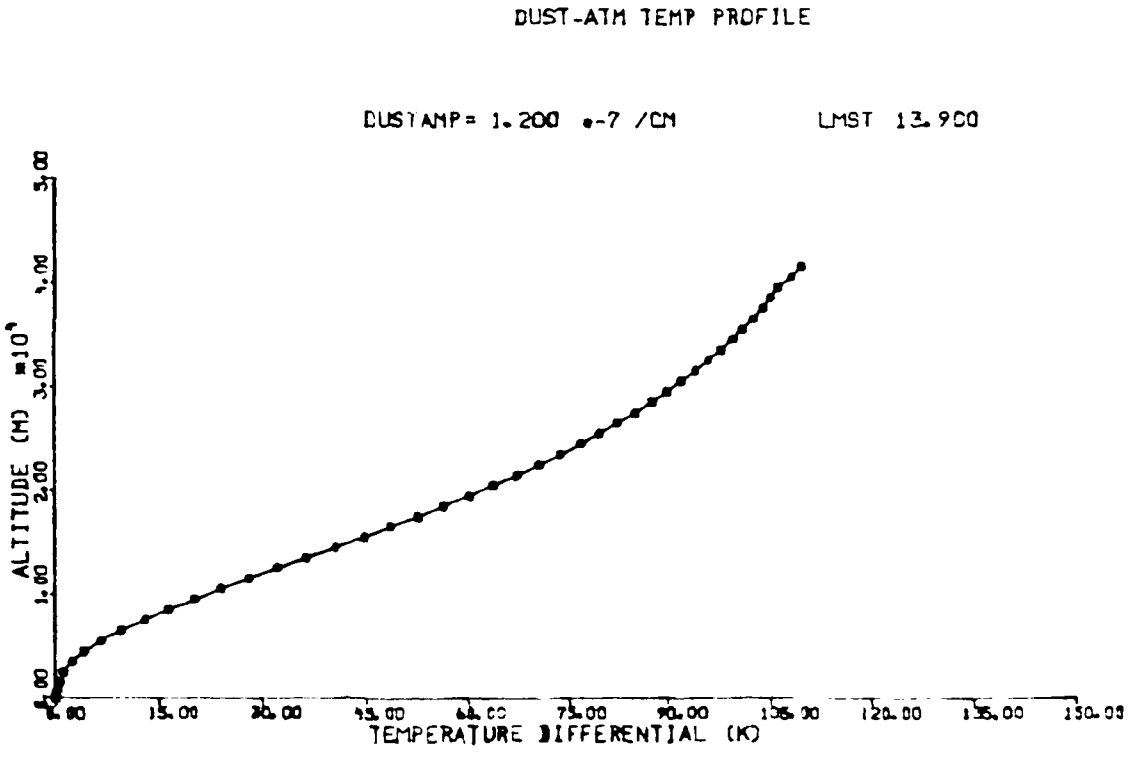

Fig. A.36 Dust-Atm Temperature Profile; Light Dust Load, LMST 13.90

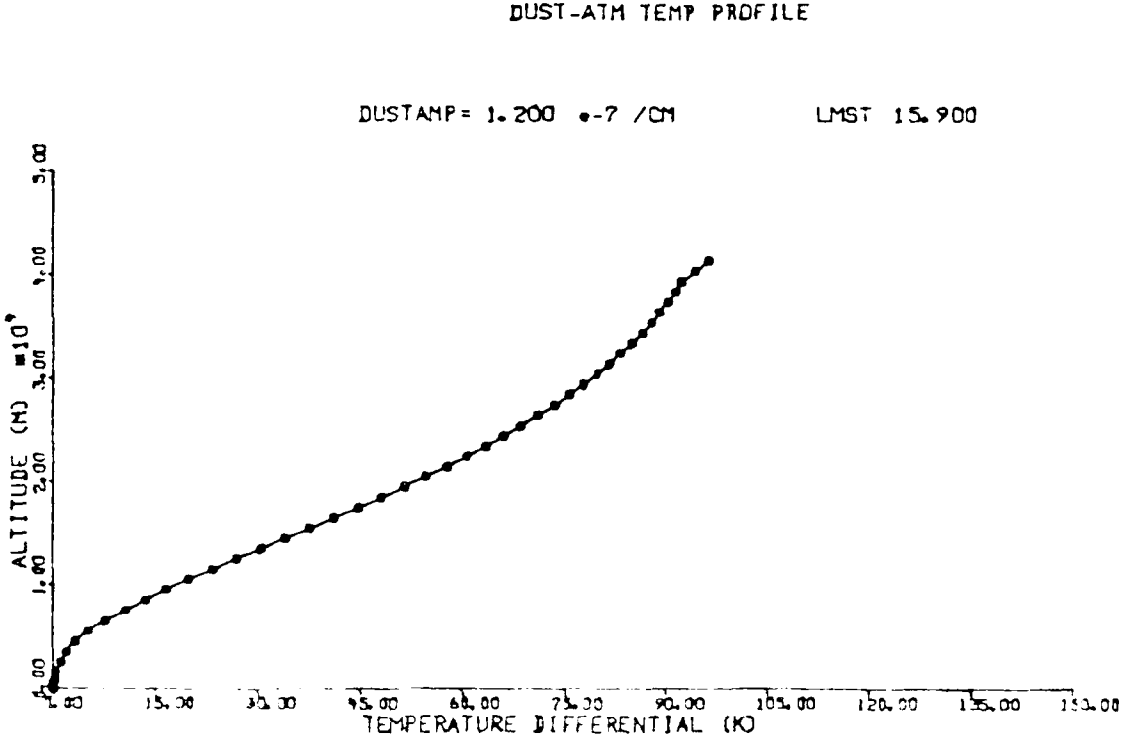

Fig. A.37 Dust-Atm Temperature Profile; Light Dust Load, LMST 15.90

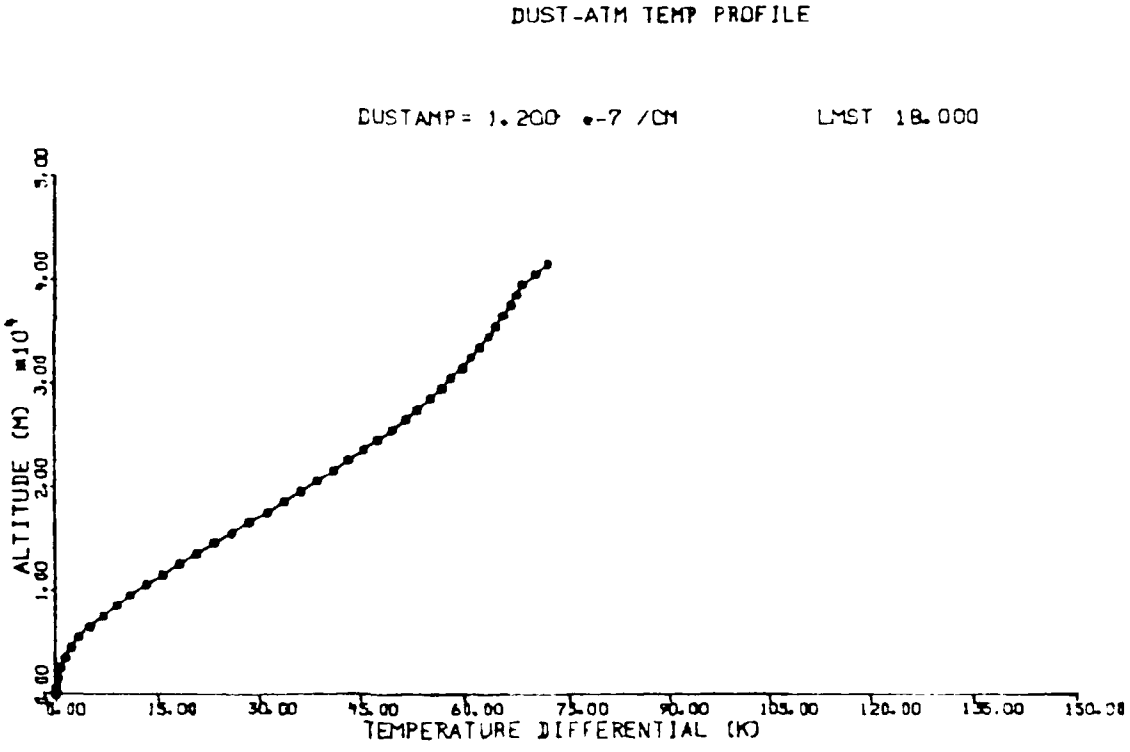

Fig. A.38 Dust-Atm Temperature Profile; Light Dust Load, LMST 18.00

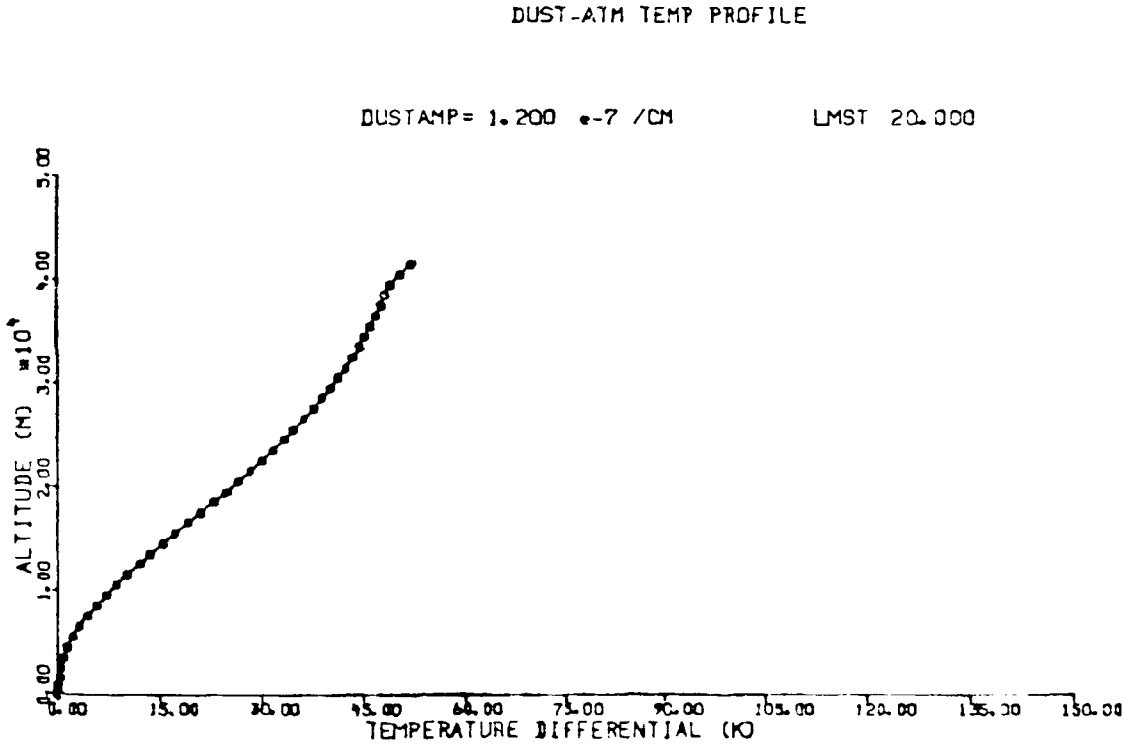

Fig. A.39 Dust-Atm Temperature Profile; Light Dust Load, LMST 20.00

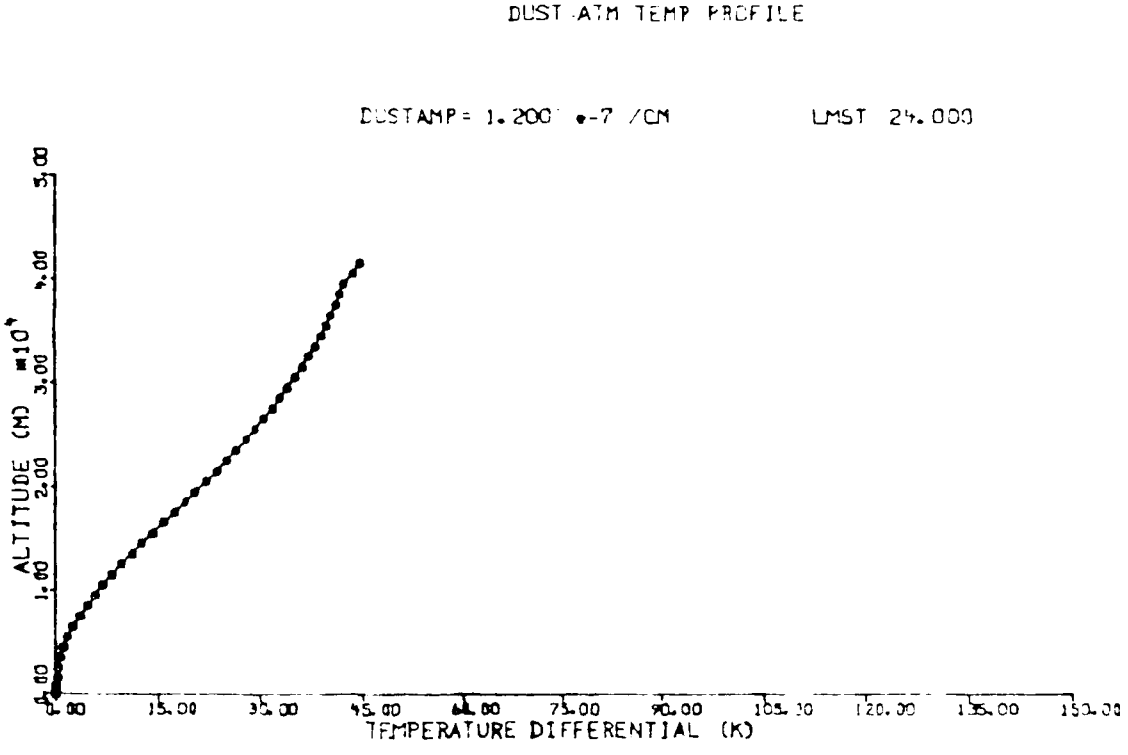

Fig. A.40 Dust-Atm Temperature Profile; Light Dust Load, LMST 24.00

TABLE 3. PROGRAM PARAMETERS;

DUSTAMP = 3.0×10^{-7} cm^{-1}

Initial Time: 16.000 LMST; Local Martian Solar Time

Number of Timesteps: 576

Timestep Interval: 10 minutes (Martian)

[4 minutes (Martian) from LMST 13.500 to 16.500]

Surface Albedo: 0.284

Surface Emissivity: 0.900

Soil Density: 1.500 g/cm^3

Soil Heat Capacity: 1.01×10^6 $J/(m^3 K)$

Soil Conductivity: 0.230 J/(s m K)

CO2 Conductivity: 0.0133 J/(s m K)

Latitude: 22.50° N

Solar Declination: 24.60°

Ratio of Mean to Actual Solar Distance: 0.9222

(This data for Viking 1 Lander; 20 Jul 1976)

Surface Pressure: 7.6 hPa (mb)

Dust Extinction Coefficient: 3.0×10^{-7} cm^{-1}

One Martian Solar Day = 24 Martian Hours = 1440

Martian Minutes; One Martian Minute = 61.6625 s

MARTIAN DUSTY ATMOSPHERE RAD-COND-CONV HEAT

TRANSFER SIMULATION: MARSDUST

Figures A.41 - A.51

Vertical Profiles of

Dust Temperature

With Medium Dust Loading

DUSTAMP = 3.0×10^{-7} cm^{-1}

Four hour intervals from LMST 20.000 to LMST 4.000;

two hour intervals otherwise.

Horizontal axis temperature range: 190 K to 240 K;

Vertical axis altitude range: 0 m to 50 000 m.

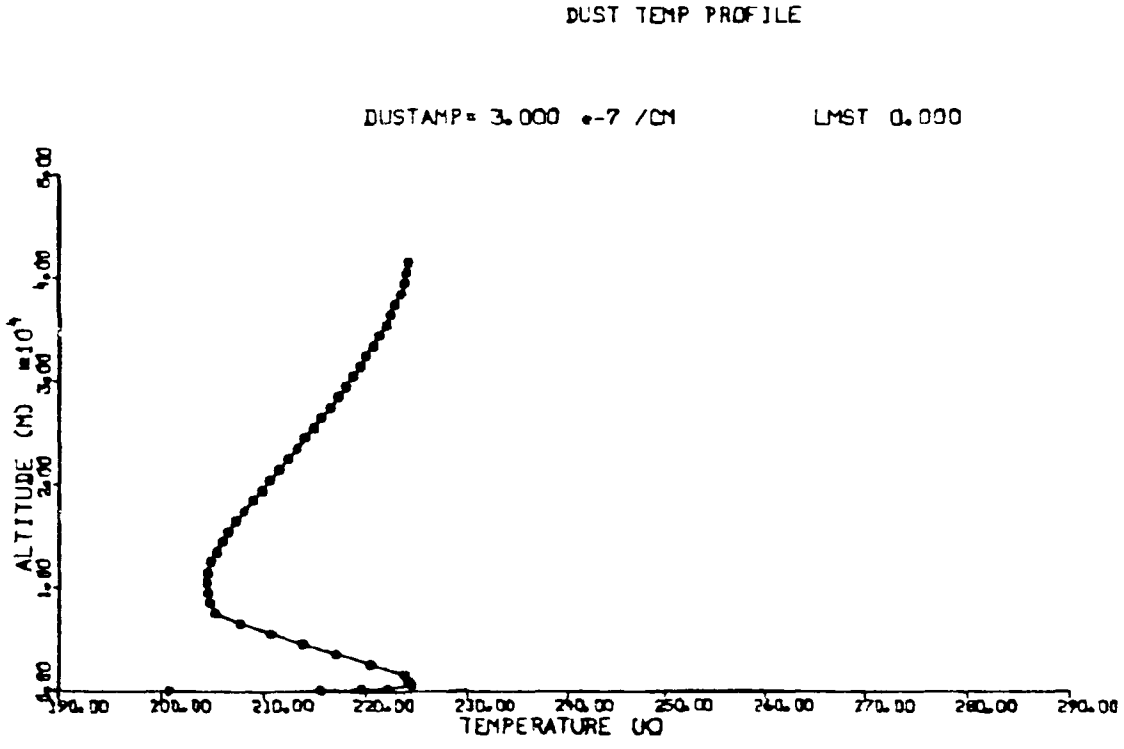

Fig. A.41 Dust Temperature Profile; Moderate Dust Load, LMST 00.00

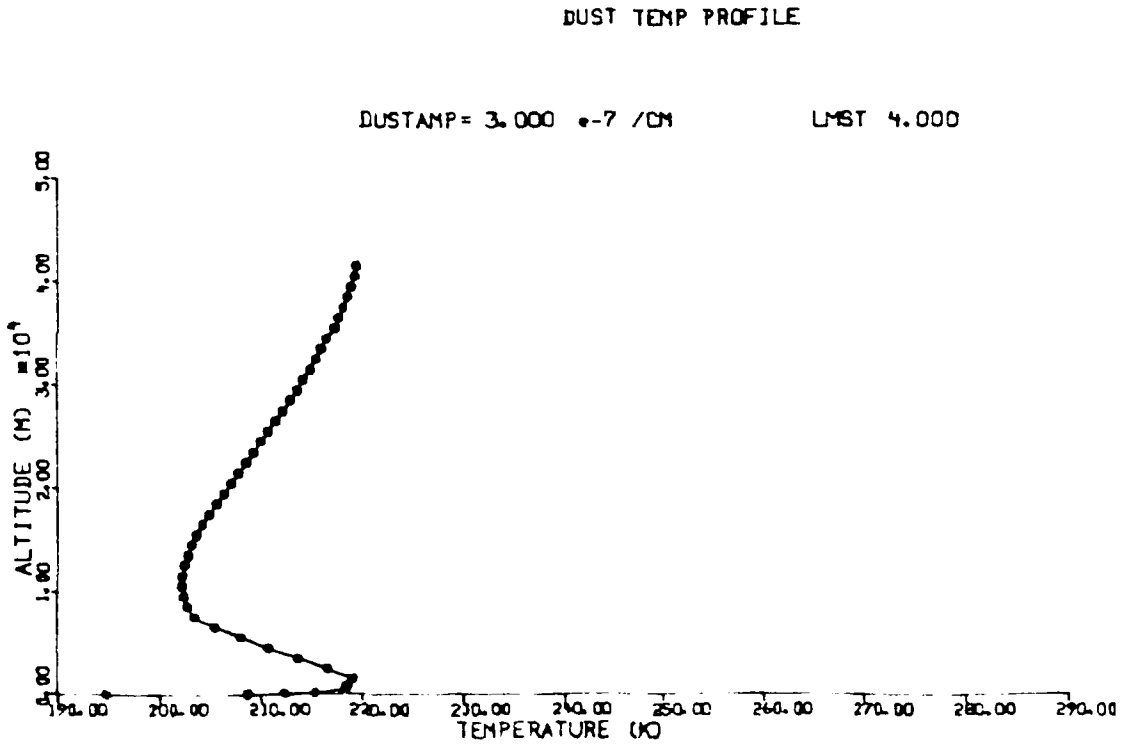

Fig. A.42 Dust Temperature Profile; Moderate Dust Load, LMST 04.00

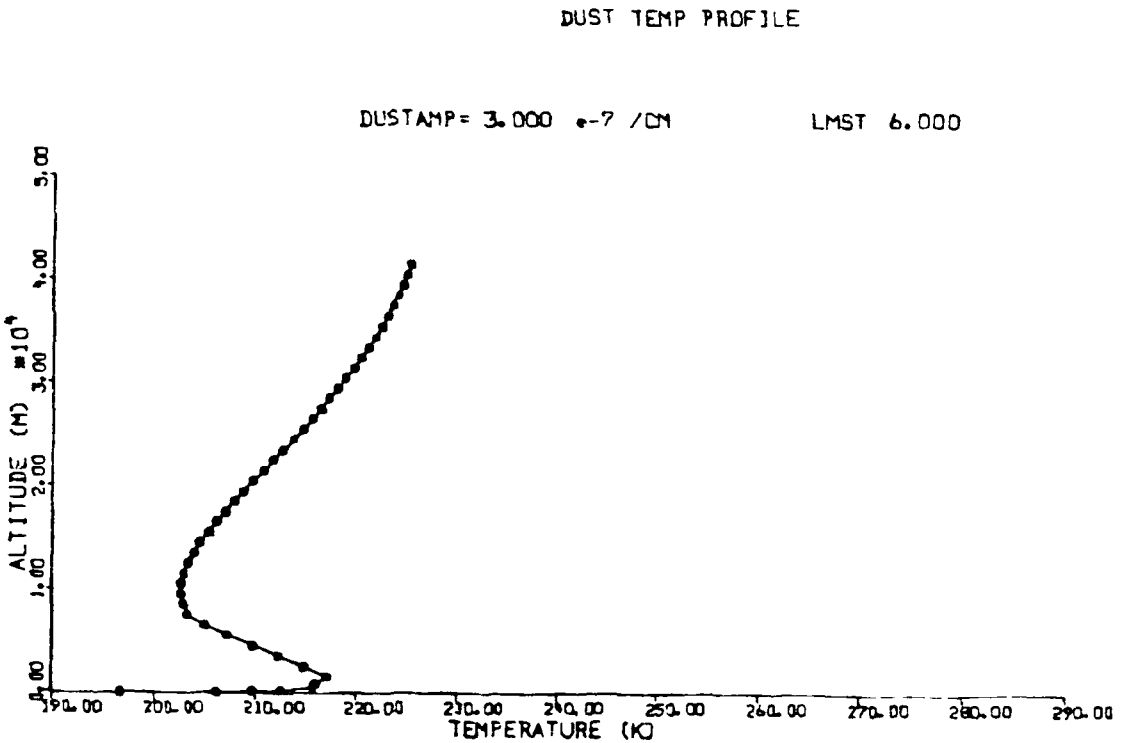

Fig. A.43 Dust Temperature Profile; Moderate Dust Load, LMST 06.00

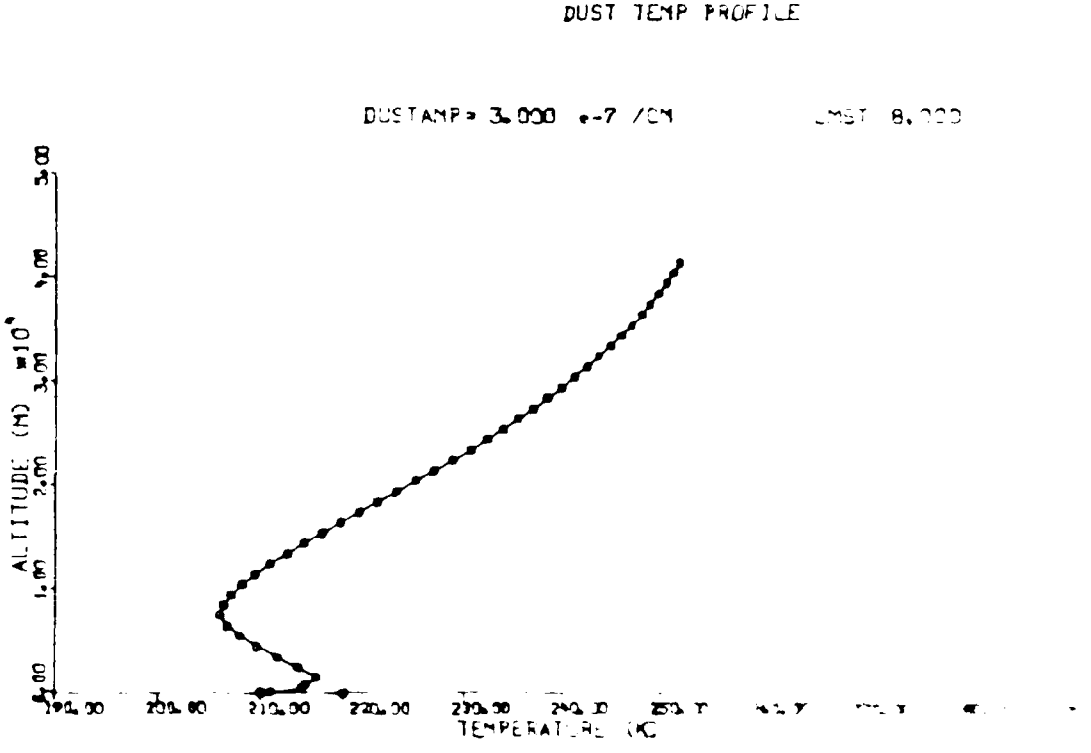

Fig. A.44 Dust Temperature Profile: Moderate

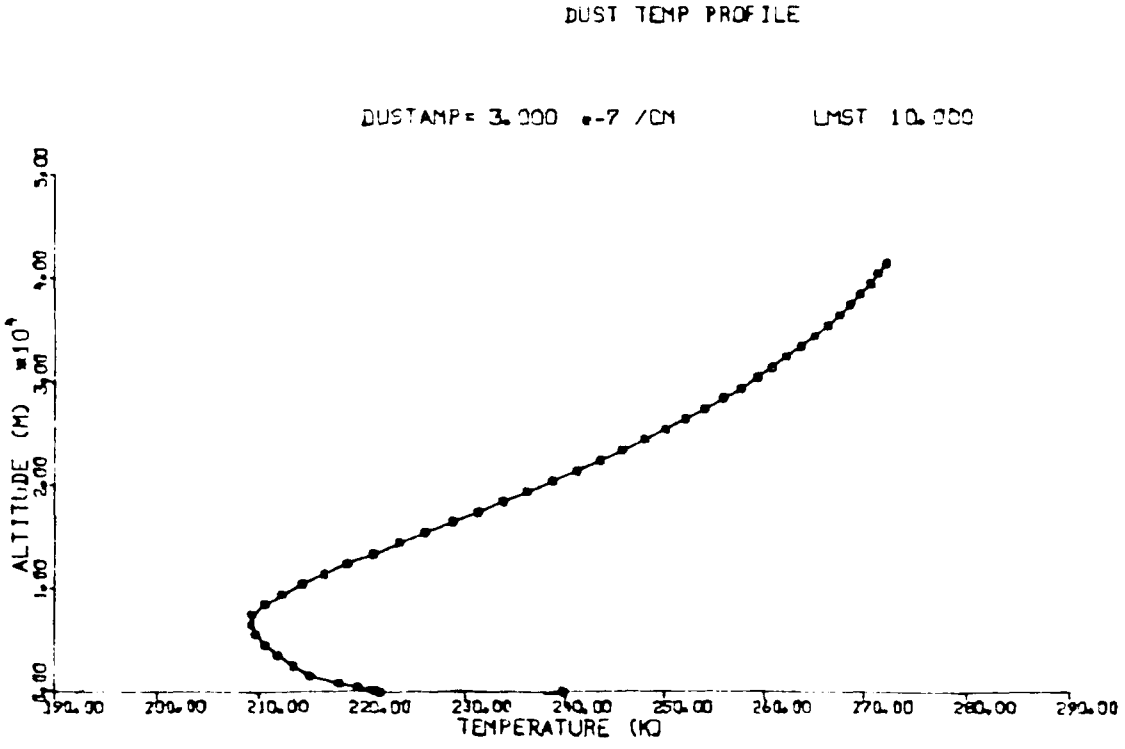

Fig. A.45 Dust Temperature Profile; Moderate Dust Load, LMST 10.00

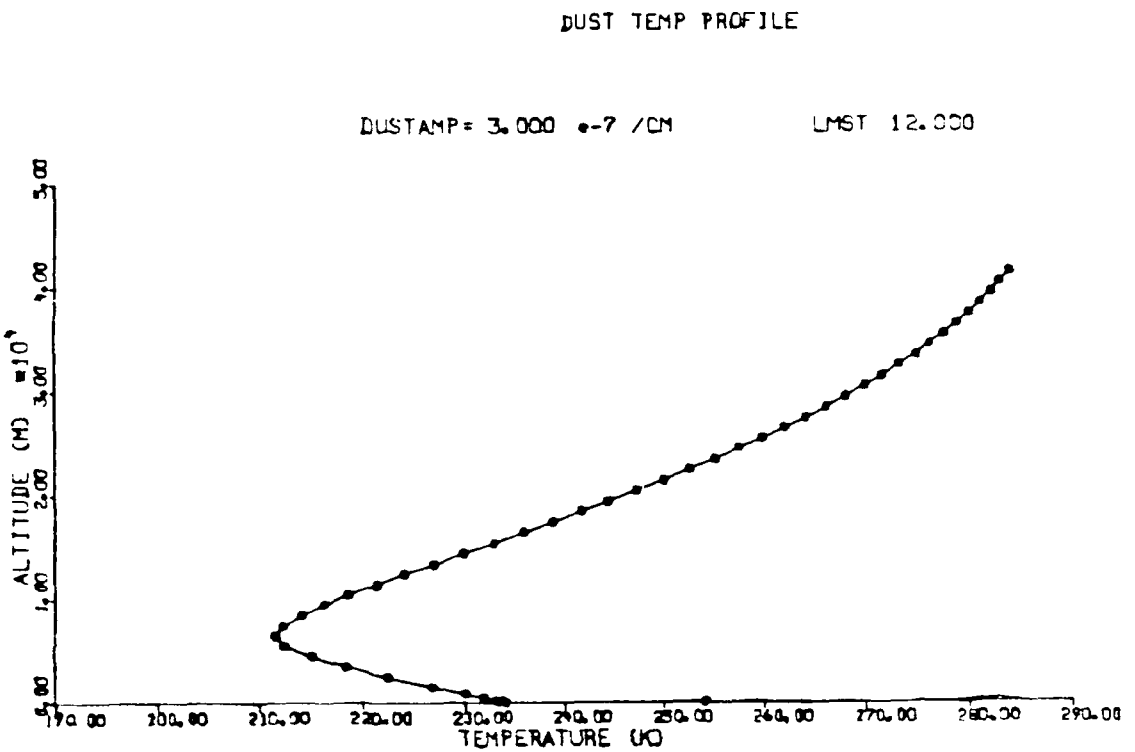

Fig. A.46 Dust Temperature Profile; Moderate Dust Load, LMST 12.00

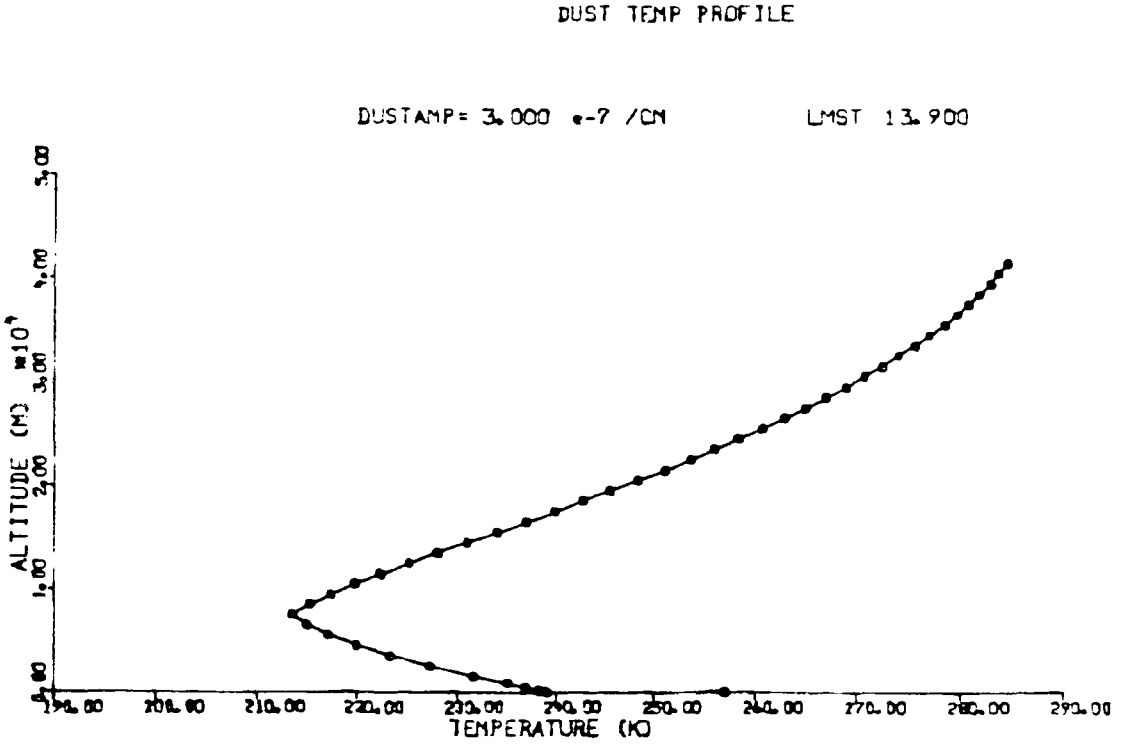

Fig. A.47 Dust Temperature Profile; Moderate Dust Load, LMST 13.90

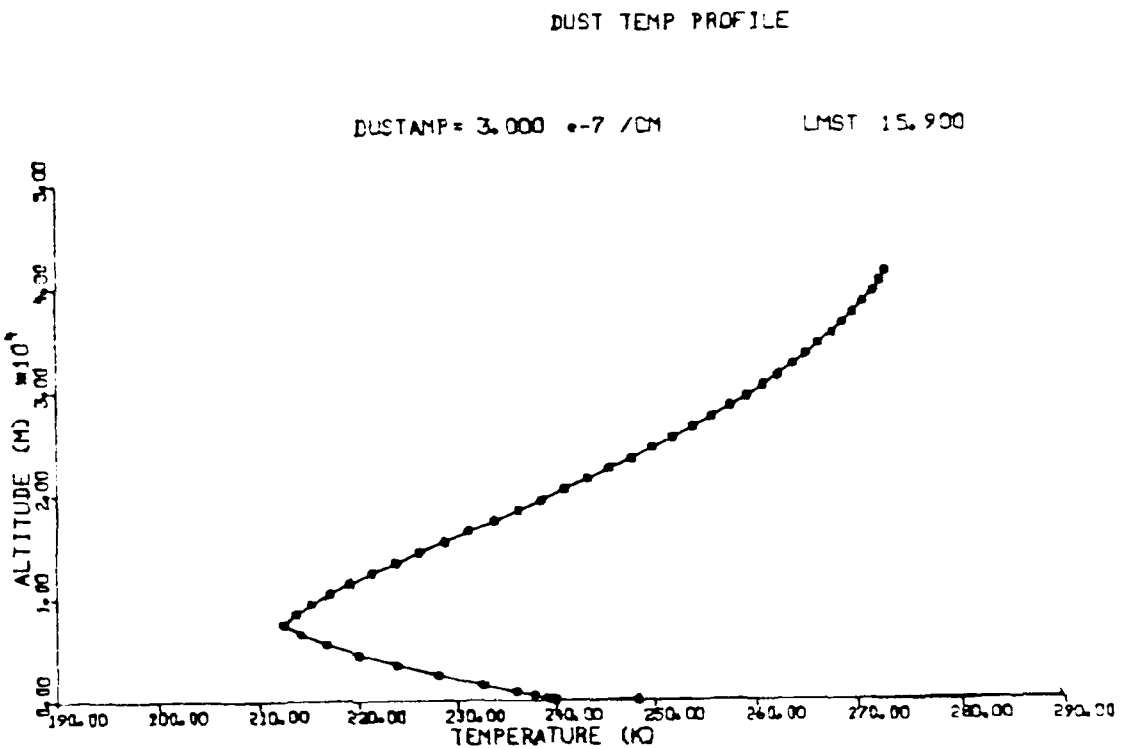

Fig. A.48 Dust Temperature Profile; Moderate Dust Load. LMST 15.90

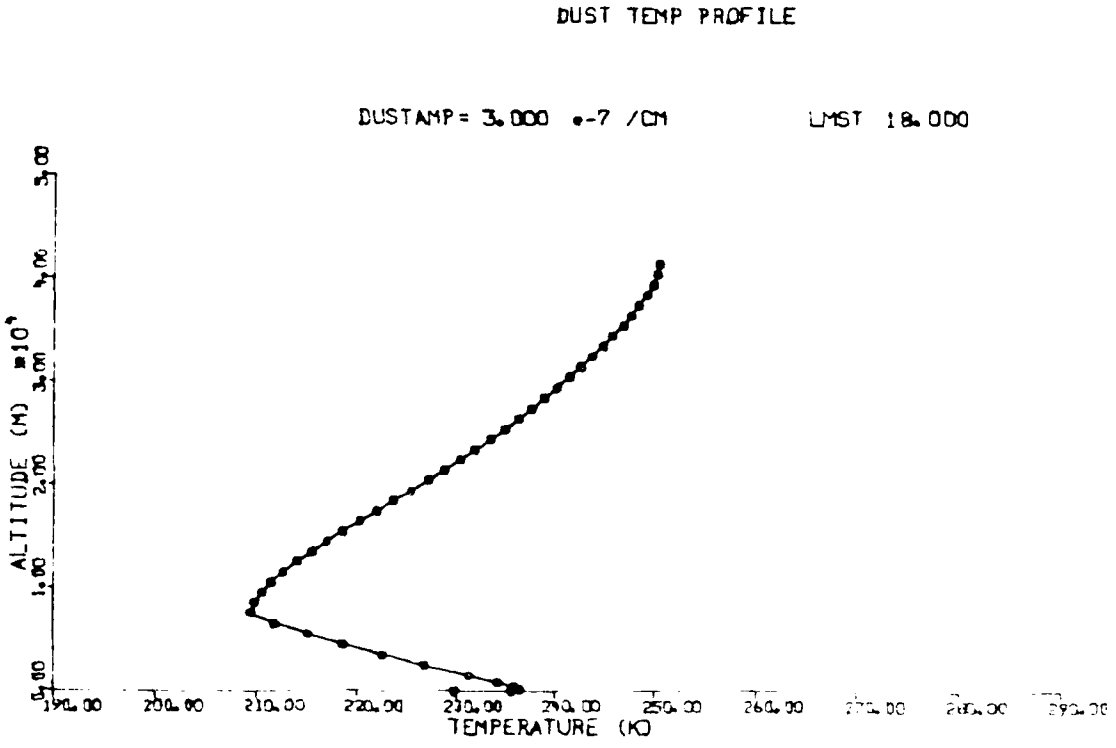

Fig. A.49 Dust Temperature Profile; Moderate Dust Load, LMST 18.00

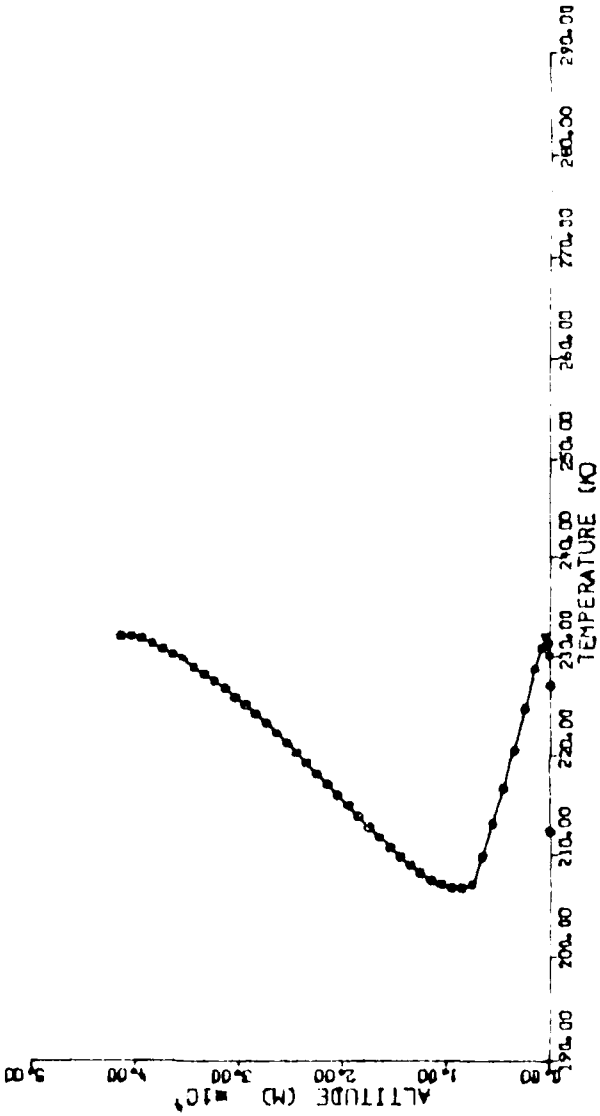

Fig. A.50 Dust Temperature Profile; Moderate Dust Load, LMST 20.00

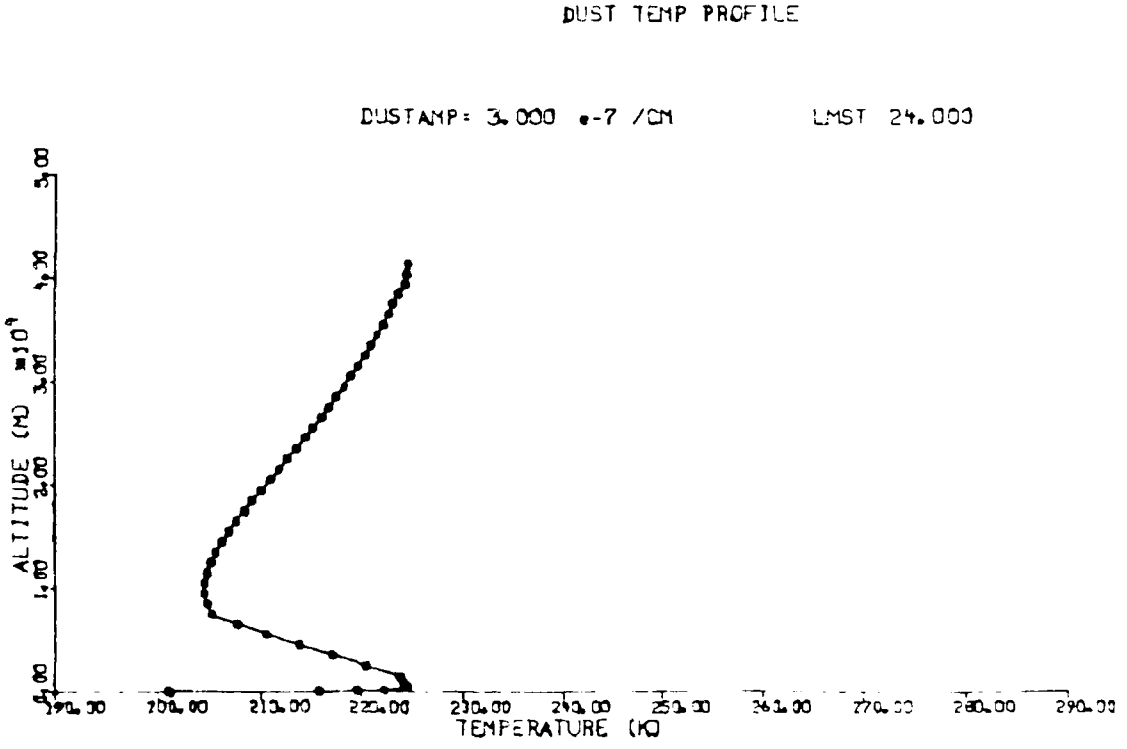

Fig. A 51 Dust Temperature Profile; Moderate Dust Load, LMST 24.00

MARTIAN DUSTY ATMOSPHERE RAD-COND-CONV HEAT

TRANSFER SIMULATION: MARSDUST

Figures A.52 - A.62

Vertical Profiles of

Dust Temperature Minus Atmospheric Temperature

With Medium Dust Loading

DUSTAMP = 3.0×10^{-7} cm^{-1}

Four hour intervals from LMST 20.000 to LMST 4.000;

two hour intervals otherwise.

Horizontal axis temperature difference range:

0 K to 150 K;

Vertical axis altitude range: 0 m to 50 000 m.

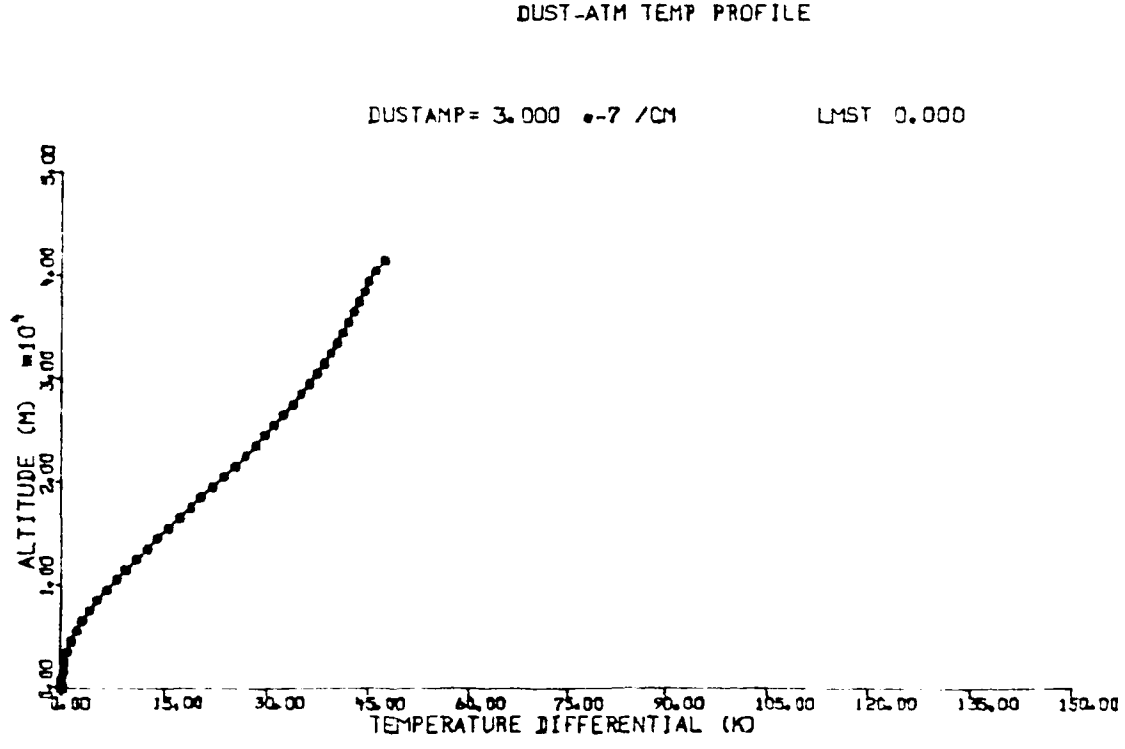

Fig. A.52 Dust-Atm Temperature Profile; Moderate Dust Load, LMST 00.00

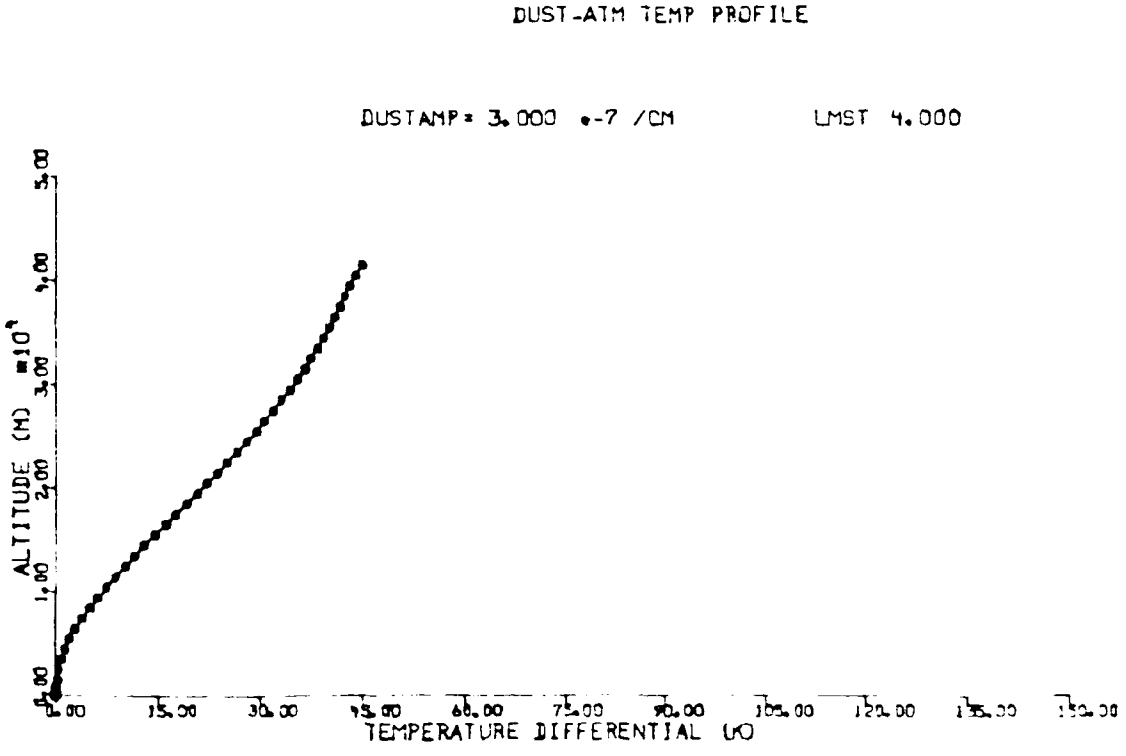

Fig A-53 Dust-Atm Temperature Profile; Moderate Dust Load, LMST 04 00

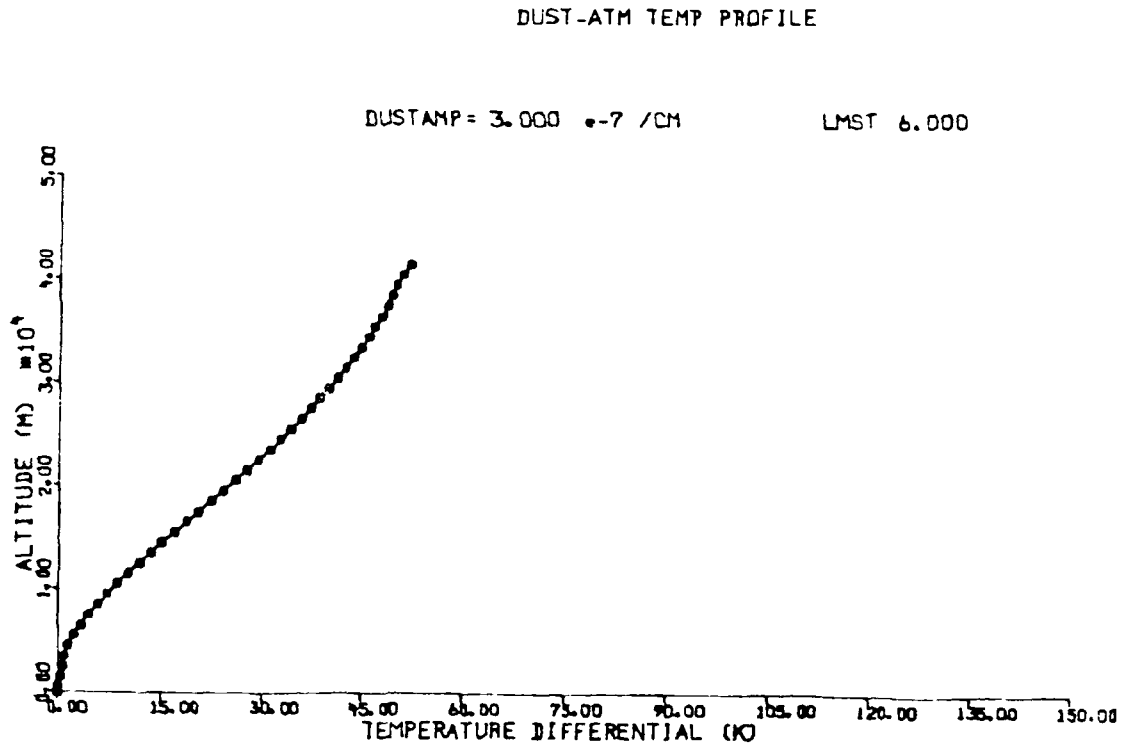

Fig. A.64 Dust-Atm Temperature Profile; Moderate Dust Load, LMST 06.00

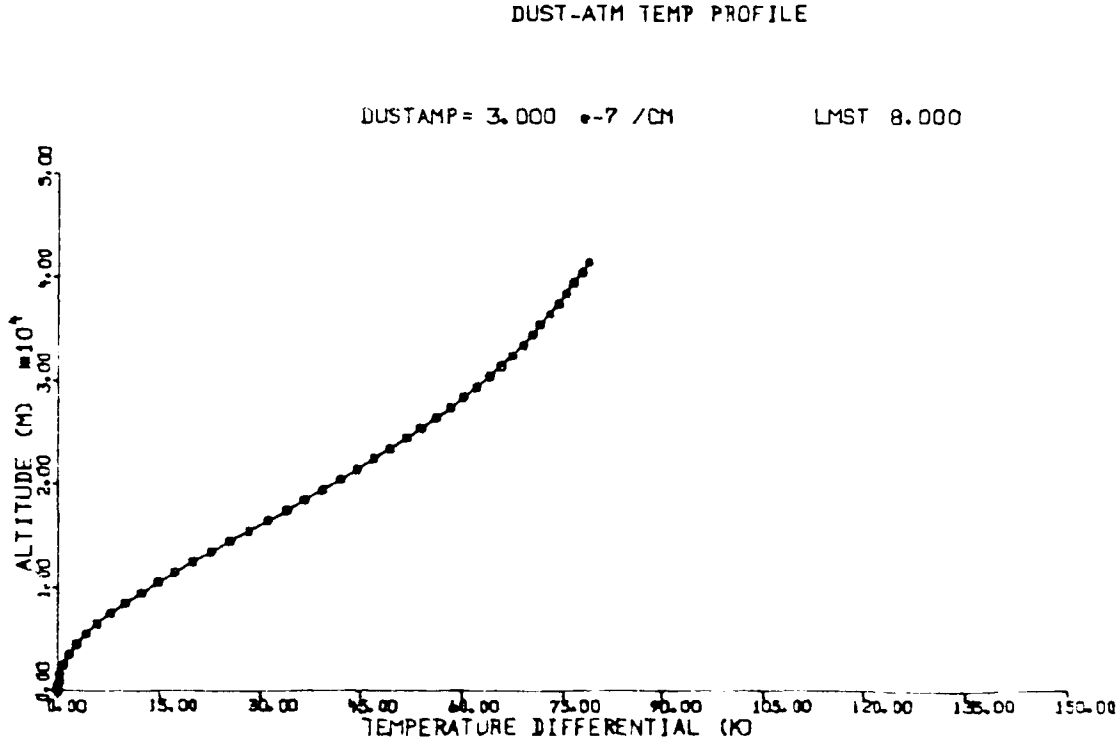

Fig. A.55 Dust-Atm Temperature Profile; Moderate Dust Load, LMST 08.00

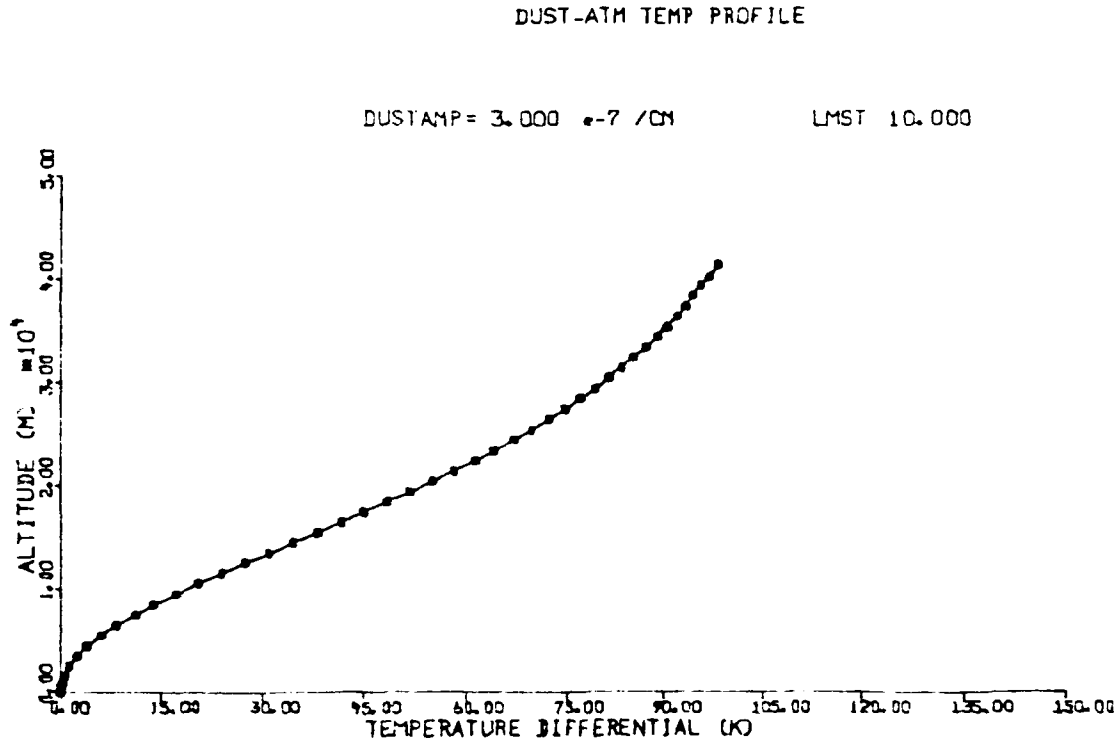

Fig. A.56 Dust-Atm Temperature Profile; Moderate Dust Load, LMST 10.00

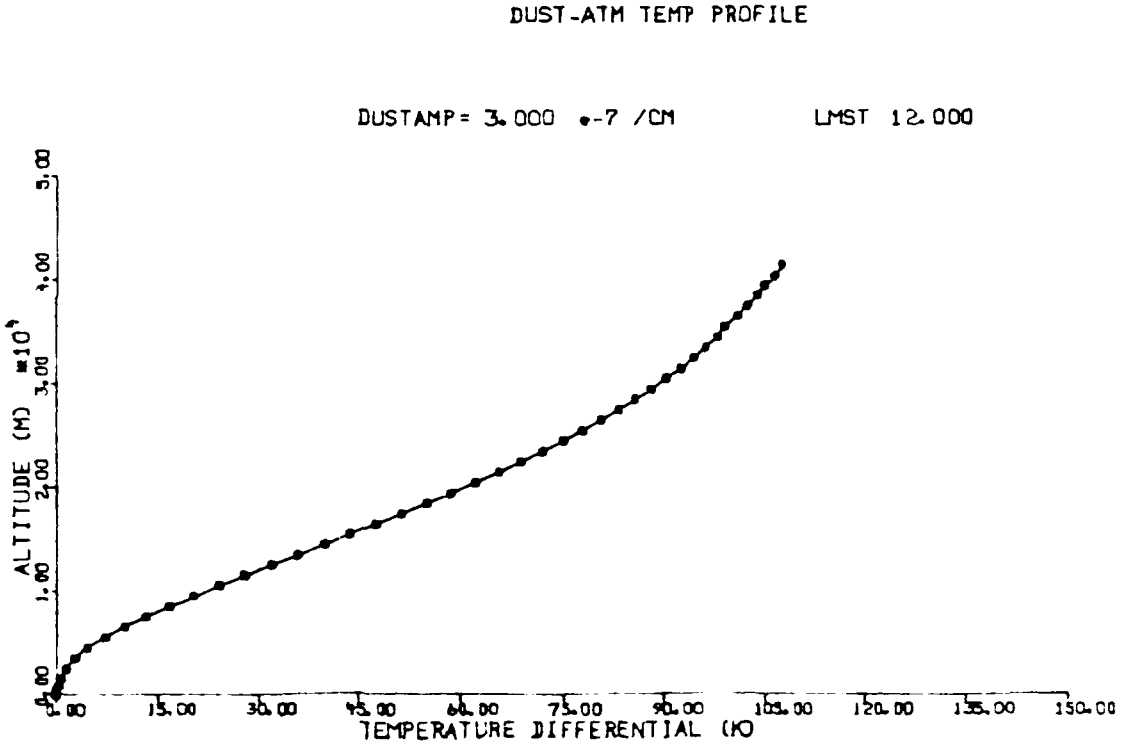

Fig A.57 Dust-Atm Temperature Profile; Moderate Dust Load, LMST 12.00

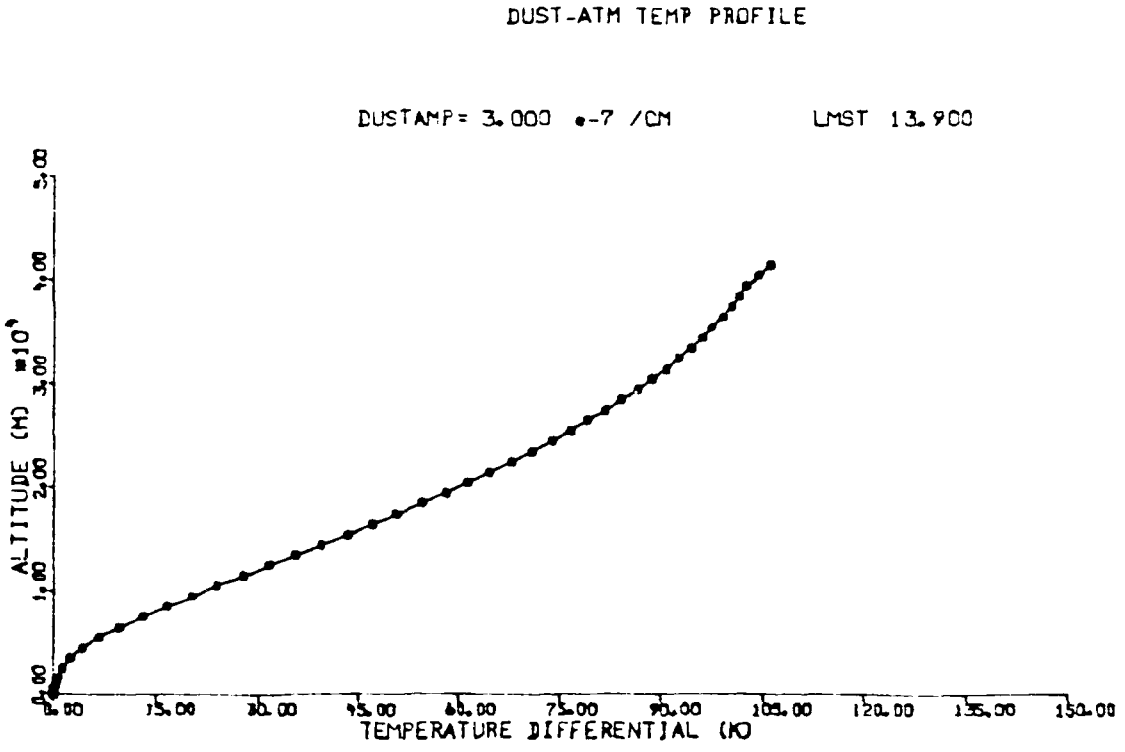

Fig. A.58 Dust-Atm Temperature Profile; Moderate Dust Load, LMST 13.90

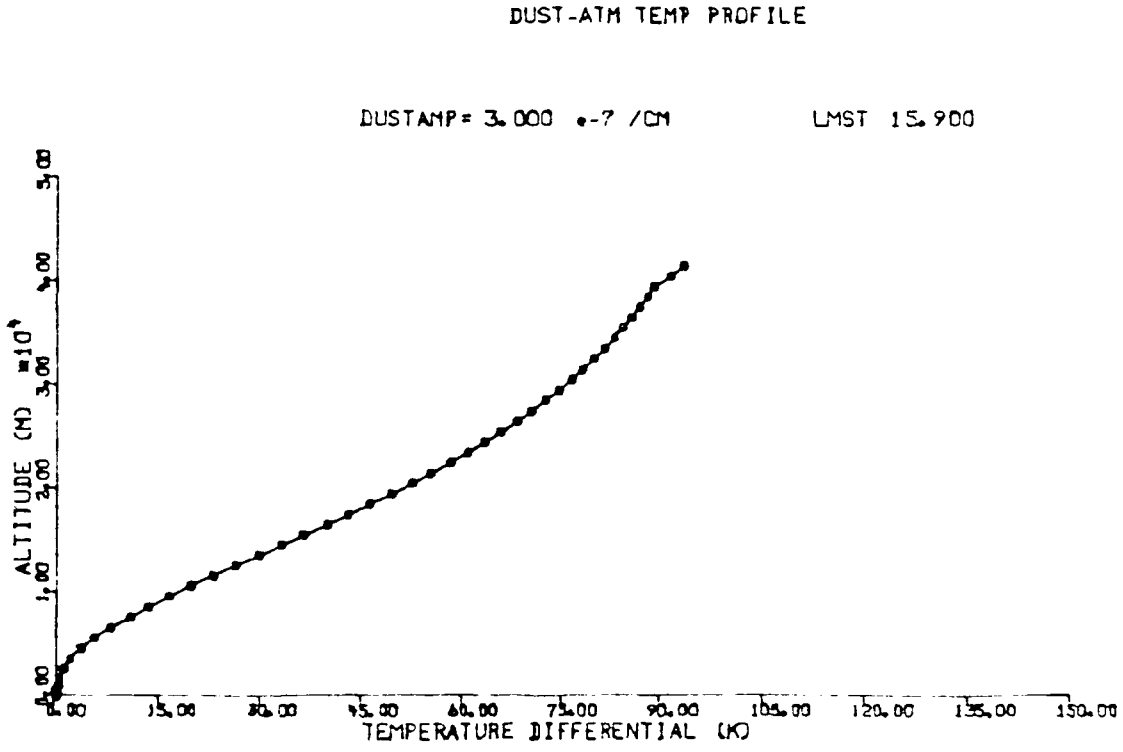

Fig. A.59 Dust-Atm Temperature Profile; Moderate Dust Load, LMST 15.90

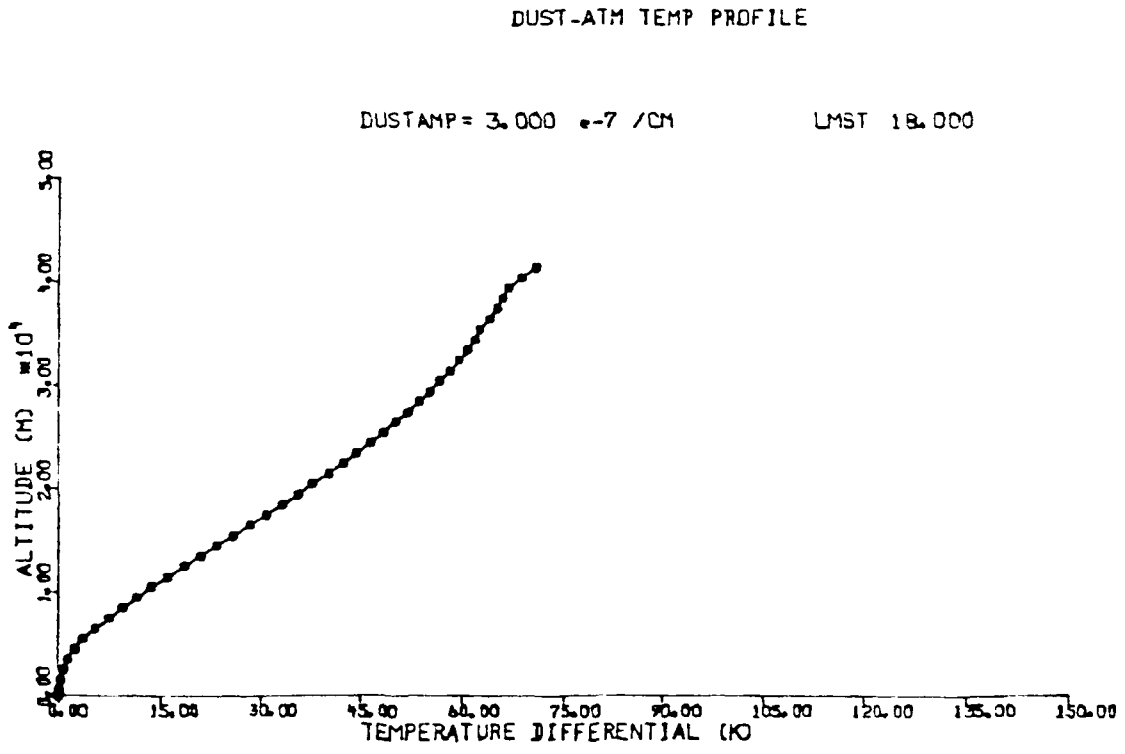

Fig. A.60 Dust-Atm Temperature Profile; Moderate Dust Load, LMST 18.00

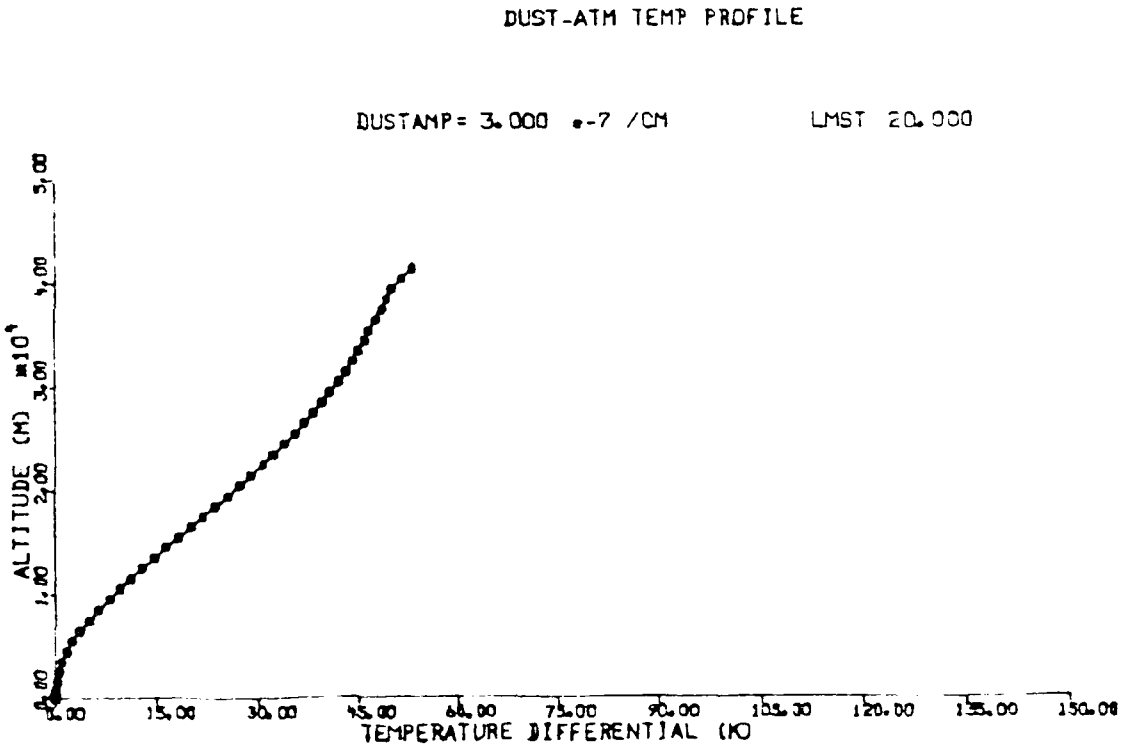

Fig. A.61 Dust-Atm Temperature Profile; Moderate Dust Load, LMST 20.00

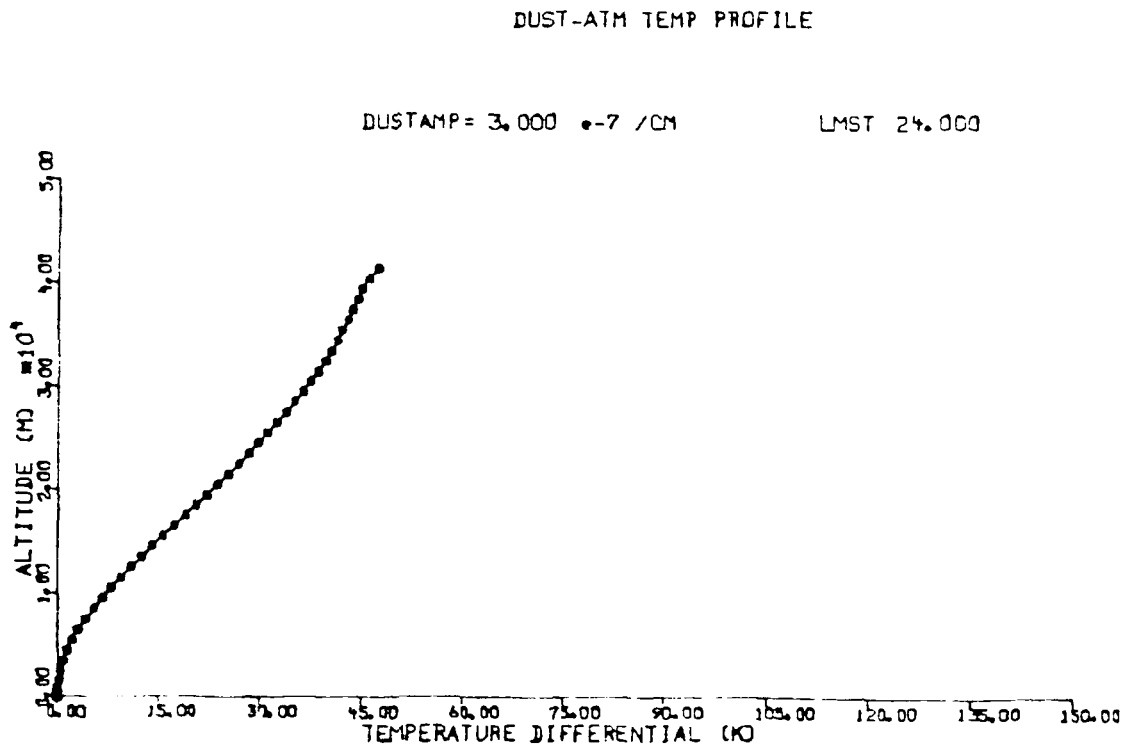

Fig. A.62 Dust-Atm Temperature Profile; Moderate Dust Load, LMST 24.00

TABLE 4. PROGRAM PARAMETERS;

DUSTAMP = 6.0×10^{-7} cm^{-1}

Initial Time: 16.000 LMST; Local Martian Solar Time

Number of Timesteps: 576

Timestep Interval: 10 minutes (Martian)

[4 minutes (Martian) from LMST 13.500 to 16.500]

Surface Albedo: 0.284

Surface Emissivity: 0.900

Soil Density: 1.500 g/cm^3

Soil Heat Capacity: 1.01×10^6 $J/(m^3\ K)$

Soil Conductivity: 0.230 J/(s m K)

CO2 Conductivity: 0.0133 J/(s m K)

Latitude: 22.50° N

Solar Declination: 24.60°

Ratio of Mean to Actual Solar Distance: 0.9222

(This data for Viking 1 Lander; 20 Jul 1976)

Surface Pressure: 7.6 hPa (mb)

Dust Extinction Coefficient: 6.0×10^{-7} cm^{-1}

One Martian Solar Day = 24 Martian Hours = 1440

Martian Minutes; One Martian Minute = 91.6625 s

MARTIAN DUSTY ATMOSPHERE RAD-COND-CONV HEAT

TRANSFER SIMULATION: MARSDUST

Figures A.63 - A.73

Vertical Profiles of

Atmospheric Temperature

With Heavy Dust Loading

DUSTAMP = 6.0×10^{-7} cm^{-1}

Four hour intervals from LMST 20.000 to LMST 4.000;

two hour intervals otherwise.

Horizontal axis temperature range: 160 K to 260 K;

Vertical axis altitude range: 0 m to 50 000 m.

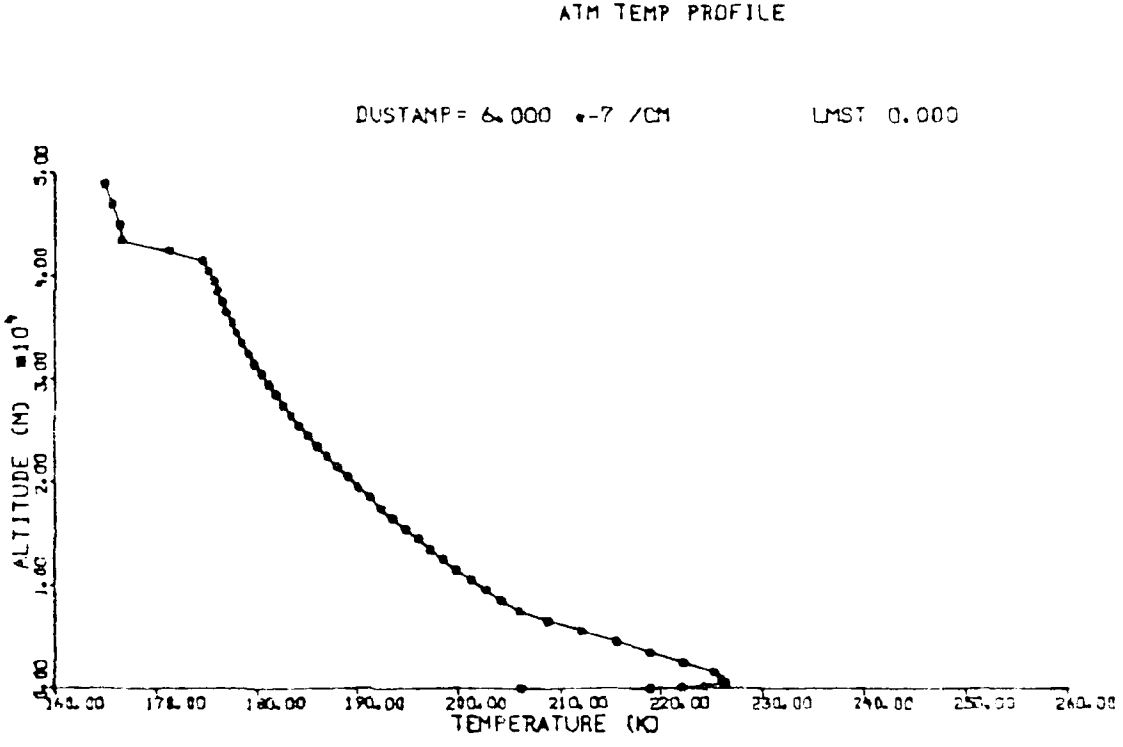

Fig. A.63 Atmospheric Temperature Profile; Heavy Dust Load, LMST 00.00

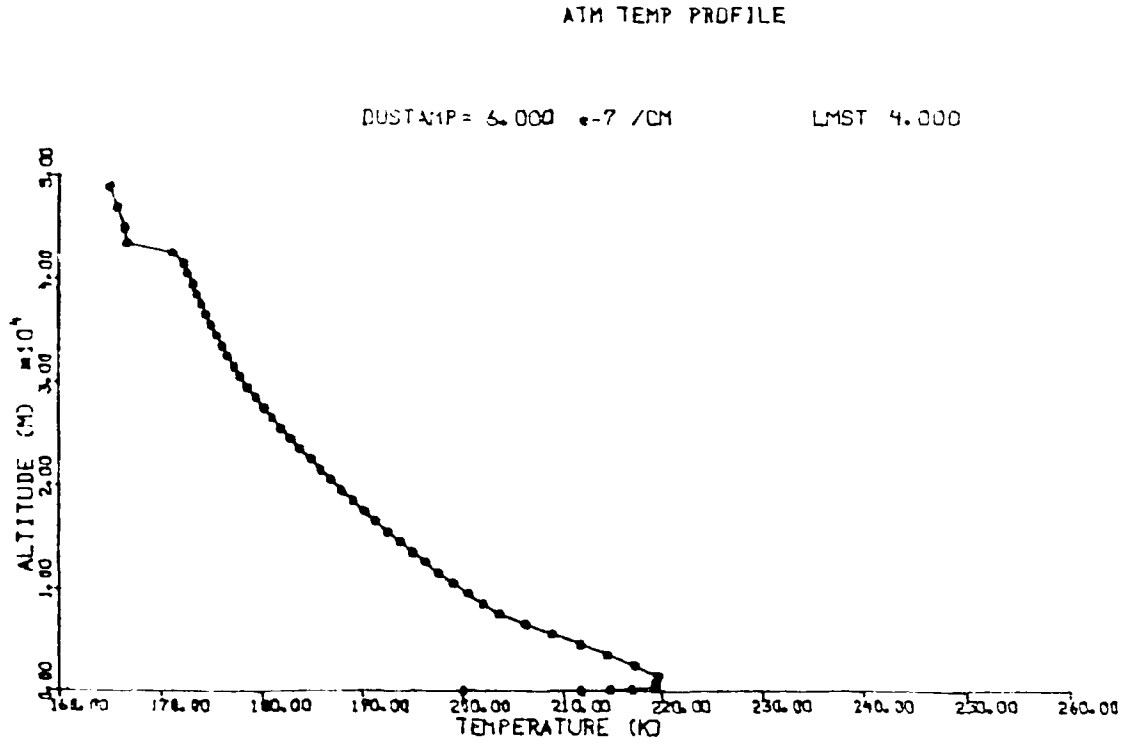

Fig. A.64 Atmospheric Temperature Profile: Heavy Dust Load, LMST 04.00

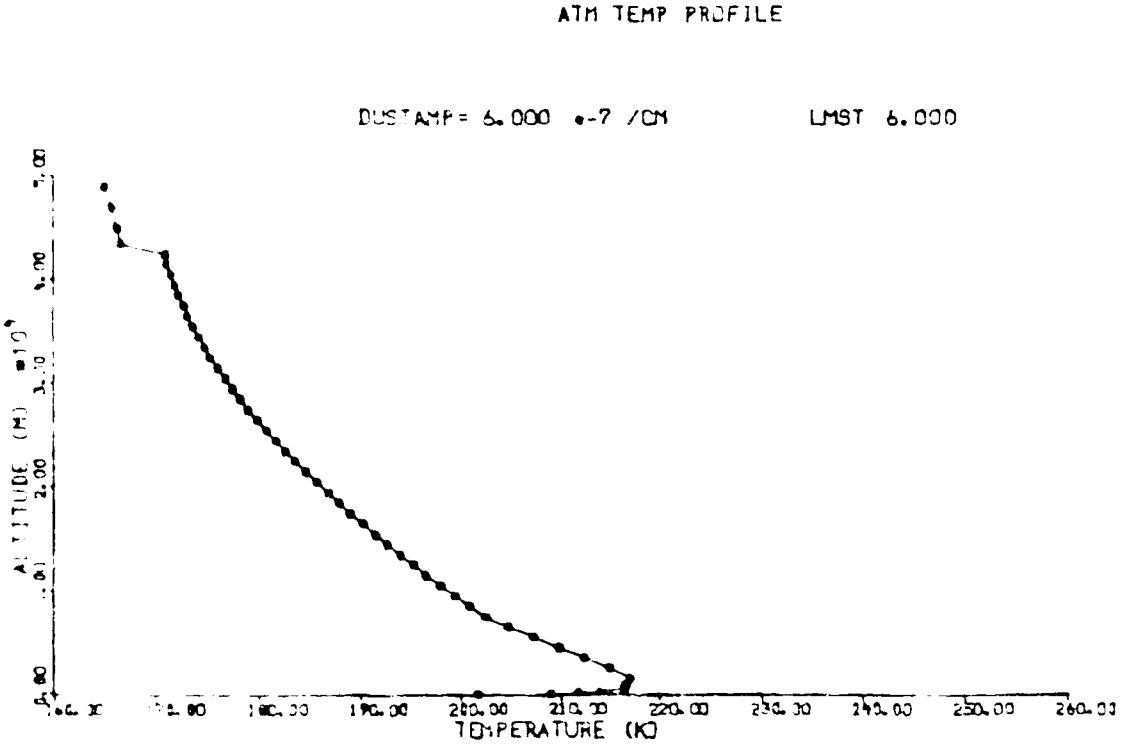

Fig. A- Atmospheric Temperature Profile: Heavy Dust Load, LMST 06:00

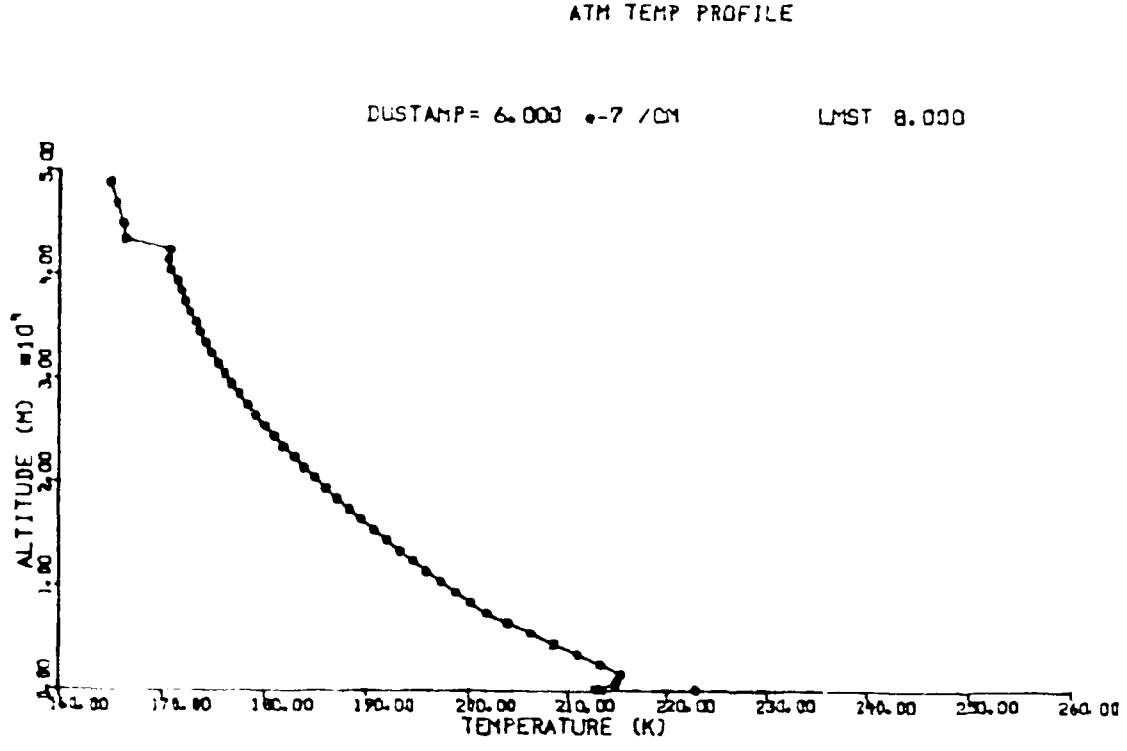

Fig A 66 Atmospheric Temperature Profile: Heavy Dust Load, LMST 08.00

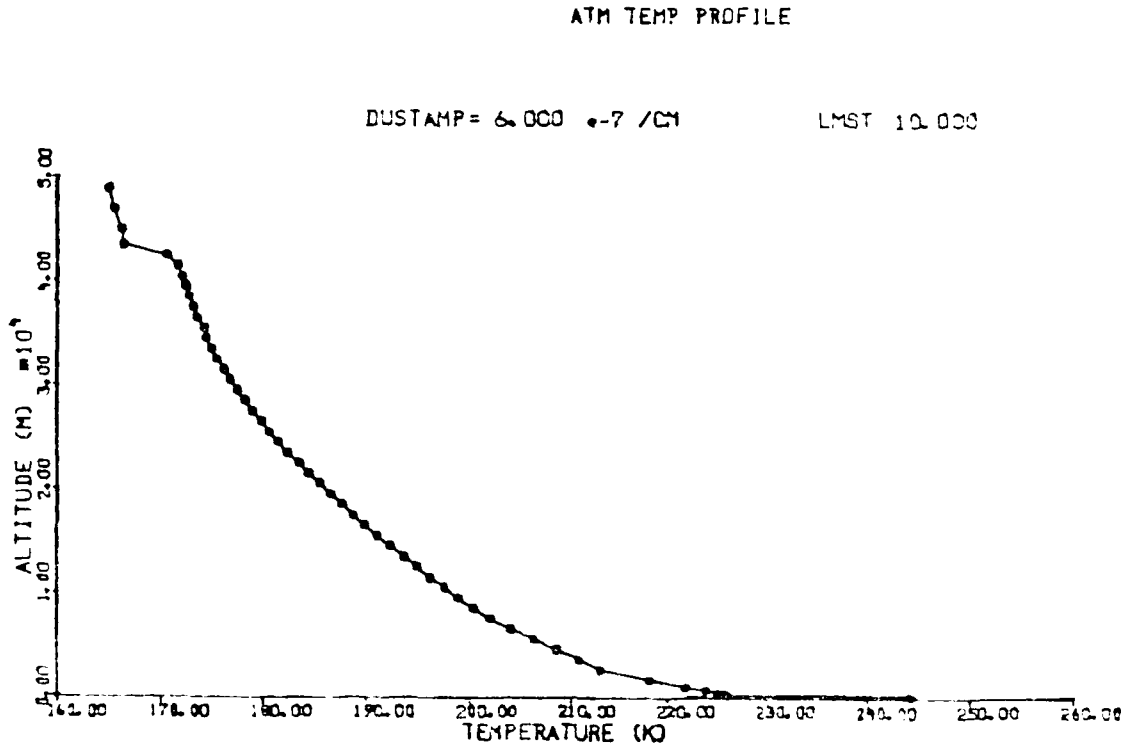

Fig. A.67 Atmospheric Temperature Profile; Heavy Dust Load, LMST 10.00

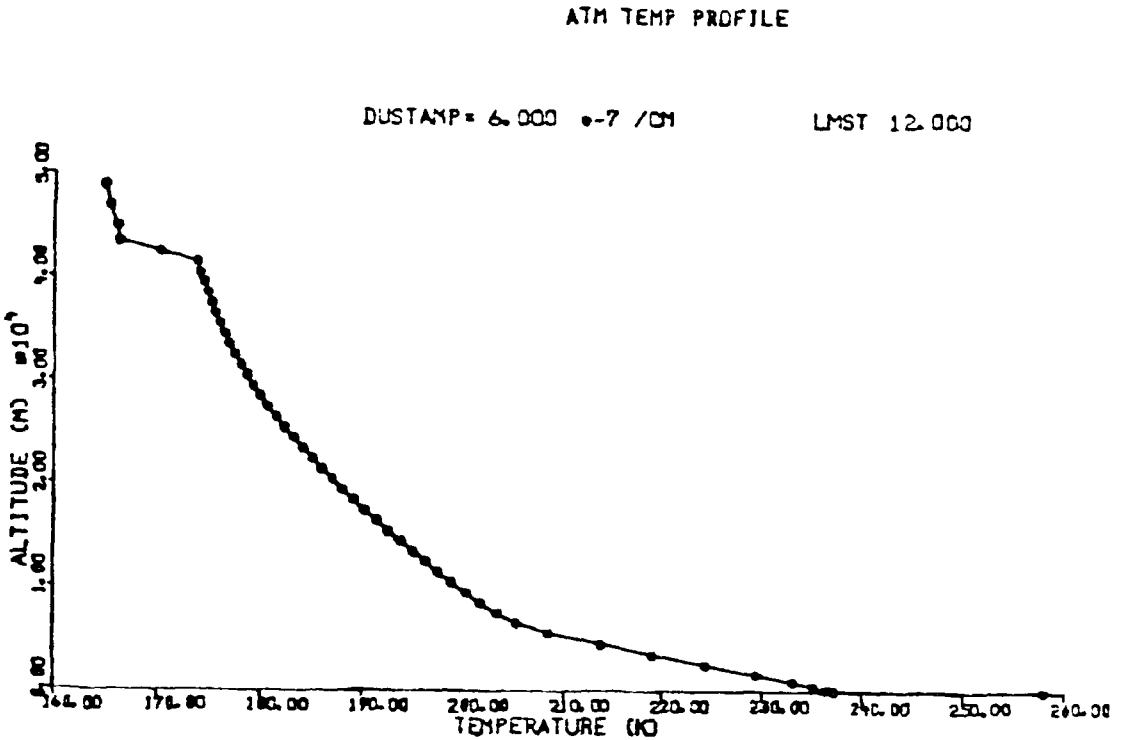

Fig. A.68 Atmospheric Temperature Profile: Heavy Dust Load, LMST 12.00

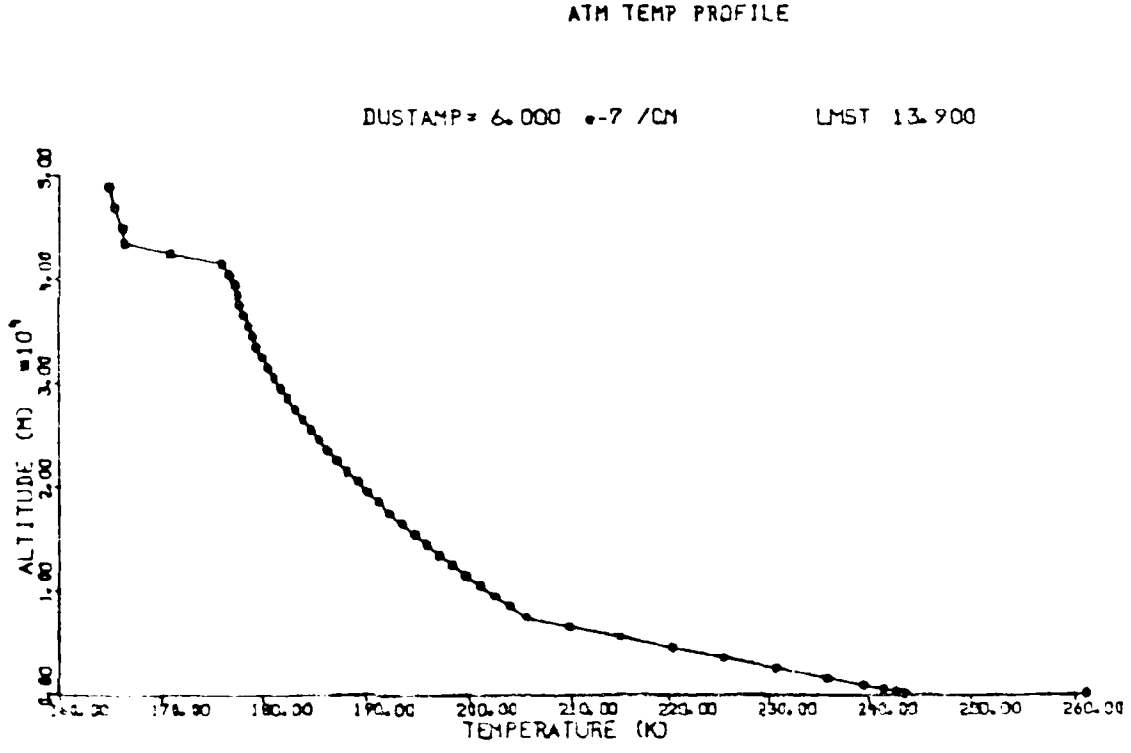

Fig. A-14. Atmospheric Temperature Profile: Heavy Dust Load, LMST 13.90

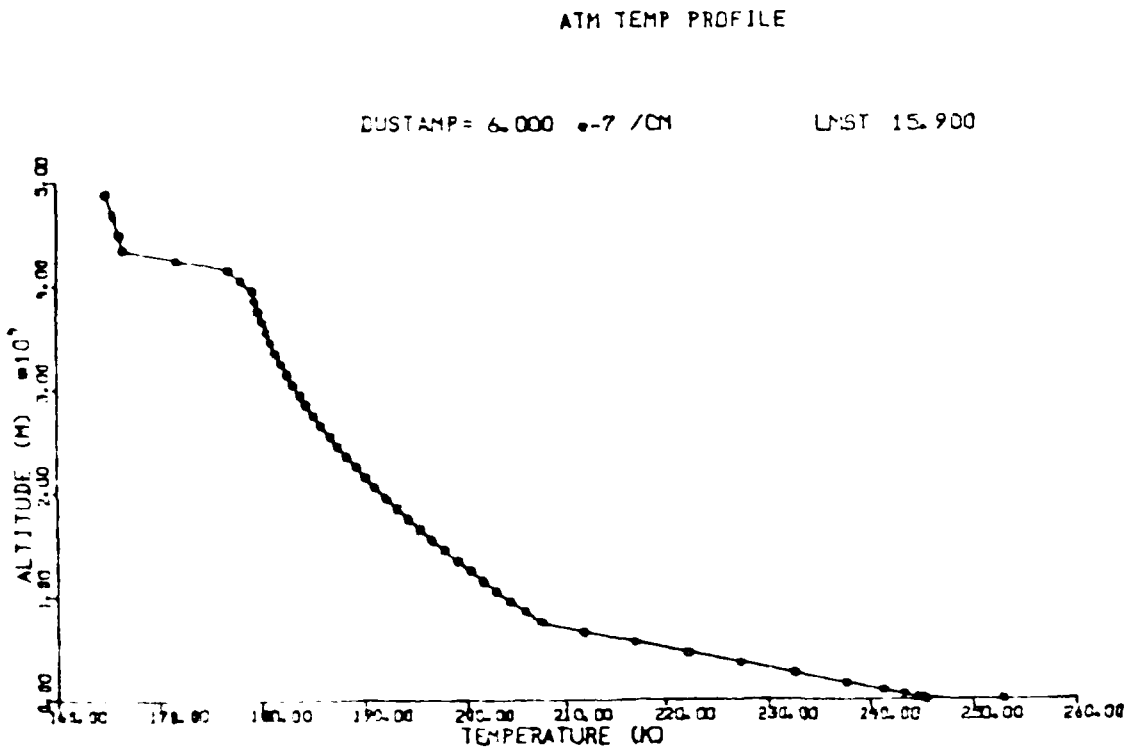

Fig A 7[illegible] Atmospheric Temperature Profile; Heavy Dust Load, LMST 15.90

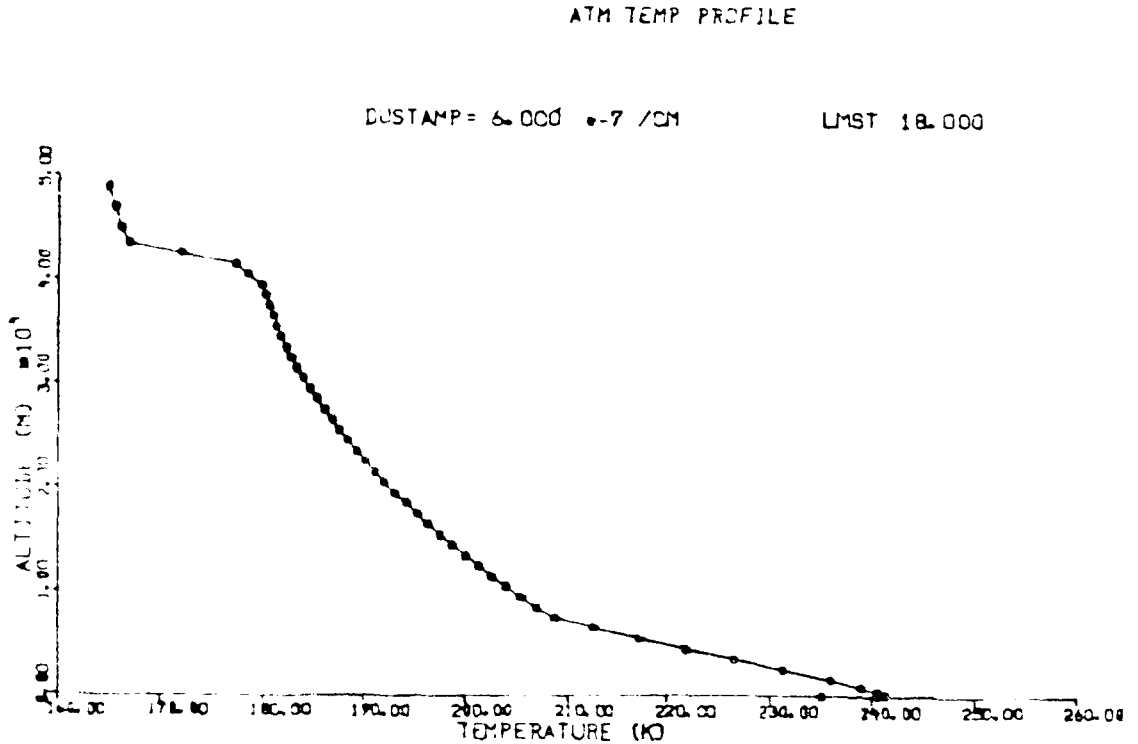

Fig. A[illegible] Atmospheric Temperature Profile; Heavy Dust Load, LMST 18.00

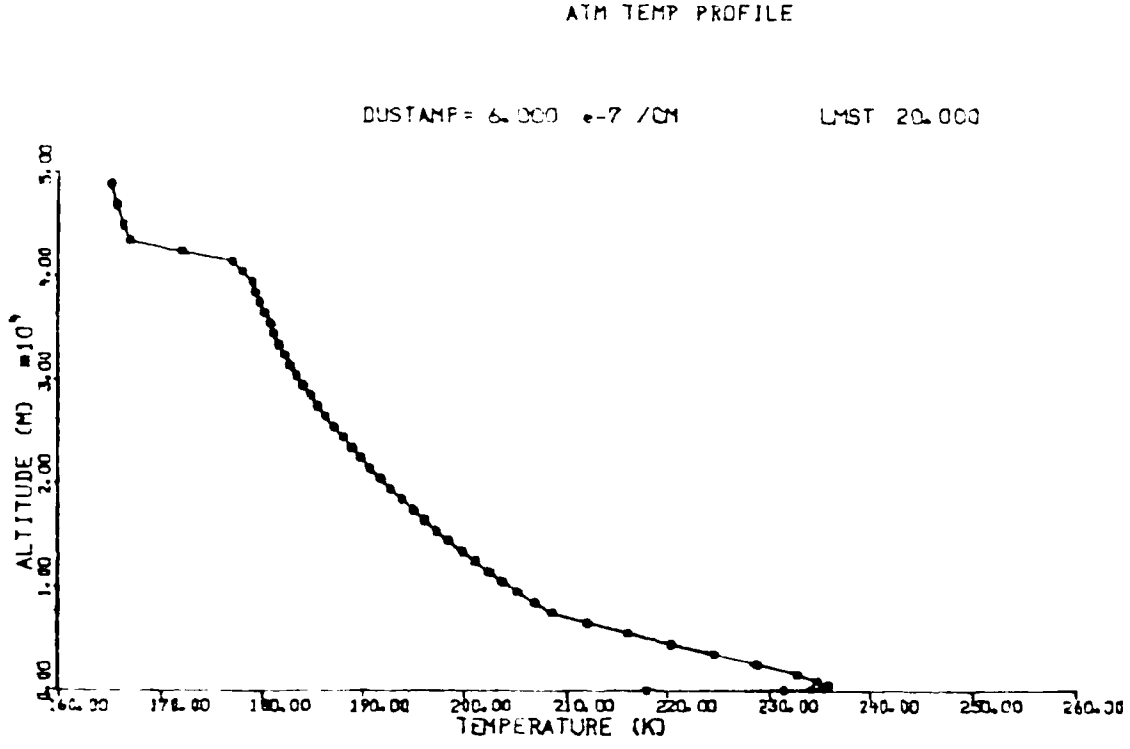

Fig. A.72 Atmospheric Temperature Profile; Heavy Dust Load, LMST 20.00

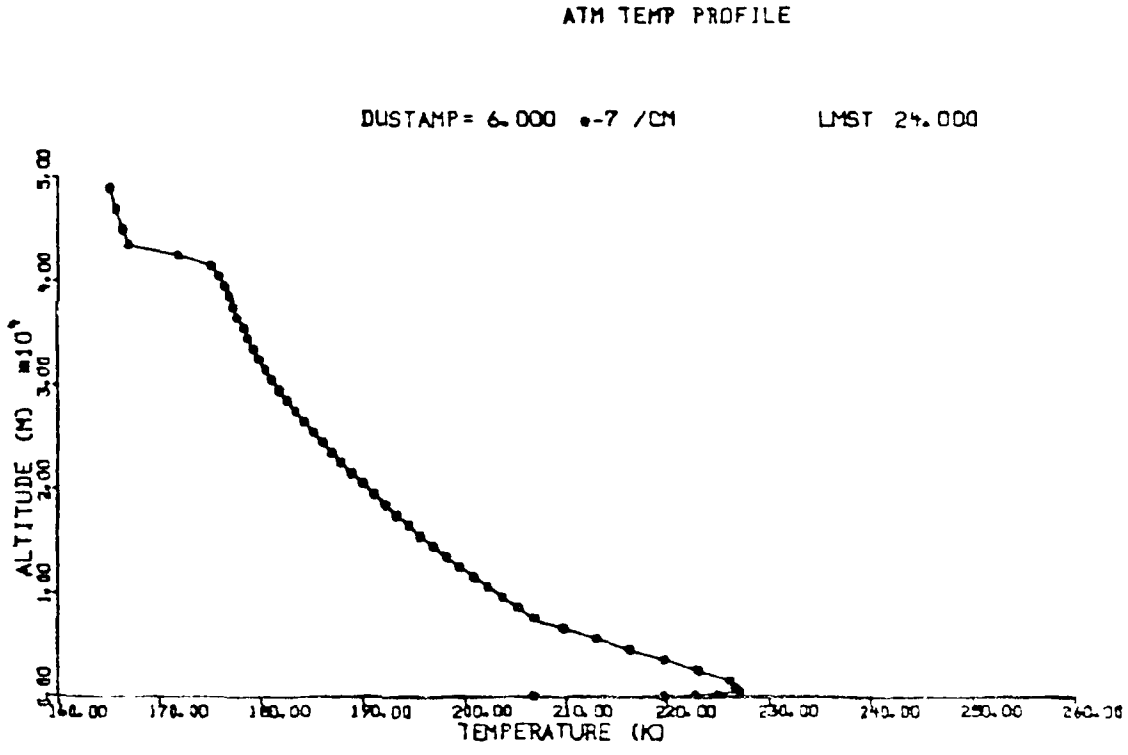

Fig. A.73 Atmospheric Temperature Profile; Heavy Dust Load, LMST 24.00

MARTIAN DUSTY ATMOSPHERE RAD-COND-CONV HEAT

TRANSFER SIMULATION: MARSDUST

Figures A.74 - A.84

Vertical Profiles of

Dust Temperature

With Heavy Dust Loading

DUSTAMP = 6.0×10^{-7} cm^{-1}

Four hour intervals from LMST 20.000 to LMST 4.000;

two hour intervals otherwise.

Horizontal axis temperature range: 190 K to 290 K;

Vertical axis altitude range: 0 m to 50 000 m.

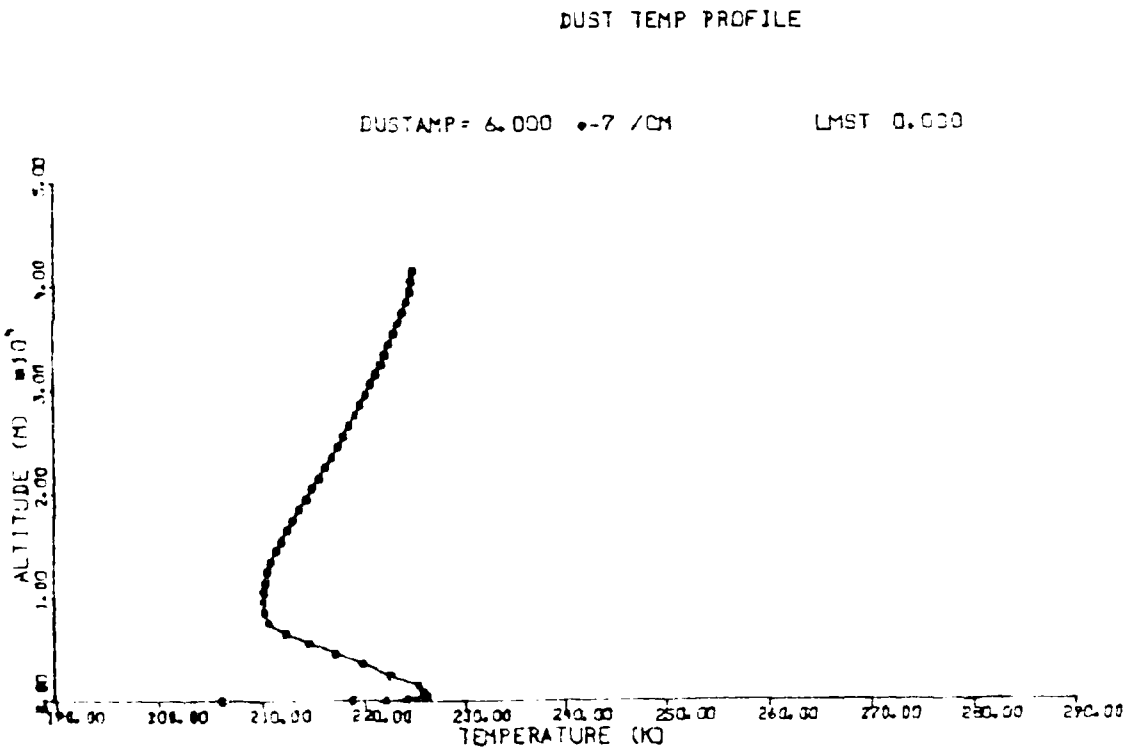

Fig A-14 Dust Temperature Profile: Heavy Dust Load, LMST 00.00

DUST TEMP PROFILE

DUSTAMP= 6.000 e-7 /CM LMST 4.000

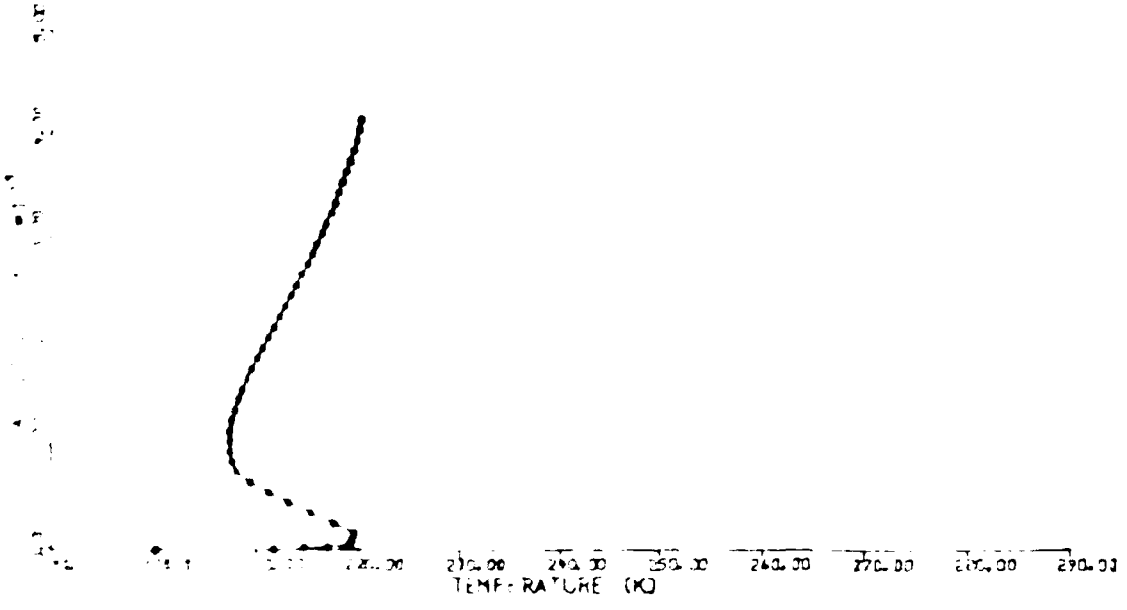

LMST 04.00

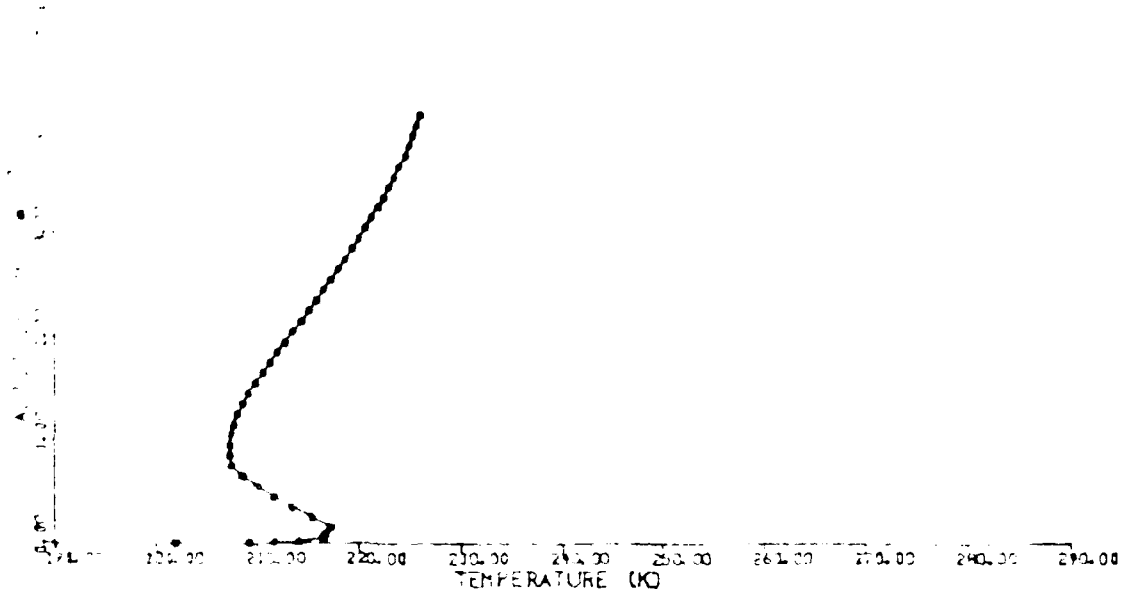

Fig. A-6 [illegible] Temperature Profiles, Heavy Dust Loading, LMST 06:00

AD-A185 888 PARTICLE-GAS TEMPERATURE DIFFERENTIALS RESULTING FROM TIME-DEPENDENT RADI (U) AIR FORCE INST OF TECH WRIGHT-PATTERSON AFB OH P J BELLAIRE 1987 3/3

UNCLASSIFIED AFIT/CI/NR-87-47T F/G 3/2 NL

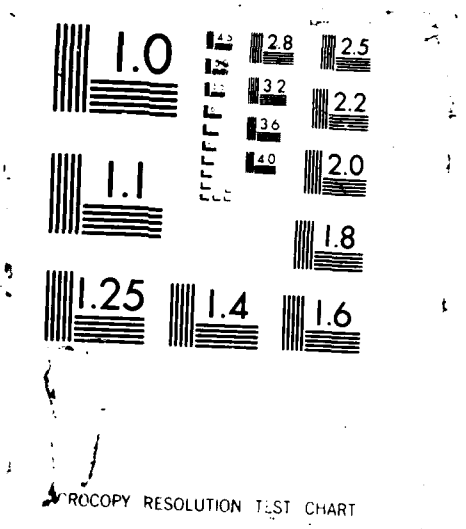
1.0
2.8
2.5
3.2
2.2
3.6
4.0
1.1
2.0
1.8
1.25
1.4
1.6
ROCOPY RESOLUTION TEST CHART

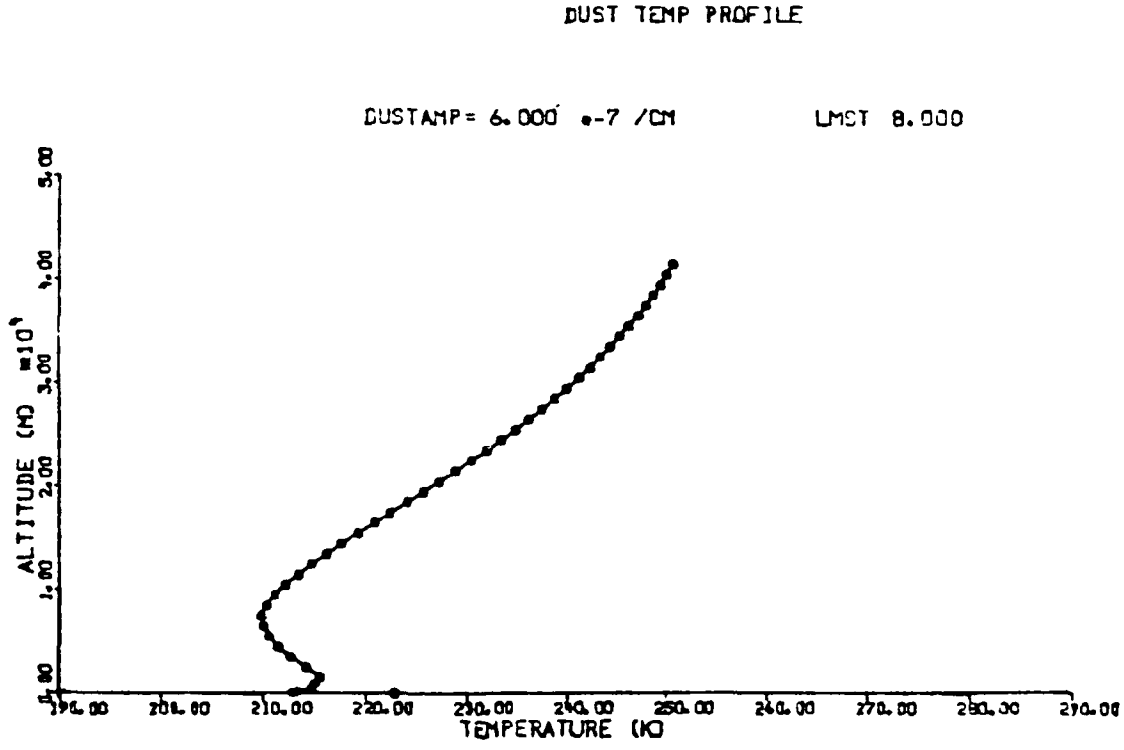

Fig. A.77 Dust Temperature Profile; Heavy Dust Load, LMST 08.00

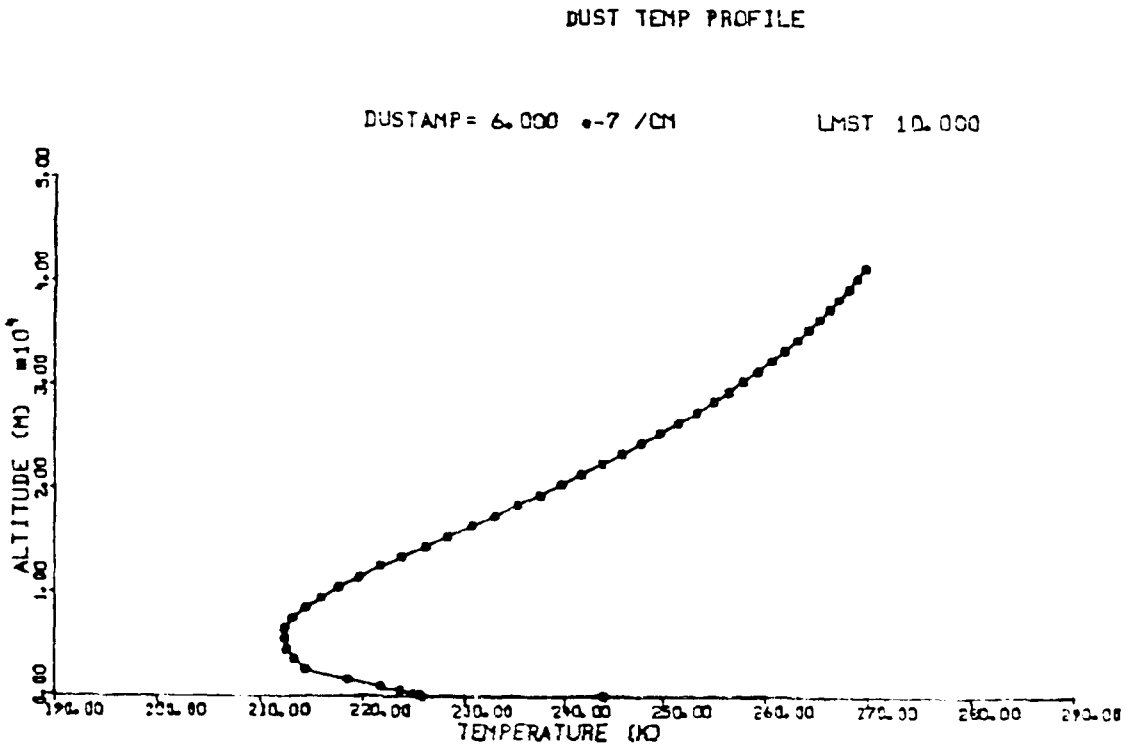

Fig. A.78 Dust Temperature Profile: Heavy Dust Load, LMST 10.00

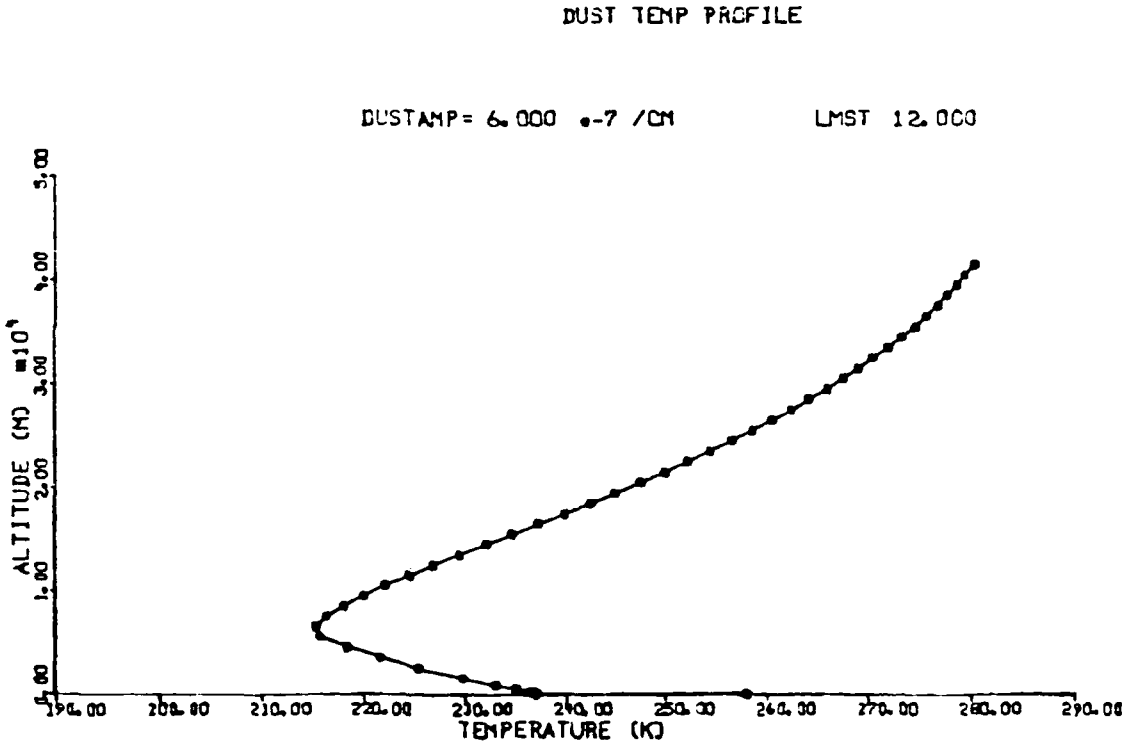

Fig. A.79 Dust Temperature Profile; Heavy Dust Load, LMST 12.00

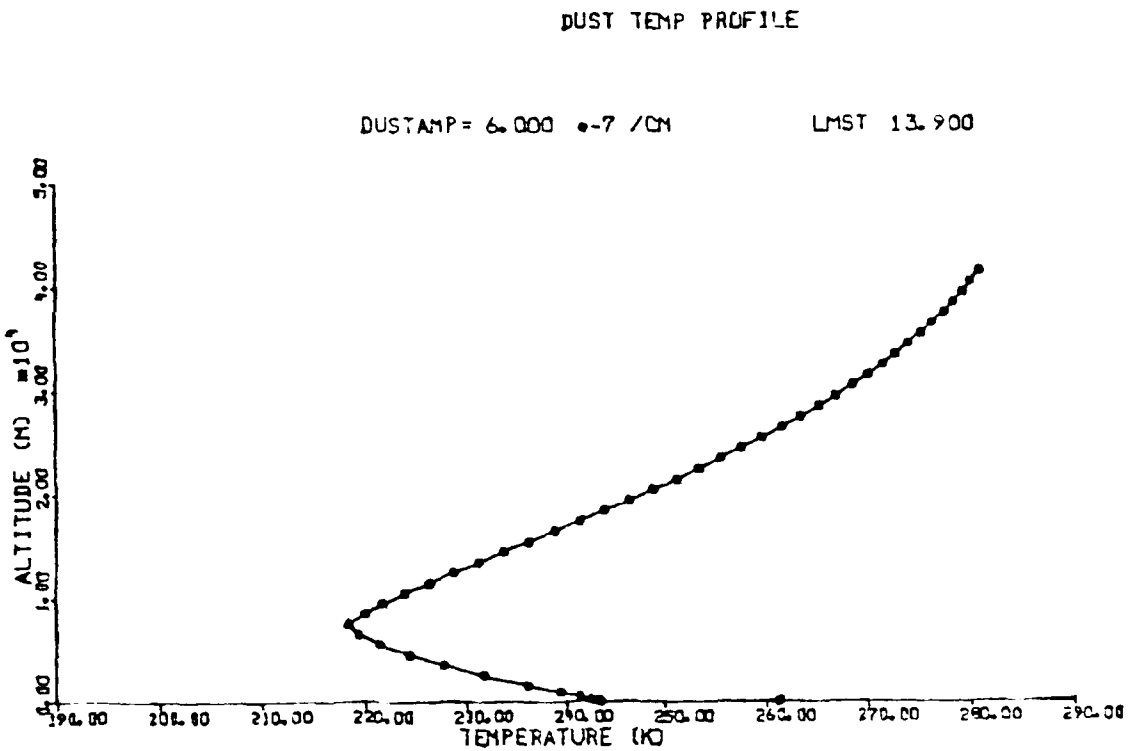

Fig. A.80 Dust Temperature Profile; Heavy Dust Load, LMST 13.90

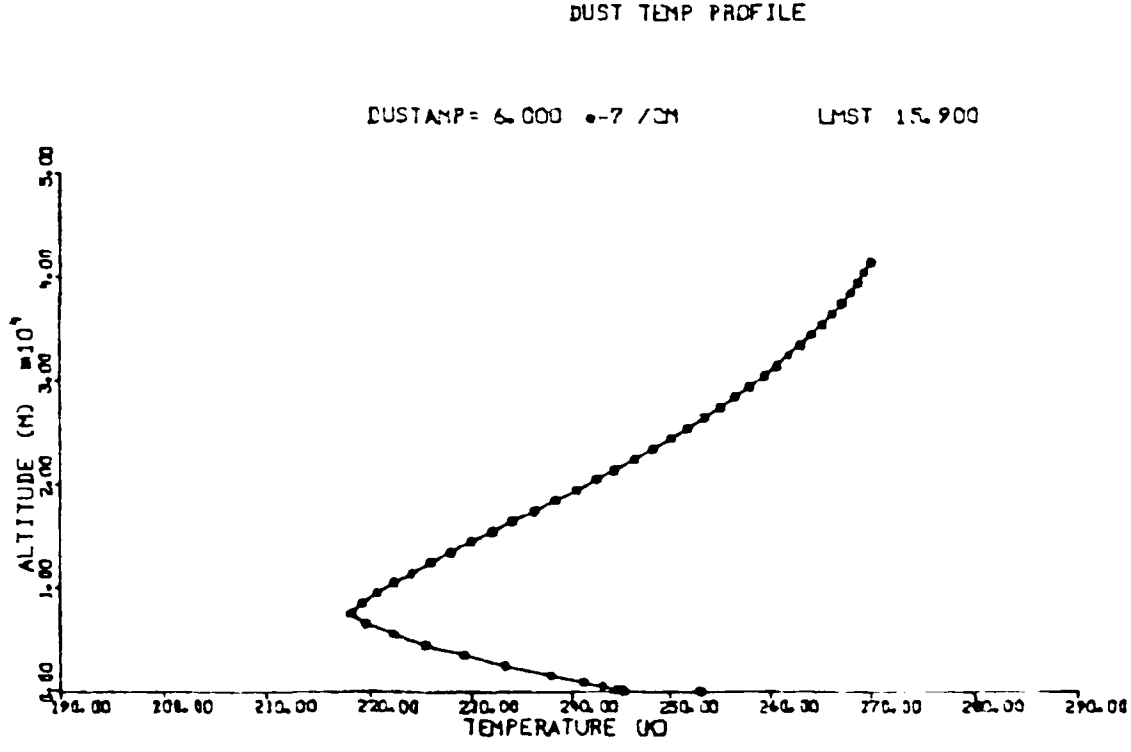

Fig. A.81 Dust Temperature Profile: Heavy Dust Load, LMST 15.90

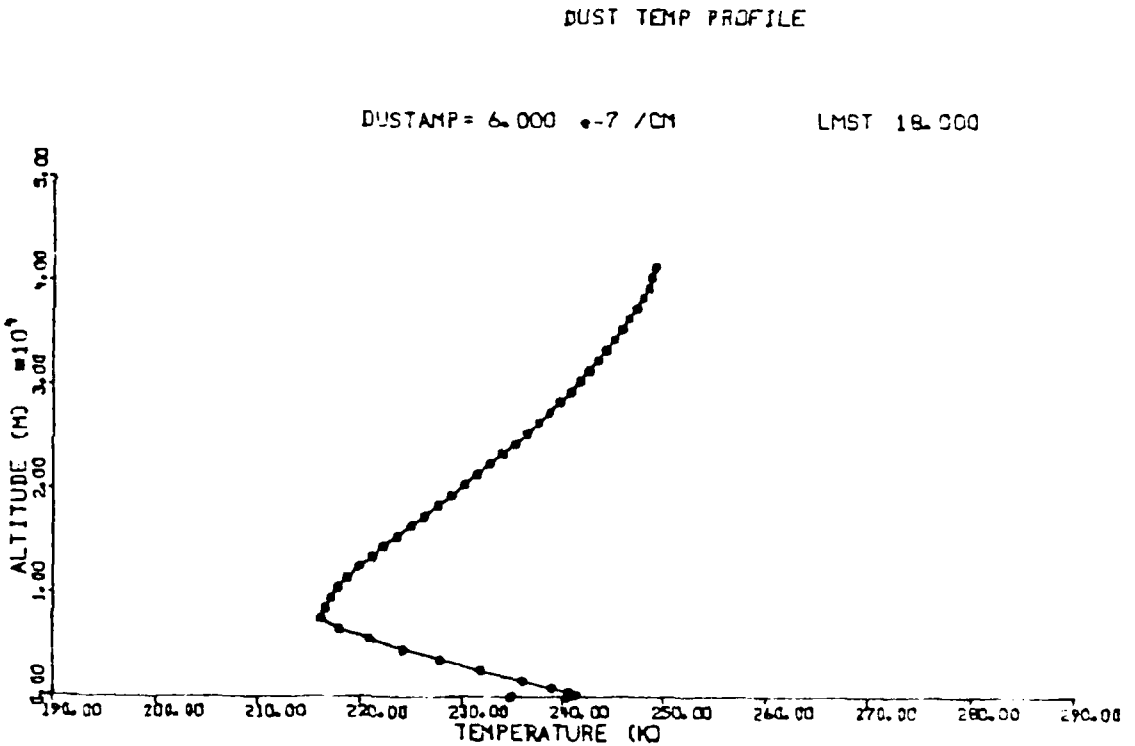

Fig. A.82 Dust Temperature Profile; Heavy Dust Load, LMST 18.00

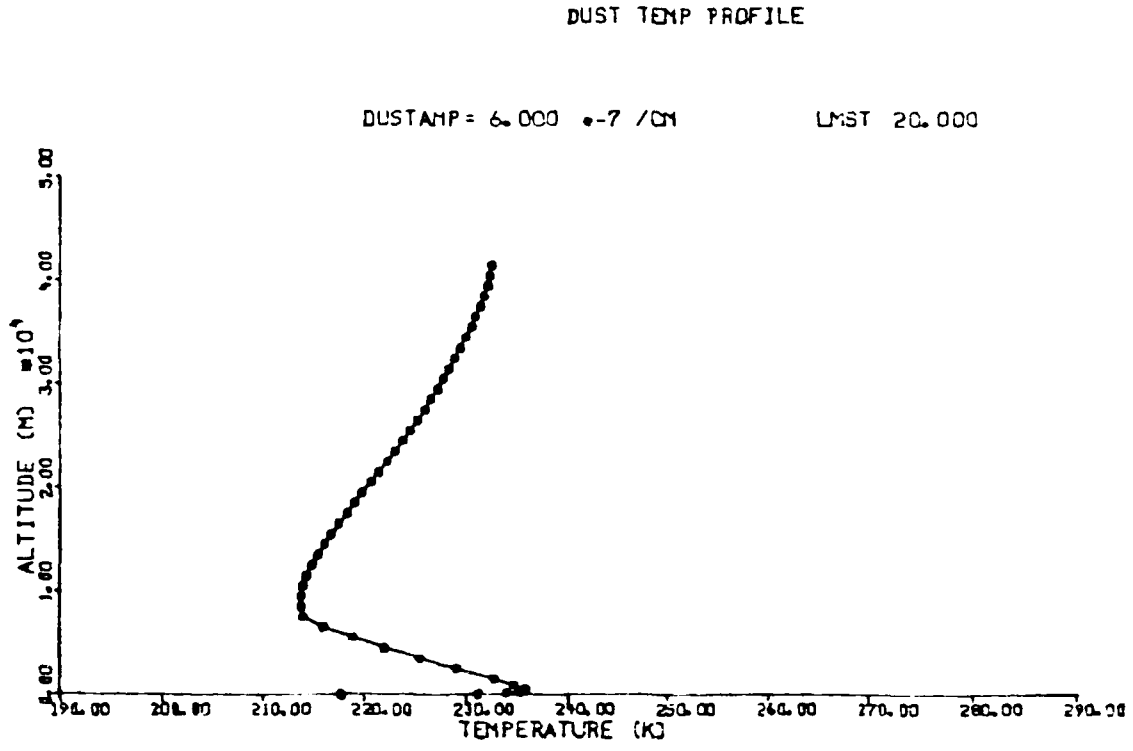

Fig. A.83 Dust Temperature Profile; Heavy Dust Load, LMST 20.00

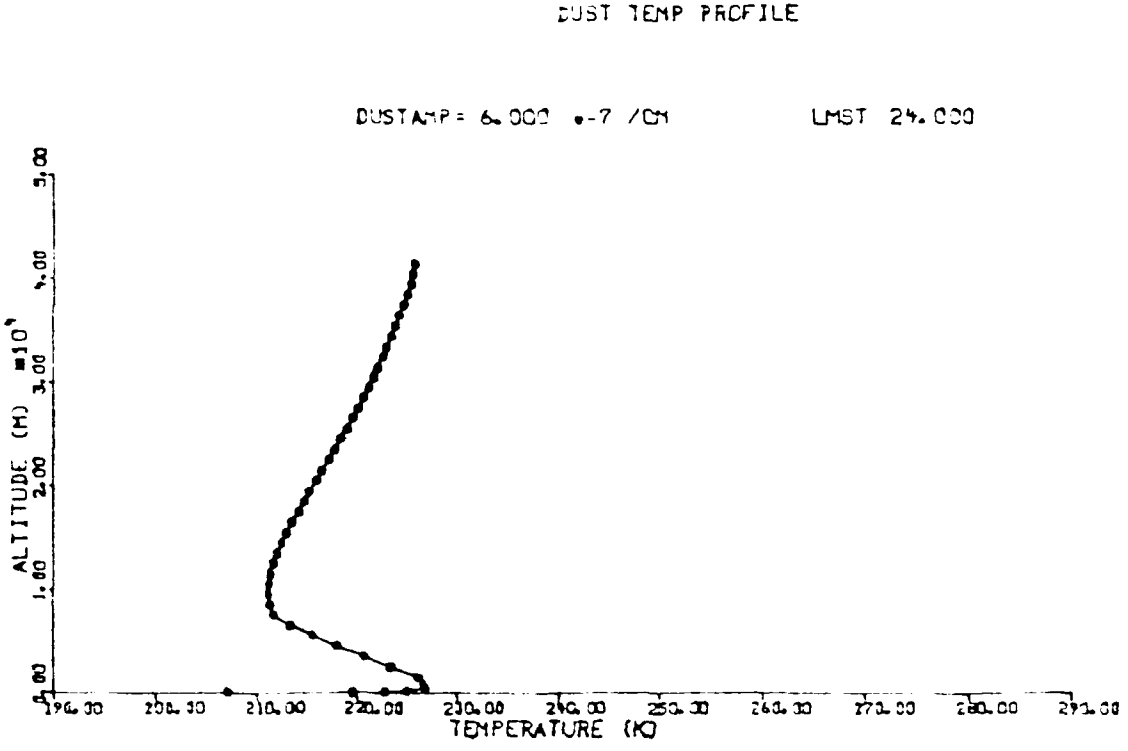

Fig. A.84 Dust Temperature Profile; Heavy Dust Load, LMST 24.00

MARTIAN DUSTY ATMOSPHERE RAD-COND-CONV HEAT

TRANSFER SIMULATION: MARSDUST

Figures A.85 - A.95

Vertical Profiles of

Dust Temperature Minus Atmospheric Temperature

With Heavy Dust Loading

DUSTAMP = 6.0×10^{-7} cm^{-1}

Four hour intervals from LMST 20.000 to LMST 4.000;

two hour intervals otherwise.

Horizontal axis temperature difference range:

0 K to 150 K;

Vertical axis altitude range: 0 m to 50 000 m.

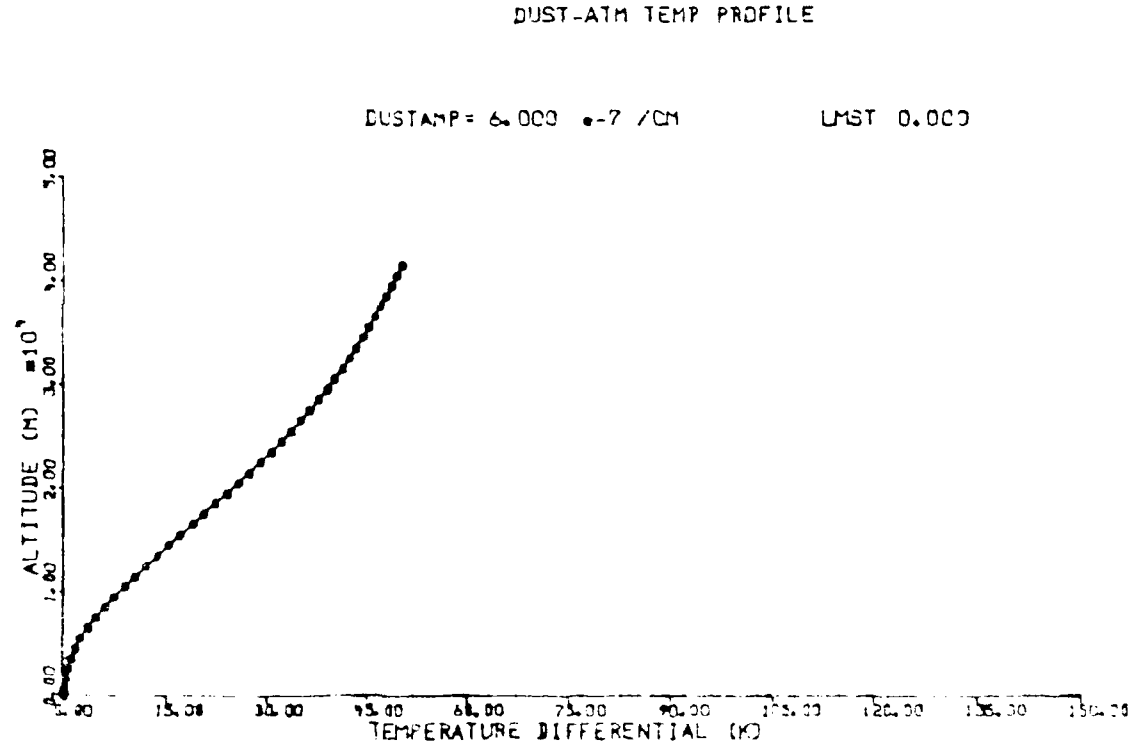

Fig. A.85 Dust-Atm Temperature Profile: Heavy Dust Load, LMST 00 00

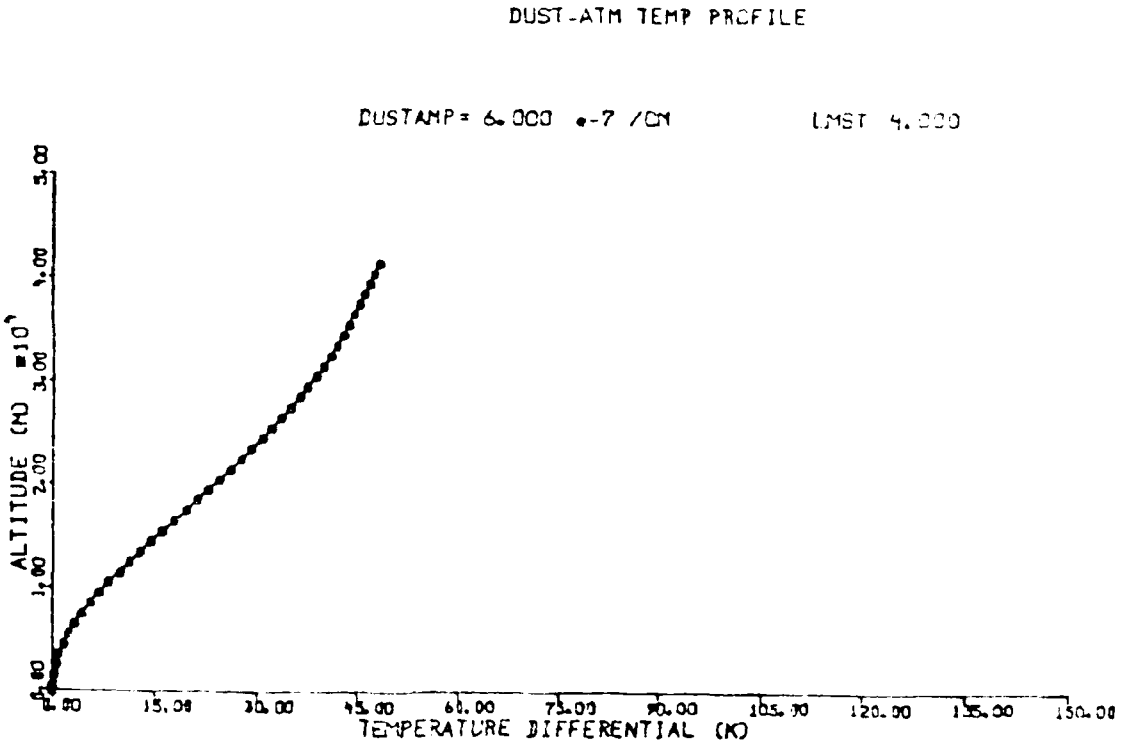

Fig. A.86 Dust-Atm Temperature Profile: Heavy Dust Load, LMST 04:00

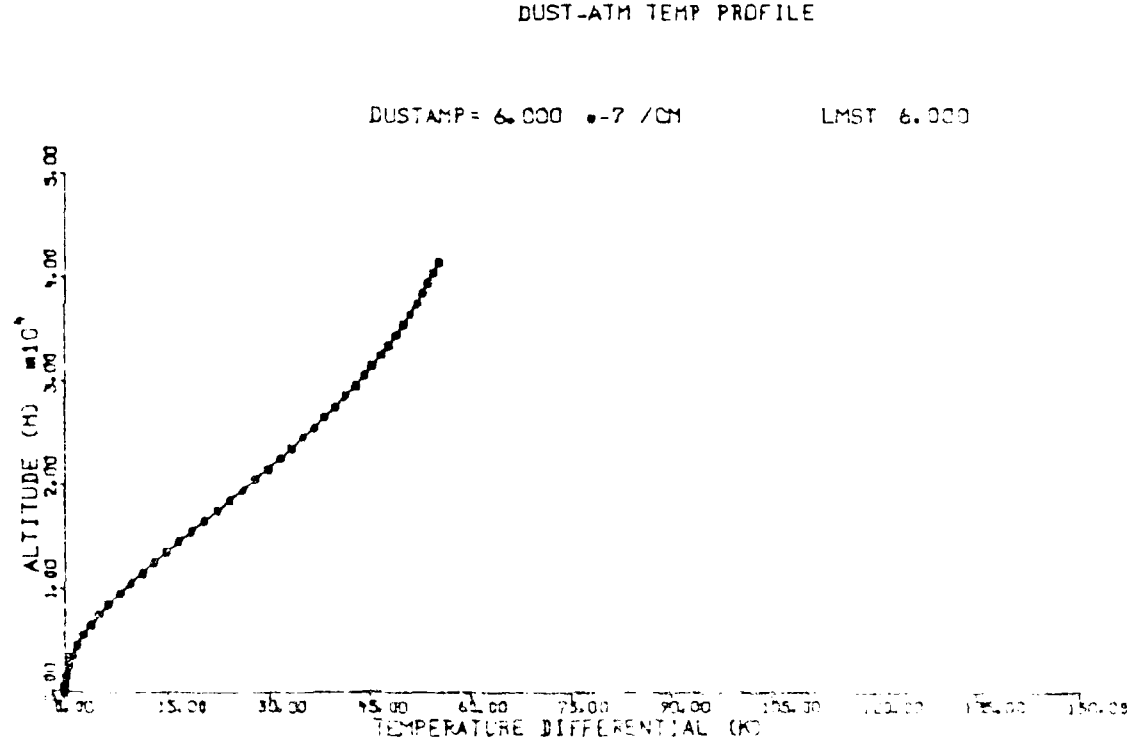

Fig A-67 Dust Atm Temperature Profiles, Heavy Dust Load, LMST 6.00

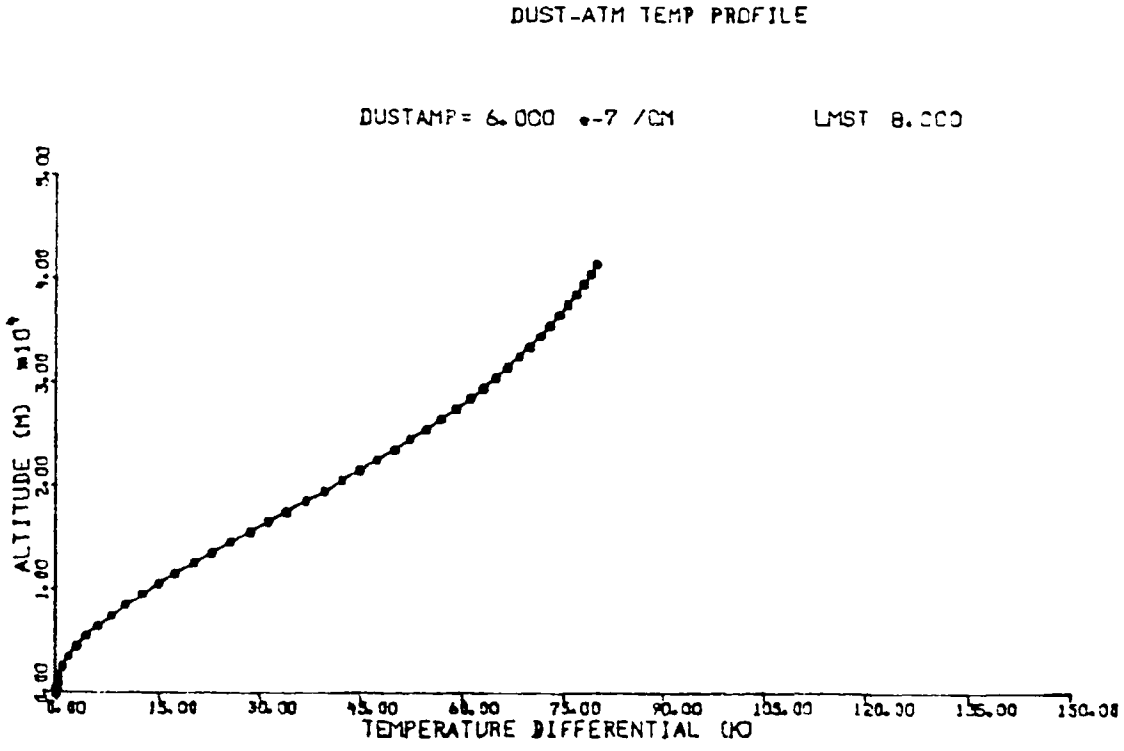

Fig. A.88 Dust-Atm Temperature Profile; Heavy Dust Load, LMST 08.00

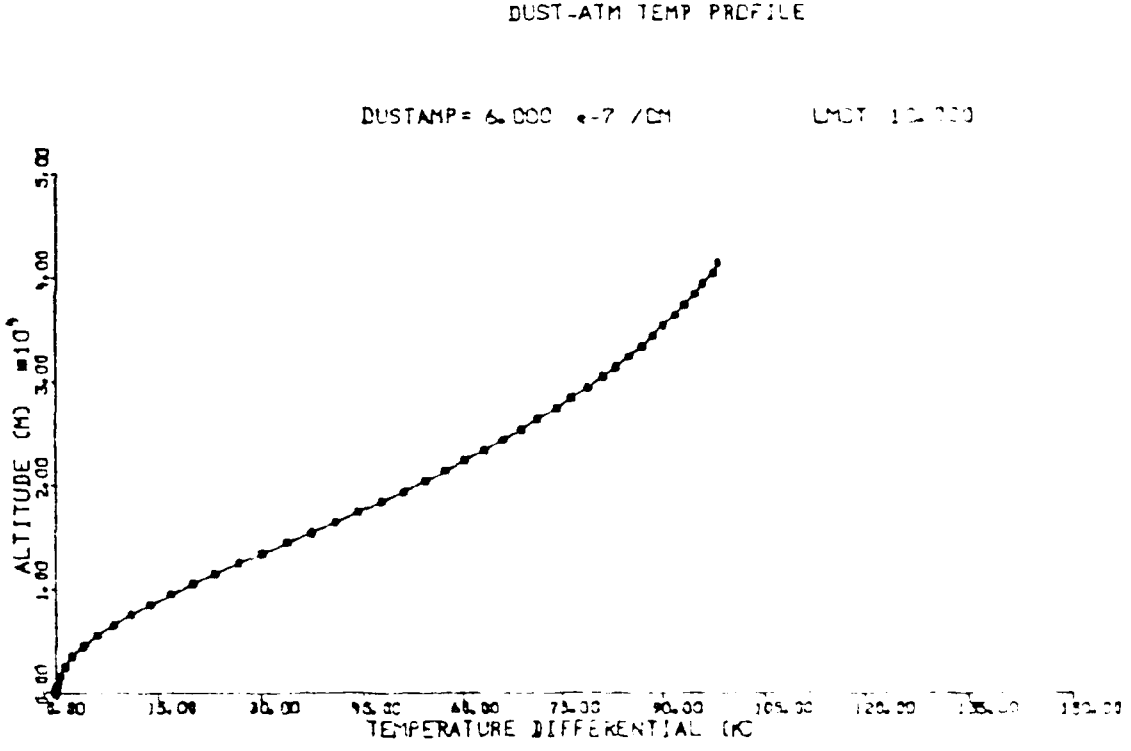

Fig. A-89 Dust-Atm Temperature Profile: Heavy Dust Load, LMST

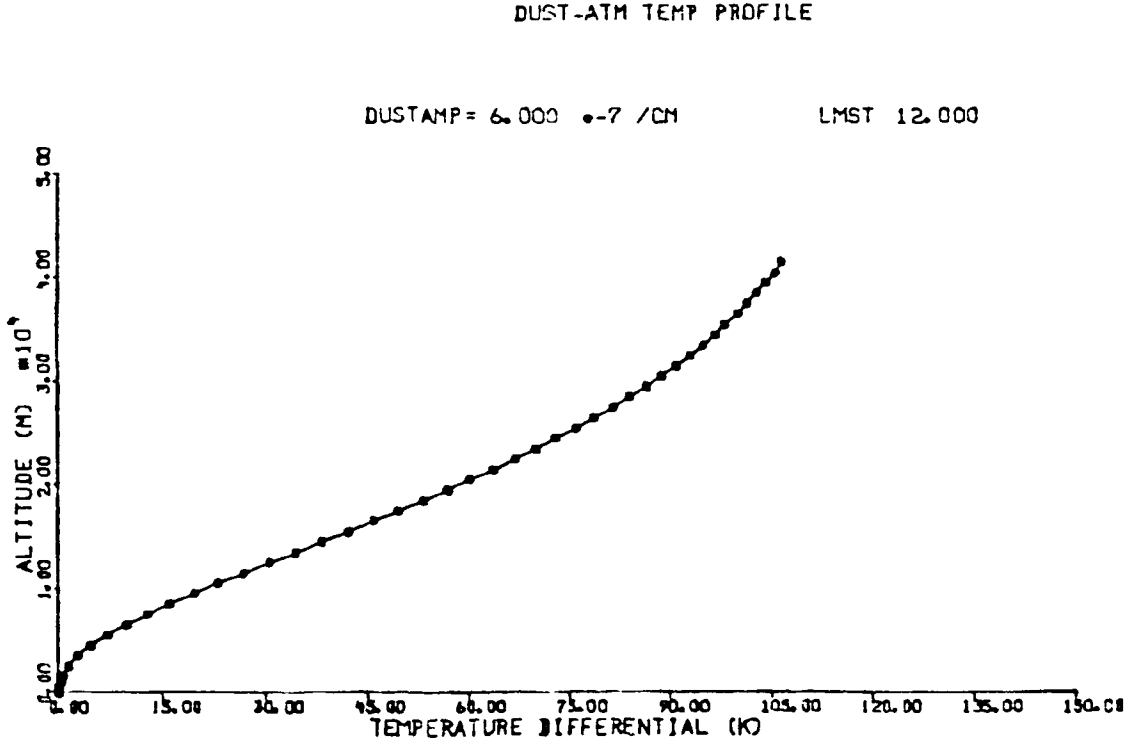

Fig. A.90 Dust-Atm Temperature Profile; Heavy Dust Load, LMST 12.00

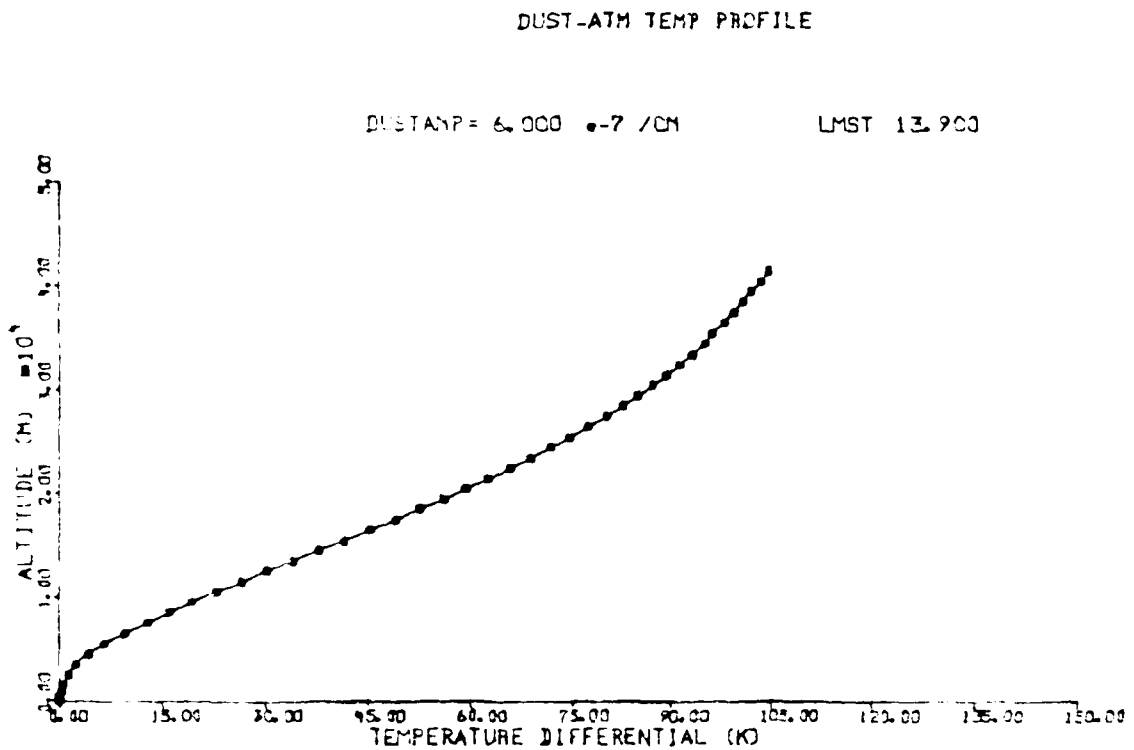

Fig. A.91 Dust-Atm Temperature Profile: Heavy Dust Load, LMST 13.90

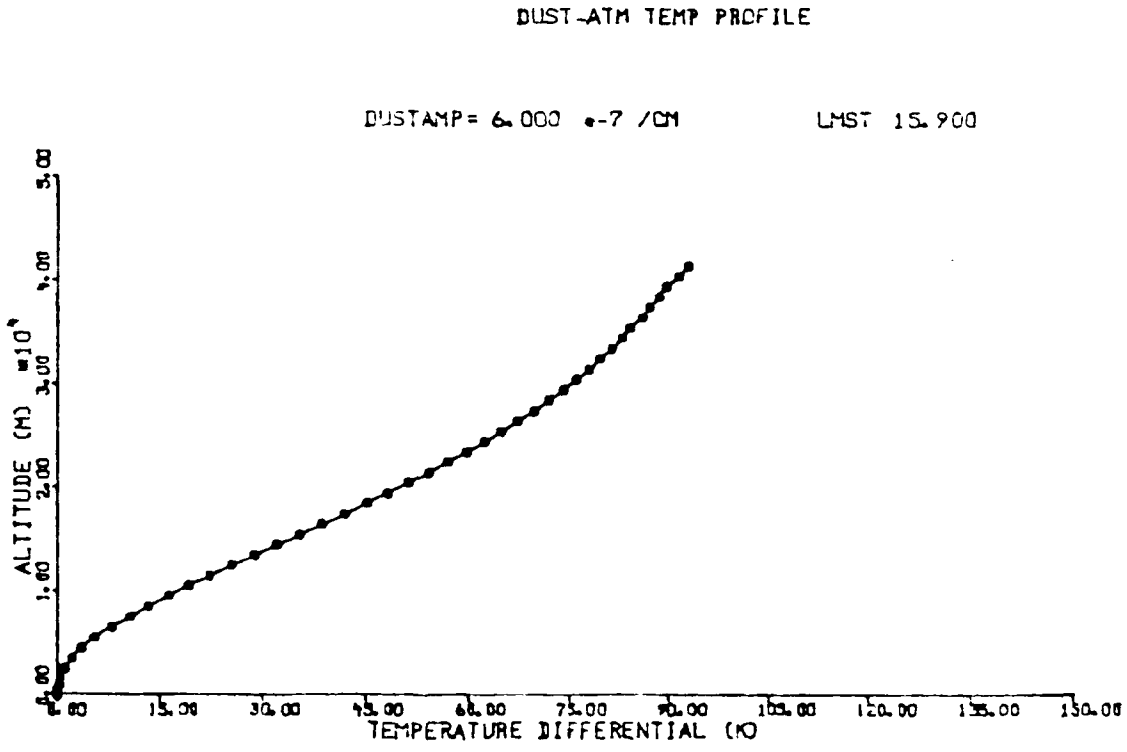

Fig. A.92 Dust-Atm Temperature Profile; Heavy Dust Load, LMST 15.90

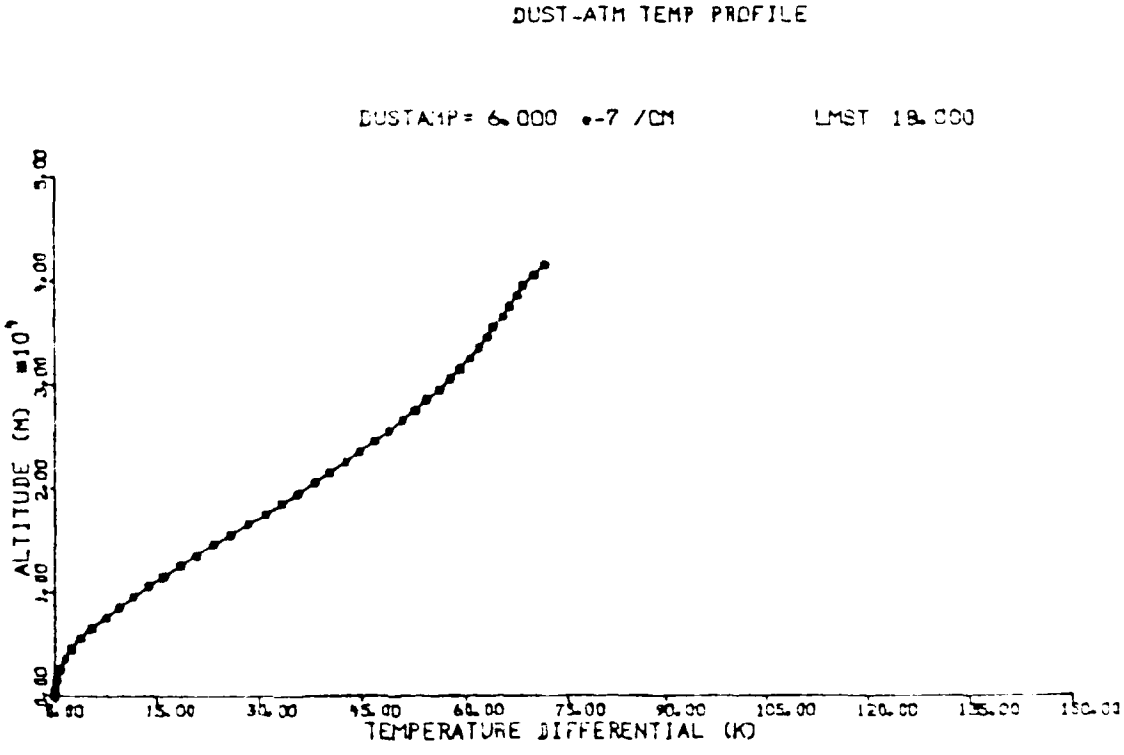

Fig. A.93 Dust-Atm Temperature Profile; Heavy Dust Load, LMST 18.00

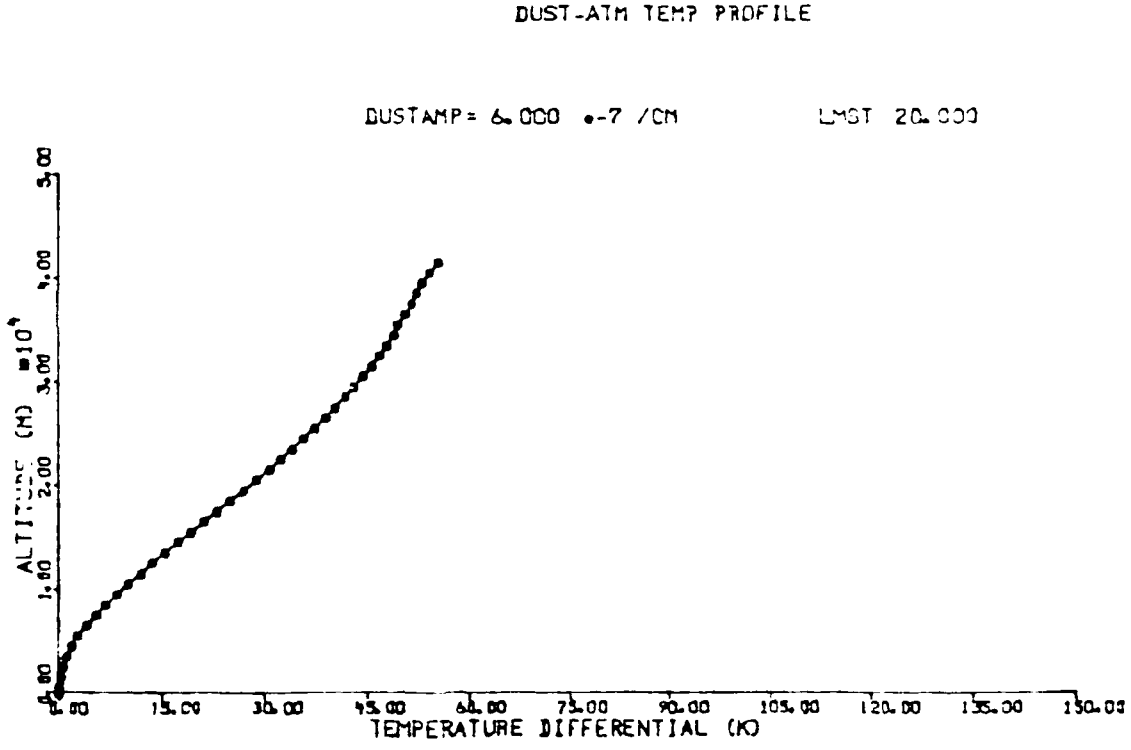

Fig. A.94 Dust-Atm Temperature Profile; Heavy Dust Load, LMST 20.00

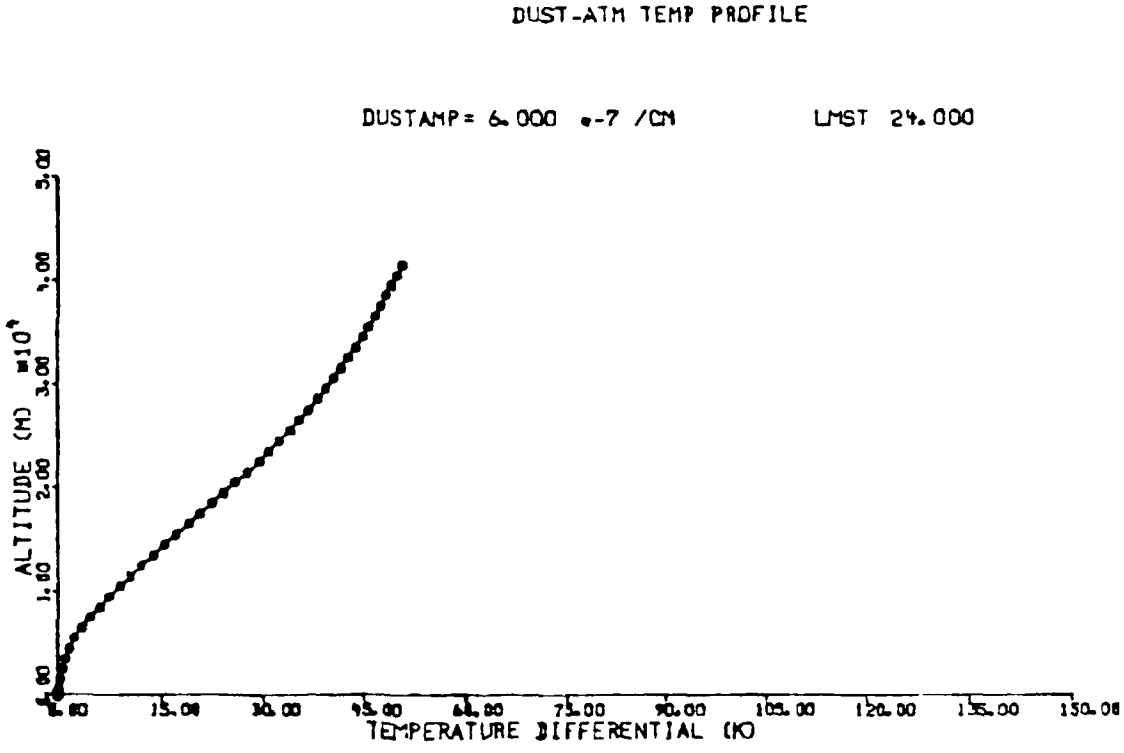

Fig. A.95 Dust-Atm Temperature Profile; Heavy Dust Load, LMST 24.00

BIBLIOGRAPHY

Journal articles:

Cadle, R.D., and G.W. Grams, 1975; Stratospheric aerosol particles and their optical properties; Rev. Geophys. and Space Phys., v. 13, # 4, pp. 475-501.

Chylek, P., and G.W. Grams, 1978; Scattering by nonspherical particles and optical properties of Martian dust; Icarus, v. 36, pp. 198-203.

Clough, S.A., et al., 1981; Atmospheric spectral transmittance and radiance: FASCOD1B; SPIE Vol. 277 Atmospheric Transmission, pp. 152-166.

Cordell, B.M., 1986; Mars, Earth, and ice; Sky and Telescope, v. 72, # 1, pp. 16-22.

Dannevick, W.P., and A.J. Pallmann, 1974; Mariner 9-based simulation of radiative convective temperature changes in the Martian dust-laden atmosphere-soil system; Riv. Ital. di Geofis., v. 23, # 3/4, pp. 201-206.

Davies, R., et al., 1984; Spectral absorption of solar radiation in cloudy atmospheres: A 20 cm-1 model; J. Atm. Sci., v. 41, pp. 2126-2137.

Egan, W.G., et al., 1980; High-resolution Martian atmosphere modeling; Icarus, v. 41, pp. 166-174.

Fiocco, G., et al., 1975; Equilibrium temperatures of small particles in the Earth's upper atmosphere (50-110 km); J. Atm. and Terr. Phys., v. 37, pp. 1327-1337.

Fiocco, G., et al., 1976; Energy exchange and temperature of aerosols in the Earth's atmosphere (0-60 km); J. Atm. Sci., v. 33, pp. 2415-2424.

Gierasch, P.J., and R.M. Goody, 1973; A model of a Martian great dust storm; J. Atm. Sci., v. 30, pp. 169-179.

Goody, R.M., and M. Belton, 1967; Radiative relaxation times for Mars: A discussion of Martian atmospheric dynamics; Planet. Space Sci., v. 15, pp. 247-256.

Haberle, R.M., 1986; The climate of Mars; Sci. Amer., v. 254, # 5, pp. 54-62.

Haberle, R.M., et al., 1982; Some effects of global dust storms on the atmospheric circulation of Mars; Icarus, v. 50, pp. 322-367.

Hansen, J.E., 1969; Exact and approximate solutions for multiple scattering by cloudy and hazy planetary atmospheres; J. Atm. Sci., v. 26, pp. 478-487.

Hess, S.L., 1979; Static stability and thermal wind in an atmosphere of variable composition: Applications to Mars; J. Geophys. Res.; v. 84, # B6, pp. 2969-2973.

Hunt, G.E., 1979; Thermal infrared properties of the Martian atmosphere 4. Predictions of the presence of dust and ice clouds from Viking IRTM spectral measurements; J. Geophys. Res.; v. 84, # B6, pp. 2865-2874.

Hunt, G.E., and P.B. James, 1985; Martian cloud systems: Current knowledge and future observations; Adv. Space Res., v. 5, # 8, pp. 93-99.

Iviev, L.S., and S.I. Popova, 1973; The complex refractive indices of substances in the atmospheric-aerosol dispersed phase; Izv., Atm. and Ocean. Phys., v. 9, # 10, pp. 1034-1043.

Joseph, J.H., et al., 1976; The delta-Eddington approximation for radiative flux transfer; J. Atm. Sci., v. 33, pp. 2452-2459.

Leovy, C.B., and R.W. Zurek, 1979; Thermal tides and Martian dust storms: Direct evidence for coupling; J. Geophys Res., v. 84, # B6, pp. 2956-2968.

Liou, K.N., and T. Sasamori, 1975; On the transfer of solar radiation in aerosol atmospheres; J. Atm. Sci., v. 32, pp. 2166-2177.

McCormick, M.P., et al., 1982; Polar stratospheric cloud sightings by SAM II; J. Atm. Sci., v. 39, pp. 1387-1397.

Martin, T.Z., and H.H. Kieffer, 1979; Thermal infrared properties of the Martian atmosphere 2. The 15- m band measurements; J. Geophys. Res., v. 84, # B6, pp. 2843-2852.

Martin, T.Z., et al., 1979; Thermal infrared properties of the Martian atmosphere 1. Global behavior at 7,9,11, and 20 m; J. Geophys. Res., v. 84, # B6, pp. 2830-2842.

Mugnai, A., et al., 1978; Effects of aerosol optical properties and size distributions on heating rates induced by stratospheric aerosols; Quart. J. R. Met. Soc., v. 104, pp. 783-796.

Pallmann, A.J., 1977; Effect of haze absorption and scattering on radiative-convective-conductive heat flux divergence in Martian CO2 atmosphere and ground; Riv. Ital. di Geofis. e Sci. Aff., v. 4, # 1/2, pp. 47-56.

Pallmann, A.J., 1983; The thermal structure of the atmospheric surface boundary layer on Mars as modified by the radiative effect of aeolian dust; J. Geophys. Res., v. 88, # C9, pp. 5483-5493.

Peterfreund, A.R., and H.H. Kieffer, 1979; Thermal infrared properties of the Martian atmosphere 3. Local dust clouds; J. Geophys. Res., v. 84, # B6, pp. 2853-2863.

Pollack, J.B., and O.B. Toon, 1982; Quasi-periodic climate changes on Mars: A review; Icarus, v. 50, pp. 259-287.

Pollack, J.B., et al., 1979; Properties and effects of dust particles suspended in the Martian atmosphere; J. Geophys. Res., v. 84, # B6, pp. 2929-2945.

Rothman, L.S., et al., 1983; AFGL atmospheric absorption line parameters compilation: 1982 edition; Appl. Opt., v. 22, # 15, pp. 2247-2256.

Singer, R.B., 1985; Spectroscopic observation of Mars; Adv. Space Res., v. 5, # 8, pp. 59-68.

Stephens, G.L., 1983; The influence of radiative transfer on the mass and heat budgets of ice crystals falling in the atmosphere; J. Atm. Sci., v. 40, pp. 1729-1739.

Thomas, P., and P.J. Gierasch, 1985; Dust devils on Mars; Science, v. 230, pp. 175-177.

Thorpe, T.E., 1981; Mars atmospheric opacity effects observed in the northern hemisphere by Viking Orbiter imaging; J. Geophys. Res., v. 86, # A13, pp. 11419-11429.

Toon, O.B., et al., 1977; Physical properties of the particles composing the Martian dust storm of 1971-1972; Icarus, v. 30, pp. 663-696.

Wells, E.N., et al., 1984; Mars: experimental study of albedo changes caused by dust fallout; Icarus, v. 58, pp. 331-338.

Wiscombe, W.J., 1977[a]; The delta-M method: Rapid yet accurate radiative flux calculations for strongly asymmetric phase functions; J. Atm. Sci., v. 34, pp. 1408-1421.

Zurek, R.W., 1976; Solar heating of the dusty Martian atmosphere; Icarus, v. 35, pp. 196-206.

Zurek, R.W., 1981; Inference of dust opacities for the 1977 Martian great dust storms from Viking Lander 1 pressure data; Icarus, v. 45, pp. 202-219.

Zurek, R.W., 1982; Martian great dust storms: An update; Icarus, v. 50, pp. 288-310.

Special publications:

American Geophysical Union (AGU), 1977; Scientific Results of the Viking Project; Reprinted from J. Geophys. Res., v. 82, # 28, pp. 3959-4680.

Conrath, B.J., et al., 1973; Atmosphere and Surface Properties of Mars Obtained by IR Spectroscopy on Mariner 9; Mariner Mars 1971 Project Final Report, Vol. IV: Science Results, Jet Propulsion Laboratory, Pasadena, California.

Fernandez, W., 1973; Martian Ice Cap - Desert Breeze: A Simulation; M.S. Thesis, Saint Louis University, pp. 54.

Isaacs, R.G., et al., 1986; Multiple Scattering Treatment for Use in the LOWTRAN and FASCODE Models; AFGL-TR-86-0073, Air Force Geophysics Laboratory, Hanscom AFB, Massachusetts, pp. 234.

Mechtly, E.A., 1973; The International System of Units, Physical Constants and Conversion Factors; NASA SP-7012; National Aeronautics and Space Administration, Washington, D.C., pp. 21.

NASA/JPL, 1984; Viking, The Exploration of Mars; NASA EP-208, National Aeronautics and Space Administration, Washington, D.C., pp. 56.

Pallmann, A.J., 1976; Effective Mie-scattering and CO2 Absorption in the Dust-laden Martian Atmosphere and its Impact on Radiative-Convective Temperature Changes in the Lower Scale Heights; PLATMOS Research Report #10, Planetary Atmospheres Research Project, NASA Grant 26-006-042, Saint Louis University, Missouri, pp. 124.

Sekera, Z., 1963; Radiative Transfer in a Planetary Atmosphere with Imperfect Scattering; R-413-PR, The RAND Corporation, Santa Monica, California, pp. 64.

Souders, S.W., 1970; Relative Geometries of the Earth, Sun, and Mars from the Year 1973 to the Year 2000; NASA SP-3053; National Aeronautics and Space Administration, Washington, D.C., pp. 128.

Wiscombe, W.J., 1977[b]; The delta-Eddington Approximation for a Vertically Inhomogeneous Atmosphere; NCAR/TN-121+STR; National Center for Atmospheric Research, Boulder, Colorado.

Books:

Deirmendjian, D., 1969; Electromagnetic Scattering on Spherical Polydispersions; R-456-PR, The RAND Corporation, Santa Monica, California, 290 pp.

Howell, J.R., and R. Siegel, 1969; Thermal Radiation Heat Transfer, Volume II: Radiation Exchange Between Surfaces and in Enclosures; NASA SP-164, National Aeronautics and Space Administration, Washington, D.C., pp. 285.

Liou, K.N., 1980; An Introduction to Atmospheric Radiation; Academic Press, New York, N.Y., [illegible] pp.

NASA, 1976; The Martian Landscape; NASA SP-425, National Aeronautics and Space Administration, Washington, D.C., pp. 166.

Pasachoff, J.M., 1979; Astronomy: From the Earth to the Universe; Saunders College Publishing, Philadelphia, Pennsylvania, pp. 559.

Siegel, R., and J.R. Howell, 1971; Thermal Radiation Heat Transfer, Volume III: Radiation Transfer with Absorbing, Emitting, and Scattering Media; NASA SP-164, National Aeronautics and Space Administration, Washington, D.C., pp. 359.

van de Hulst, H.C., 1957; Light Scattering by Small Particles; J. Wiley and Sons, New York, N.Y., pp. 470.

van de Hulst, H.C., 1980; Multiple Light Scattering, Vols. I and II; Academic Press; New York, N.Y., pp. 739.

VITA AUCTORIS

Paul John Bellaire, Jr. was born on the 27th of June, 1956, in Pittsburgh, Pennsylvania. After attending primary schools in Delaware and Florida, he graduated in 1974 from Lake Worth High School in Lake Worth, Florida, where he earned a National Merit Scholarship. In his senior year of high school, the author concurrently attended Palm Beach Junior College in Lake Worth, Florida, earning college credit in chemistry. He graduated from the University of California at Los Angeles (UCLA) in 1978 with the degree of Bachelor of Science in Physics.

The author served from 1978 to 1980 as a secondary school science and mathematics teacher in Malaysia with the United States Peace Corps. In August 1984, he graduated from the United States Air Force Officer Training School in San Antonio, Texas, where he received his Commission. He was accepted into the Graduate School of Saint Louis University in the fall of 1985 after completing the Air Force Basic Meteorology Program at the University. The author is currently a student member of the American Meteorological Society and the American Geophysical Union.

END

DATE

FILMED

DEC.

1987